Numerical Investigation of Theories of Strain-Gradient Plasticity

Nothando Precious Mhlongo (MHLNOT006@myuct.ac.za)
University of Cape Town (UCT)

Supervised by: Prof. B.D. Reddy
University of Cape Town, South Africa

Dissertation presented for the degree of Master of Science in the Department of Mathematics and Applied Mathematics,

University of Cape Town

Declaration

I, the undersigned, hereby declare that the work contained in this research project is my original work, and that any work done by others or by myself previously has been acknowledged and referenced accordingly.

Signed by candidate

NOTHANDO Precious Mhlongo, 31 July 2018

Abstract

In this work, a higher-order irrotational strain gradient plasticity theory is studied in the small strain regime. This theory is based on that originally developed by Gurtin and Anand, and includes both dissipative and energetic contributions. A detailed numerical study is based on the problem of simple shear of a homogeneous and a non-homogeneous block. Combinations of micro-hard and micro-free boundary conditions are used. The elastic gap, that is, elastic behaviour following a change in the plastic regime from micro-free to micro-hard boundary conditions, is clearly evident. A second phenomenon studied is that of strengthening and hardening with increase in dissipative and energetic length scales, respectively. For the purely dissipative theory, it has been shown that the flow relation in terms of Cauchy stress is necessarily global in terms of the dissipation function. This relation cannot be inverted in closed form to obtain a relation in terms of a global yield function. Approximations to the yield function are proposed using a maximisation relation, and these predictions of yield are compared with actual yield determined numerically.

Contents

Chapter 1

Introduction

Experiments on metallic specimens at the micro scale (approximately 10μm to 100μm) show significant size-dependence which conventional theories of plasticity are not able to capture. These include experiments on torsion (Fleck et al., 1994), indentation (Begley and Hutchinson (1998), Swadener et al. (2002), Stelmashenko et al. (1993), Ma and Clarke (1995)), bending (Stölken and Evans, 1998) and thin film applications (Xiang and Vlassak, 2006). For all these cases there may be different explanations; however, there is general agreement about a size-dependence of hardening (the increase in the stress needed to obtain a given plastic shear with the increase of the energetic length scale) and/or strengthening (the increase of the initial yield stress with the increase of the dissipative length scale magnitude) due to geometrically necessary dislocations (GND), hence clear motivation for the inclusion of material length scales in the constitutive models.

Size-dependent effects may be incorporated in conventional plasticity theories by assuming, for example, that the yield stress depends on the plastic strain and its gradient. Aifantis (1984), (1987), and Mühlhaus and Aifantis (1991) introduced the Laplacian plastic strain measure in the classical yield criterion to construct a plastic flow rule that also incorporates Bauschinger's effect. Gurtin (2004) then Gurtin and Anand (2005) presented an alternative, thermodynamically consistent approach, with the latter referred to as Gurtin's distortion gradient plasticity theory. Its starting point is the principle of virtual power in which microstresses $\boldsymbol{\rho}$ and $\mathbb{K}$ power conjugate to the plastic strain rate $\dot{\boldsymbol{\epsilon}}^p$ and its gradient $\nabla\dot{\boldsymbol{\epsilon}}^p$, respectively, are included. This leads to the equilibrium and microforce balance equations governing the gradient model.

The initial boundary value problem corresponding to the model of Gurtin and Anand (2005) is formulated as a variational inequality, and its well-posedness explored by Reddy, Ebobisse, and McBride (2008). Moreover, Gudmundson (2004) presented a theoretical framework that has the potential to cover a large range of strain gradient plasticity effects in isotropic materials

for both incremental plasticity and viscoplasticity. He shows that there is a close coonnection between the surface energy of an interface and boundary conditions in terms of plastic strains and moment stresses. Following the strategy of Gudmundson (2004), Fleck and Willis (2009a, 2009b) developed a phenomenological flow theory version of strain-gradient plasticity which involves a tensorial and/or scalar plastic multiplier as the primary kinematic unknown in addition to the displacement rate. The theory they developed is constructed such that stress measures, work-conjugate to plastic strain and its gradient, satisfy a yield condition. They consider energetic and dissipative stresses, with a flow rule that is equivalent to the J_2 classical flow theory in the absence of gradient terms. This constitutive framework for both rate-dependent and rate-independent solids can be implemented numerically using standard finite element methods based on minimization problems.

In the strain-gradient model, the flow relation is given in terms of the microscopic stresses. This cannot be used to determine when yield has occurred locally, since the microscopic stresses are unknown. Reddy (2011) showed that the flow relation can be expressed in terms of the Cauchy stress through a global formulation using the dissipation function. The form of the flow relation in terms of the yield function and a normality law can then be obtained from a dualisation procedure. However, it is not possible to invert this relation in closed form to obtain the generalized plastic strain rate as the normal to a global yield function, as shown by Carstensen et al. (2017).

In recent work by McBride, Reddy and Steinmann (2018), micromorphic continua are introduced as a framework for extended models of plasticity. It is shown that while a local determination of the admissible region is not possible for the general energetic-dissipative case and the fully dissipative case in micromorphic plasticity, the hybrid energetic-dissipative case, defined in the paper, permits a local treatment. They introduce and develop the global problem, then deduce that determining the admissible region for it is non-trivial, and derive an upper bound for the yield function. Using the thoroughly researched one-dimensional strip subjected to shear, approximations to the yield strength are investigated.

Fleck, Hutchinson and Willis (2014) introduced the elastic gap phenomenon which arises as a result of non-proportional loading. The elastic gap is defined as the elastic response to change of microscopic boundary conditions at some time during the plastic phase of the analysis. Two types of strain-gradient plasticity theories were examined and consequences due to their differences were investigated for two examples with non-proportional loading. Pantheghini and Bardella (2016), Martínez-Pañeda, Niordson, Bardella (2016) and Bardella (2010) investigate the significant influence of the plastic shear strain and spin due to a mechanism associated with higher-order boundary conditions. The first two publications and Carstensen et al. (2017) also

investigate the 'elastic gap' as a result of non-proportional loading. Fleck and Willis (2014, 2015) observed the elastic gap in a dissipative plane-strain tension analysis of a strip subjected to passivation of the lateral boundaries. They further observed that the size of the elastic gap is not affected by the presence of energetic terms.

Polizzotto (2010) investigated a rate-independent theory to describe strengthening in terms of state variables, whilst Chiricotto, Giacomelli, Tomassetti (2016) developed and investigated a rate-independent theory to describe both strengthening and hardening. Other computational studies include strain gradient crystal plasticity modelling with particular reference to the material length scales involved (Bardella, 2007), fracture in SGP (Martínez-Pañeda and Niordson, 2016), lower order strain gradient plasticity theories (Niordson and Hutchinson, 2003), and size-effects in plane strain sheet-necking (Niordson and Redanz, 2004).

The main aim of this project is to implement a higher-order strain gradient plasticity algorithm with energetic and dissipative contributions as a user element in ABAQUS (Systemes, 2015). This work is restricted to small deformation plastically and irrotational materials. The model used is based on rate-independent, viscoplastic and strain-gradient plasticity theory of Gurtin and Anand (2005) with the rate-independent formulation of Reddy (2011) and defect energy based on Nye's tensor (Nye, 1953) as adapted by Panteghini and Bardella (2016). The energetic contribution is incoporated through a defect energy whilst the dissipitive contribution is captured in the flow relation.

We use the problem of simple shear of a block as a vehicle to investigate various aspects of a strain-gradient plasticity theory. Like Fleck and Willis (2015), Polizzotto (2010) and Chiricotto, Giacomelli, Tomassetti (2016), we investigate strengthening and hardening; the elastic gap in the case of non-proportional loading; and the global flow relation for the purely dissipative problem. We further we use the discrete problem to explore numerically the global formulation of the flow relation and yield function.

The rest of this work is organised as follows. We introduce the basic principles of continuum mechanics in Chapter 2; the classical elastic problem section of our model is presentend in Section 2.5. Chapter 3 presents the classical plasticity problem under small strain conditions; the equations governing our SGP model are presented in Section 3.2. In Chapter 4 we derive the weak formulation of our model and present the finite element approximations, in Section 4.7 we derive a global flow relation in terms of finite element approximation terminology. Results are presented in Chapter 5 and our conclusions are presented in Chapter 6.

Chapter 2

Continuum mechanics

The study of the response of continuous materials to different loading conditions is known as continuum mechanics. The response, particularly deformation, can either be geometrically significant or insignificant (small). This work considers the small deformation case. Since the continuum is assumed to be continuous, all physical quantities such as density, velocity and stress are assumed to vary smoothly with position and time. Literature discussing these assumptions and theories in detail include Allan, (2012), Rubin et al.,(2012), de Souza Neto et al., (2011) and Lai et al.,(2009). Allan (2012) also states that, though these assumptions are set out for macroscopic response of material, they provide a reasonably accurate response measure for shorter length scales with some relation of the deformation to macroscopic response.

This chapter discusses the relevant mathematical model of deformable solid behaviour. We assume isothermal behaviour throughout this work. Firstly, we define notation. We then discuss kinematics of continuous media in Section 2.1. The types of forces considered are discussed in Section 2.2, then the laws governing continua are presented in Section 2.3. A brief review of linear elasticity is presented in Section 2.4, and lastly the boundary value problem for an elastic material is formulated in Section 2.5.

Notation

We adopt the following conventions:

- Light-faced letters A, a, ... represent scalar valued functions and scalars.
- Bold letters $\mathbf{a}$, $\mathbf{A}$, ... represent vectors and tensors.
- Light sans serif font letters A, ... represent matrices.

We assume a fixed Cartesian coordinate system x_i where $i = 1, 2, 3$, with basis vectors $\mathbf{e}_i$. A vector $\mathbf{a}$ can be expressed in terms of its components with respect to this basis as

$$\mathbf{a} = a_1\mathbf{e}_1 + a_2\mathbf{e}_2 + a_3\mathbf{e}_3 = \sum_{i=1}^{3} a_i\mathbf{e}_i. \tag{2.1}$$

Using Einstein's summation convention, we drop the summation sign, and it is understood that for the index i, summation over the index range (three in this case) is implied. Then the components of $\mathbf{a}$ are denoted by a_i, and the components of a tensor $\mathbf{A}$ are represented by A_{ij}, A_{ijk}, A_{ijkl} for second-order, third-order and fourth-order tensors, respectively. The magnitude of a vector $\mathbf{a}$ is defined by $|\mathbf{a}| = \sqrt{\mathbf{a} \cdot \mathbf{a}}$, where $\mathbf{a} \cdot \mathbf{a} = a_i a_i$ is the inner product. The Kronecker delta is defined by

$$\delta_{ij} = \begin{cases} 1 & \text{if } i = j, \\ 0 & \text{if } i \neq j, \end{cases} \tag{2.2}$$

and ε_{ikl} denotes the alternating symbol:

$$\varepsilon_{ikl} = \begin{cases} 1 & \text{for } \{i,k,l\} \text{ an even permutation of } \{1,2,3\}, \\ -1 & \text{for } \{i,k,l\} \text{ an odd permutation of } \{1,2,3\}, \\ 0 & \text{for } \{i,k,l\} \text{ not a permutation of } \{1,2,3\}. \end{cases} \tag{2.3}$$

Regarding second-order-tensor operations, we adopt the standard notation for cartesian tensors:

$$\mathbf{A} = A_{ij}\ \mathbf{e}_i \otimes \mathbf{e}_j \tag{2.4}$$

where A_{ij} are the components and $\mathbf{e}_i \otimes \mathbf{e}_j$ is the basis. The inner product of tensors $\mathbf{A}$ and $\mathbf{B}$ is defined by

$$\mathbf{A} : \mathbf{B} = A_{ij}B_{ij}, \tag{2.5}$$

whilst the product $\mathbf{AB}$ is the tensor with components

$$A_{ij}B_{jk}. \tag{2.6}$$

The Euclidean norm of a tensor $\mathbf{A}$ is defined by $|\mathbf{A}| = \sqrt{\mathbf{A} : \mathbf{A}}$, and the transpose, trace, and determinant of $\mathbf{A}$ are represented by $\mathbf{A}^T$, tr$\mathbf{A}$ and det$\mathbf{A}$, respectively. The symmetric part of

a tensor sym $\mathbf{A}$ and the skew part skw $\mathbf{A}$ are defined by

$$\text{sym } \boldsymbol{A} = \frac{1}{2}(\boldsymbol{A} + \boldsymbol{A}^T), \tag{2.7}$$

$$\text{skw } \boldsymbol{A} = \frac{1}{2}(\boldsymbol{A} - \boldsymbol{A}^T), \tag{2.8}$$

respectively. The deviator dev $\mathbf{A}$ of a tensor $\mathbf{A}$ is defined by

$$\text{dev } \mathbf{A} = \boldsymbol{A} - \frac{1}{3}(\text{tr}\boldsymbol{A})\boldsymbol{I}, \tag{2.9}$$

where $\boldsymbol{I}$ is the identity tensor. The gradient of a tensor $\mathbf{A}(x)$ and vector $\mathbf{a}(\mathbf{x})$ is defined by the vector field

$$\nabla\mathbf{A}(\mathbf{x}) = \frac{\partial A_{ij}}{\partial x_k}\ \mathbf{e}_i \otimes \mathbf{e}_j \otimes \mathbf{e}_k, \tag{2.10}$$

$$\nabla\mathbf{a}(\mathbf{x}) = \frac{\partial a_i}{\partial x_j}\ \mathbf{e}_i \otimes \mathbf{e}_j, \tag{2.11}$$

and the divergence of a tensor $\mathbf{A}(\mathbf{x})$ is the vector defined by

$$\text{div } \boldsymbol{A} = \frac{\partial A_{ij}}{\partial x_j}\mathbf{e}_i. \tag{2.12}$$

The divergence of a vector $\mathbf{a}(\mathbf{x})$ is the scalar defined by

$$\text{div } \mathbf{a} = \nabla \cdot \mathbf{a} = \frac{\partial a_i}{\partial x_i}. \tag{2.13}$$

The curl of a vector $\mathbf{a}(\mathbf{x})$ is defined by

$$\text{curl } \boldsymbol{a} = \nabla \times \boldsymbol{a} = \varepsilon_{ijk}\frac{\partial a_k}{\partial x_j}\boldsymbol{e}_i \tag{2.14}$$

whilst the curl of a tensor $\mathbf{A}$ is defined by

$$\text{curl } \mathbf{A} = \varepsilon_{ikl}A_{jl,k}\ \mathbf{e}_i \otimes \mathbf{e}_j. \tag{2.15}$$

For third order tensors $\mathbf{A}$ and $\mathbf{B}$, the inner product is defined by

$$\mathbf{A}\vdots\mathbf{B} = A_{ijk}B_{ijk}. \tag{2.16}$$

2.1 Kinematics

Consider a material body occupying a region $\Omega_0 \subset \mathbb{R}^3$ at time t_0. We refer to this region as the reference configuration. After deformation at time t, we refer to the region $\Omega_t \subset \mathbb{R}^3$ occupied by the continuum as the deformed configuration. The spatial position at time t of a material point $\mathbf{X}$ is given by the motion

$$\mathbf{x} = \mathbf{x}(\mathbf{X}, t) \tag{2.17}$$

where $\mathbf{x}$ is the position of a particle initially at $\mathbf{X}$. The motion is assumed to be invertible; that is,

$$\mathbf{X} = \mathbf{X}(\mathbf{x}, t). \tag{2.18}$$

This requires that

$$J = \det \mathbf{F} \neq 0, \tag{2.19}$$

where

$$F_{ij} = \frac{\partial x_i}{\partial X_j}. \tag{2.20}$$

We further require $J > 0$ given that J measures the ratio of current to initial volume of infinitesimal region.

The displacement field is defined by

$$\mathbf{u}(\mathbf{X}, t) = \mathbf{x}(\mathbf{X}, t) - \mathbf{X}. \tag{2.21}$$

Therefore the position at time t in terms of displacement is

$$\mathbf{x} = \mathbf{X} + \mathbf{u}(\mathbf{X}, t). \tag{2.22}$$

Consider a particle Q_0 at a distance $d\mathbf{X}$ from the particle P_0 in the reference configuration. After deformation, point P_0 is transformed to $\mathbf{x}$ whilst Q_0 arrives at $\mathbf{x} + d\mathbf{x}$. Figure 2.1 shows the configurations, the position and the displacement vectors.

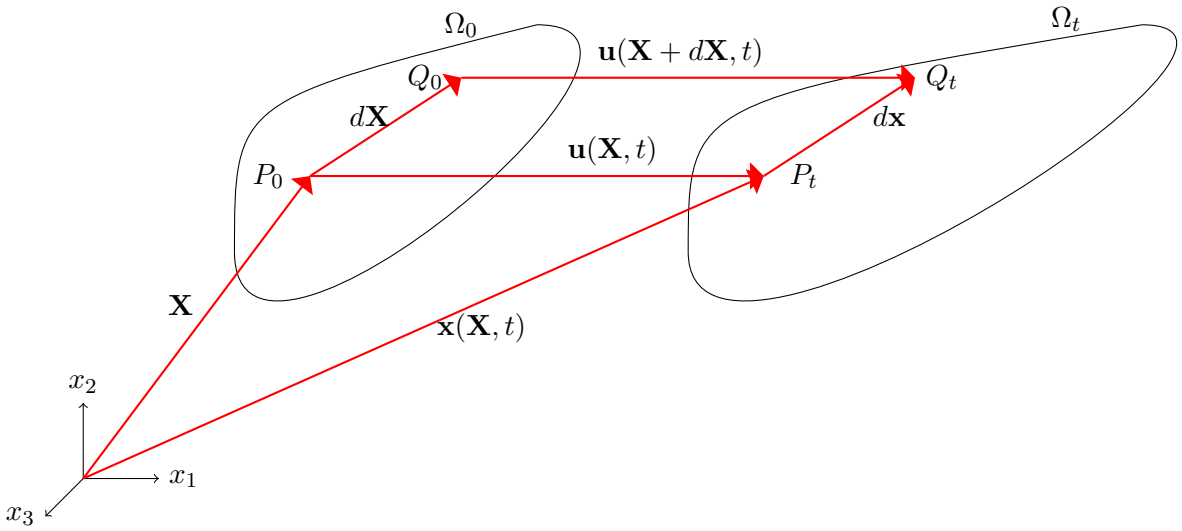

Figure 2.1: Reference and deformed configurations of a body

From Figure 2.1, it is obvious that

$$\mathbf{x}+d\mathbf{x}=\mathbf{X}+d\mathbf{X}+\mathbf{u}(\mathbf{X}+d\mathbf{X},t). \tag{2.23}$$

Subtracting equation (2.22) from (2.23) we obtain

$$d\mathbf{x}=d\mathbf{X}+\mathbf{u}(\mathbf{X}+d\mathbf{X},t)-\mathbf{u}(\mathbf{X},t), \tag{2.24}$$

which to first order becomes

$$\begin{aligned} d\mathbf{x} &= d\mathbf{X}+(\nabla\mathbf{u})d\mathbf{X} \\ &= \mathbf{F}d\mathbf{X}, \end{aligned} \tag{2.25}$$

where $\nabla\mathbf{u}$ is referred to as the displacement gradient. The deformation gradient $\mathbf{F}$ is given by

$$\mathbf{F}=\mathbf{I}+\nabla\mathbf{u}, \tag{2.26}$$

and has components

$$F_{ij}=\delta_{ij}+\frac{\partial u_i}{\partial X_j}. \tag{2.27}$$

To find the relation between the lengths of line elements in both configurations we take the dot

product of equation (2.25) with itself to obtain

$$\begin{aligned} d\mathbf{x} \cdot d\mathbf{x} &= \mathbf{F}d\mathbf{X} \cdot \mathbf{F}d\mathbf{X} \\ &= d\mathbf{X} \cdot (\mathbf{F}^T\mathbf{F})d\mathbf{X}. \end{aligned} \tag{2.28}$$

The quantity $\mathbf{F}^T\mathbf{F}$ is known as the right Cauchy-Green deformation tensor, denoted $\mathbf{C}$. From (2.26),

$$\mathbf{C} = \mathbf{F}^T\mathbf{F} \tag{2.29}$$

$$= (\mathbf{I} + \nabla\mathbf{u})^T(\mathbf{I} + \nabla\mathbf{u}) \tag{2.30}$$

$$= \mathbf{I} + \nabla\mathbf{u} + (\nabla\mathbf{u})^T + (\nabla\mathbf{u})^T\mathbf{u}. \tag{2.31}$$

We define the Lagrangian strain tensor $\mathbf{E}$ by

$$\mathbf{E} = \frac{1}{2}(\mathbf{C} - \mathbf{I}); \tag{2.32}$$

therefore we have

$$\mathbf{E} = \frac{1}{2}(\nabla\mathbf{u} + (\nabla\mathbf{u})^T + (\nabla\mathbf{u})^T(\nabla\mathbf{u})). \tag{2.33}$$

In this work we assume small strains; that is,

$$|(\nabla\mathbf{u})^T(\nabla\mathbf{u})| << |(\nabla\mathbf{u})|. \tag{2.34}$$

Hence, from equation (2.33) we define the small-strain tensor $\boldsymbol{\epsilon}$ by

$$\boldsymbol{\epsilon} = \frac{1}{2}[\nabla\mathbf{u} + (\nabla\mathbf{u})^T], \tag{2.35}$$

which is the symmetric part of the displacement gradient. Its components are given by

$$\epsilon_{ij} = \frac{1}{2}\left(\frac{\partial u_i}{\partial X_j} + \frac{\partial u_j}{\partial X_i}\right). \tag{2.36}$$

2.2 Stress

The motion described above is a result of forces acting on the body Ω. This section focuses on these forces and their distribution. There are two types of forces (de Souza Neto et al., 2011):

1. Body force $\mathbf{b}(\mathbf{x}, t)$ per unit mass acting on the body;
2. Surface traction $\mathbf{t}$ per unit area acting on a surface with outward unit normal $\mathbf{n}$:

$$\mathbf{t} = \mathbf{t}(\mathbf{x}, t, \mathbf{n}) \quad \text{or } \mathbf{t}_{\mathbf{n}}(\mathbf{x}, t). \tag{2.37}$$

Using Newton's second law, Cauchy's theorem asserts that the dependence of the surface traction on the normal is linear. Thus equation (2.37) can be expressed in the form

$$\mathbf{t} = \boldsymbol{\sigma}\mathbf{n}. \tag{2.38}$$

The linear transformation $\boldsymbol{\sigma}$ is referred to as the stress tensor.

2.3 Balance Laws

The deformations of continuous media are governed by balance laws which provide universal rules to which a continuum body, say Ω, should adhere. For isothermal problems, these are the balance of mass, and linear and angular momentum. We express them as local principles.

Conservation of mass

The conservation of mass principle states that the rate of change of mass of an arbitrary material volume is always zero. This balance law takes the form

$$\dot{\rho} + \rho \text{ div } \dot{\boldsymbol{u}} = 0, \tag{2.39}$$

where ρ is the mass density, and div $\dot{\boldsymbol{u}} = \dfrac{\partial \dot{u}_i}{\partial x_i}$ denotes the divergence of the velocity $\dot{\boldsymbol{u}}$.

Balance of linear momentum

To formulate the principle of balance of the linear momentum, we define the resultant force on an arbitrary volume $V_t \subset \Omega_t$ of a continuum with boundary S_t using (2.38) :

$$\mathbf{F} = \int_{S_t} \boldsymbol{\sigma}\mathbf{n} \, dS + \int_{V_t} \rho\mathbf{b} \, dV, \tag{2.40}$$

and the linear momentum of the volume as

$$\mathbf{P} = \int_{V_t} \rho \dot{\boldsymbol{u}} \, dV. \tag{2.41}$$

Balance of linear momentum states that the resultant force acting on an arbitrary part of a continuum body is equal to its rate of change of momentum. Hence

$$\int_{S_t} \boldsymbol{\sigma}\mathbf{n} \, dS + \int_{V_t} \rho\mathbf{b} \, dV = \frac{d}{dt}\bigg(\int_{V_t} \rho \dot{\boldsymbol{u}} \, dV \bigg). \tag{2.42}$$

Applying the divergence theorem to the first term to change it into a volume integral, we have

$$\int_{S_t} \boldsymbol{\sigma}\mathbf{n} \, dS = \int_{V_t} \operatorname{div} \boldsymbol{\sigma} \, dV. \tag{2.43}$$

Evaluating the right hand side of (2.42) we obtain, after taking account of the fact that V_t depends on time,

$$\frac{d}{dt}\bigg(\int_{V_t} \rho \dot{\boldsymbol{u}} \, dV \bigg) = \int_{V_t} \rho \ddot{\boldsymbol{u}} \, dV. \tag{2.44}$$

Thus balance of linear momentum is expressed as

$$\int_{V_t} \Big(\operatorname{div} \boldsymbol{\sigma} + \rho\mathbf{b} - \rho \ddot{\boldsymbol{u}} \Big) \, dV = 0. \tag{2.45}$$

Since it should hold for every volume in the continuum, we must have

$$\operatorname{div} \boldsymbol{\sigma} + \rho\mathbf{b} = \rho\ddot{\mathbf{u}}. \tag{2.46}$$

Equation (2.46) is known as Cauchy's equation of motion.

Balance of angular momentum

Balance of angular momentum states that the moment about a fixed point $\mathbf{x}$ of the resultant forces acting on V_t is equal to the rate of change of the volume about that point. Mathematically,

$$\int_{S_t} \mathbf{x} \times \boldsymbol{\sigma}\mathbf{n} \, dS + \int_{V_t} \mathbf{x} \times \rho\mathbf{b} \, dV = \frac{d}{dt}\bigg(\int_{V_t} \mathbf{x} \times \rho \dot{\boldsymbol{u}} \, dV \bigg). \tag{2.47}$$

Proceeding as for balance of linear momentum, we obtain the symmetry of the Cauchy stress

tensor:

$$\boldsymbol{\sigma} = \boldsymbol{\sigma}^T. \tag{2.48}$$

2.4 Elasticity

All continua conform to the above mentioned laws. What makes their responses to the same type of loading differ, are their material definitions. For a particular load, some bodies will restore the deformation with the removal of the load; however, some will have permanent deformation with the same load even after the load has been removed. The latter behaviour is known as *plasticity*, which will be discussed further in Chapter 3. This section focuses on the former behaviour, known as *elasticity*.

In addition to the characteristics above, a Hookean elastic solid's material deformations are small, the rate of loading does not have an effect, and the relation between the loading and the deformation measure is linear. Hence Hooke's law expressed in terms of the Cauchy stress tensor and the infinitesimal strain tensor states in component form that

$$\sigma_{ij} = C_{ijkl}\epsilon_{kl}, \tag{2.49}$$

where C_{ijkl} is the fourth-order elasticity tensor. We define the quadratic strain energy function $U(\epsilon_{ij})$ by

$$U = \frac{1}{2}C_{ijkl}\epsilon_{ij}\epsilon_{kl}. \tag{2.50}$$

Then $\boldsymbol{\sigma}$ is obtained from

$$\sigma_{ij} = \frac{\partial U}{\partial \epsilon_{ij}} = C_{ijkl}\epsilon_{kl}. \tag{2.51}$$

Most generally, C_{ijkl} has 81 components. However, using the symmetry properties of $\boldsymbol{\sigma}$ and $\boldsymbol{\epsilon}$ we can reduce the number of independent components drastically.

Symmetry of $\boldsymbol{\sigma}$ implies that

$$C_{ijkl} = C_{jikl}, \tag{2.52}$$

thus reducing the coefficients from 81 to 63. Using the symmetry property of the strain tensor,

the coefficients of ϵ_{ij} and ϵ_{ji} can be merged into one term, e.g. $C_{1122}\epsilon_{12} + C_{1121}\epsilon_{21}$ into $(C_{1122} + C_{1121})\epsilon_{21}$, where $C_{1122}+C_{1121}$ is treated as one term. Also, we have $C_{ijkl} = C_{ijlk}$ as a result of the symmetry of the strain tensor. These further reduce the number of independent components by 27, and we are left with 36 coefficients defining the general linearly elastic body.

Since

$$C_{ijkl} = \frac{\partial^2 U}{\partial \epsilon_{ij} \partial \epsilon_{kl}} = \frac{\partial^2 U}{\partial \epsilon_{kl} \partial \epsilon_{ij}}, \tag{2.53}$$

it follows that

$$C_{ijkl} = C_{klij}, \tag{2.54}$$

which in turn reduces the number of material coefficients to 21. The material coefficients are reduced further depending on the symmetry properties of the material.

Isotropic Linear Elasticity

A linearly elastic material is said to be isotropic if its mechanical properties can be described without reference to directions; otherwise, it is anisotropic. Assuming isotropic behaviour, the elasticity tensor C_{ijkl} remains unchanged under all orthogonal transformations. The most general form is (Lai et al., 2009)

$$C_{ijkl} = \lambda A_{ijkl} + \alpha B_{ijkl} + \beta H_{ijkl} \tag{2.55}$$

in which $A_{ijkl},\ B_{ijkl}$ and H_{ijkl} are fourth-order tensors defined by

$$A_{ijkl} = \delta_{ij}\delta_{kl}, \quad B_{ijkl} = \delta_{ik}\delta_{jl}, \quad H_{ijkl} = \delta_{il}\delta_{jk} \tag{2.56}$$

and $\lambda,\ \beta$, and α are constants. Thus

$$\sigma_{ij} = C_{ijkl}\epsilon_{kl} \tag{2.57}$$

$$= \lambda \epsilon_{kk}\delta_{ij} + (\alpha + \beta)\epsilon_{ij}. \tag{2.58}$$

Setting $(\alpha + \beta) = 2\mu$, we obtain

$$\sigma_{ij} = \lambda \epsilon_{kk}\delta_{ij} + 2\mu\epsilon_{ij} \tag{2.59}$$

or in index-free form,

$$\boldsymbol{\sigma} = \lambda \text{ tr } \boldsymbol{\epsilon} + 2\mu\boldsymbol{\epsilon}. \tag{2.60}$$

The constants λ and μ are termed *Lame's constants*, and μ is known as the shear modulus. Expressed in terms of Young's modulus E and Poisson's ratio ν, they are given by

$$\nu = \frac{E}{2(1+\nu)}, \tag{2.61}$$

$$\lambda = \frac{\nu E}{(1+\nu)(1-2\nu)}. \tag{2.62}$$

2.5 Boundary value problem

We now formulate the boundary value problem for equilibrium of an isotropically elastic material: find $\boldsymbol{u}$ that satisfies

$$-\text{div } \boldsymbol{\sigma} = \rho\mathbf{b}, \tag{2.63}$$

$$\boldsymbol{\sigma} = \mathbf{C}\ \boldsymbol{\epsilon}, \tag{2.64}$$

$$\boldsymbol{\epsilon}(\boldsymbol{u}) = \tfrac{1}{2}(\nabla\boldsymbol{u} + (\nabla\boldsymbol{u})^T), \tag{2.65}$$

in Ω together with the boundary conditions

$$\boldsymbol{u} = \overline{\boldsymbol{u}} \quad \text{on } \partial\Omega_D, \tag{2.66}$$

$$\boldsymbol{\sigma}\ \boldsymbol{n} = \bar{\boldsymbol{t}} \quad \text{on } \partial\Omega_N. \tag{2.67}$$

Here $\partial\Omega = \partial\Omega_D \cup \partial\Omega_N$ is the boundary of Ω with $\partial\Omega_D \cap \partial\Omega_N = \emptyset$, $\mathbf{F}$ is the body force and $\overline{\boldsymbol{u}}$ and $\bar{\boldsymbol{t}}$ are respectively a prescribed displacement and traction.

Chapter 3

Plasticity

Under small strain conditions, materials such as metals obey Hooke's law. However, as the strain is increased, many materials then depart from the linear response and accumulate permanent or plastic deformation. The material is then said to have yielded, and the point at which yielding occurs is referred to as the yield point or the proportional limit. Upon release of the load, elastic unloading takes place. Figure 3.1 shows schematically the elastic and plastic phases and elastic unloading for an elasto-plastic material until the point of failure.

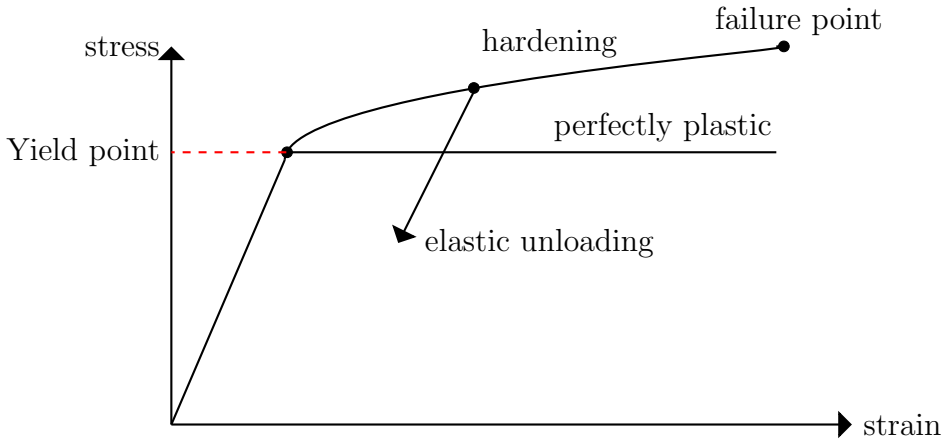

Figure 3.1: A stress-strain graph for an elasto-plastic material

In Section 3.1, the constitutive relations for classical elastoplasticity are presented including the yield criteria, the plastic flow rule and the hardening rule. Then in Section 3.2 we discuss the extension of the classical theory so as to capture size-dependent effects through the constitutive relations for gradient plasticity. Further background to details of both classical and strain-gradient plasticity may be found in (Han and Reddy, 2012).

3.1 Classical Plasticity

Conventional plasticity theory applies to materials that exhibit the following characteristics (see for example (de Souza Neto et al., 2011)):

1. A range of stresses where the material obeys Hooke's law: linear proportionality;
2. Further loading of the material after the yield point results in the evolution of plastic deformation, a process known as plastic yielding;
3. In addition to plastic yielding, hardening, corresponding to a positive slope of the stress-strain curve, may be observed in the plastic phase;
4. Upon removal of the loading, elastic behaviour takes place.

These characteristics are the guidelines to formulating the constitutive equations modelling the behaviour of an elasto-plastic material. In this section the constitutive equations for classical plasticity are presented.

First, the strain tensor $\boldsymbol{\epsilon}$ is decomposed into elastic and plastic constituents $\boldsymbol{\epsilon}^e$ and $\boldsymbol{\epsilon}^p$, respectively:

$$\boldsymbol{\epsilon} = \boldsymbol{\epsilon}^e + \boldsymbol{\epsilon}^p. \tag{3.1}$$

Hence the elastic relation (2.49) becomes

$$\boldsymbol{\sigma} = \mathbf{C}(\boldsymbol{\epsilon} - \boldsymbol{\epsilon}^p). \tag{3.2}$$

A further assumption is that there is no volume change accompanying plastic behaviour; that is,

$$\text{tr } \boldsymbol{\epsilon}^p = \epsilon^p_{ii} = 0. \tag{3.3}$$

The elastic relation may be obtained from a quadratic (elastic) free energy of the form

$$\begin{aligned} \Phi(\boldsymbol{\epsilon}, \boldsymbol{\epsilon}^p) &= \Phi^e(\boldsymbol{\epsilon} - \boldsymbol{\epsilon}^p) \\ &= \tfrac{1}{2}\, \boldsymbol{\epsilon}^e : \mathbf{C}\boldsymbol{\epsilon}^e. \end{aligned} \tag{3.4}$$

Then

$$\begin{aligned}\boldsymbol{\sigma} &= \frac{\partial \Phi}{\partial \boldsymbol{\epsilon}^e} \\ &= \mathbf{C}\, \boldsymbol{\epsilon}^e. \end{aligned} \tag{3.5}$$

From the second law of thermodynamics we have the dissipation inequality

$$\dot{\Phi} \leq \boldsymbol{\sigma} : \dot{\boldsymbol{\epsilon}}. \tag{3.6}$$

Using the free energy in equation (3.4), the dissipation inequality becomes

$$\begin{aligned} 0 &\geq \frac{\partial \Phi^e}{\partial \boldsymbol{\epsilon}^e} : \dot{\boldsymbol{\epsilon}}^e - \boldsymbol{\sigma} : (\dot{\boldsymbol{\epsilon}}^e + \dot{\boldsymbol{\epsilon}}^p) \\ &= \mathbf{C}\boldsymbol{\epsilon}^e : \dot{\boldsymbol{\epsilon}}^e - \boldsymbol{\sigma} : (\dot{\boldsymbol{\epsilon}}^e + \dot{\boldsymbol{\epsilon}}^p) \\ &= (\mathbf{C}\boldsymbol{\epsilon}^e - \boldsymbol{\sigma}) : \dot{\boldsymbol{\epsilon}}^e - \boldsymbol{\sigma} : \dot{\boldsymbol{\epsilon}}^p. \end{aligned}$$

Using (3.5), this reduces to

$$\boldsymbol{\sigma} : \dot{\boldsymbol{\epsilon}}^p \geq 0. \tag{3.7}$$

Equation (3.7) is known as the reduced dissipation inequality and is the basis for constructing a flow relation.

Yield surface

The stresses at a material point in an elastoplastic body are constrained to lie in a set $\mathcal{S}$ of admissible stresses. This set may be defined by a scalar yield function $\Upsilon(\boldsymbol{\sigma})$; that is,

$$\mathcal{S} = \{\boldsymbol{\sigma} \mid \Upsilon(\boldsymbol{\sigma}) \leq 0\}. \tag{3.8}$$

The boundary of the set $\mathcal{S}$ is the set of stresses for which yielding may occur: this is called the yield surface, and it is defined by

$$\Psi = \{\boldsymbol{\sigma} \mid \Upsilon(\boldsymbol{\sigma}) = 0\}. \tag{3.9}$$

The region where $\Upsilon(\boldsymbol{\sigma}) < 0$ is the elastic region, defined by

$$\mathcal{E} = \{\boldsymbol{\sigma} \mid \Upsilon(\boldsymbol{\sigma}) < 0\}. \tag{3.10}$$

Different criteria are used to define the yield function for a plastic material. The most commonly used include the criteria of Tresca, von Mises, Mohr-Coulomb and Drucker-Prager. More about these criteria can be found in de Souza Neto et al.(2011). We will briefly discuss the von Mises and Tresca criteria.

The von Mises yield criterion

We first write the stress as the sum of a spherical component, $\boldsymbol{\sigma}^{\text{sph}}$, and a deviatoric component $\boldsymbol{\sigma}^{\text{dev}}$: that is,

$$\boldsymbol{\sigma} = \boldsymbol{\sigma}^{\text{dev}} + \boldsymbol{\sigma}^{\text{sph}} \tag{3.11}$$

in which

$$\boldsymbol{\sigma}^{\text{sph}} = \tfrac{1}{3}(\text{tr}\boldsymbol{\sigma})\boldsymbol{I} \tag{3.12}$$

and

$$\boldsymbol{\sigma}^{\text{dev}} = \boldsymbol{\sigma} - \boldsymbol{\sigma}^{\text{sph}}. \tag{3.13}$$

In index form, the deviatoric stress is given by

$$\sigma_{ij}^{\text{dev}} = \sigma_{ij} - \tfrac{1}{3}\sigma_{kk}\delta_{ij}. \tag{3.14}$$

The second invariant J_2 of the deviatoric stress is defined by

$$J_2 = \tfrac{1}{2}\sigma_{ij}^{\text{dev}}\sigma_{ij}^{\text{dev}} = \tfrac{1}{2}|\boldsymbol{\sigma}^{\text{dev}}|^2. \tag{3.15}$$

The von Mises criterion states that only the deviatoric stress influences plastic yielding and that plastic flow starts when J_2 reaches a critical value. The yield function for this criterion is

$$\Upsilon(\boldsymbol{\sigma}) = \sqrt{3J_2(\boldsymbol{\sigma})} - \sigma_y. \tag{3.16}$$

It is also worth noting that the von Mises yield function is an isotropic function of the stress tensor. The spherical stress does not affect plastic yielding in the von Mises yield criterion as it is pressure-insensitive. Both properties are also shared by the Tresca yield function, to be discussed next.

The Tresca yield criterion

To discuss the Tresca yield criterion we first write the stress tensor in spectral form as

$$\boldsymbol{\sigma} = \sum_{i=1}^{3} \sigma_i \, \boldsymbol{p}_i \otimes \boldsymbol{p}_i \tag{3.17}$$

where σ_i are the principal stresses and $\boldsymbol{p}_i$ $(i = 1, 2, 3)$ are the mutually orthogonal principal directions. We order the principal stresses according to $\sigma_1 \geq \sigma_2 \geq \sigma_3$. The maximum shear stress is then given by

$$\tau_{\max} = \tfrac{1}{2}|\sigma_1 - \sigma_3|. \tag{3.18}$$

In 1868, Tresca proposed that when the maximum shear stress reaches a critical value, plastic yielding commences; that is,

$$\tfrac{1}{2}|\sigma_1 - \sigma_3| = \tau_y, \tag{3.19}$$

where τ_y is the yield stress in shear. The Tresca yield function is then defined by

$$\Upsilon(\boldsymbol{\sigma}) = \tfrac{1}{2}|\sigma_{\max} - \sigma_{\min}| - \tau_y. \tag{3.20}$$

The Tresca yield function may be written alternatively as

$$\Upsilon(\boldsymbol{\sigma}) = |\sigma_{\max} - \sigma_{\min}| - \sigma_y. \tag{3.21}$$

Similar to the von Mises yield criterion, the Tresca yield criterion is both isotropic and pressure-insensitive.

Figure 3.2 below is a graphical representation of the Tresca and von Mises yield surfaces in principal stress space, von Mises surface being the cylinder with axes equally inclined to the principal axes and the Tresca yield surface being the inscribed hexagonal cylinder.

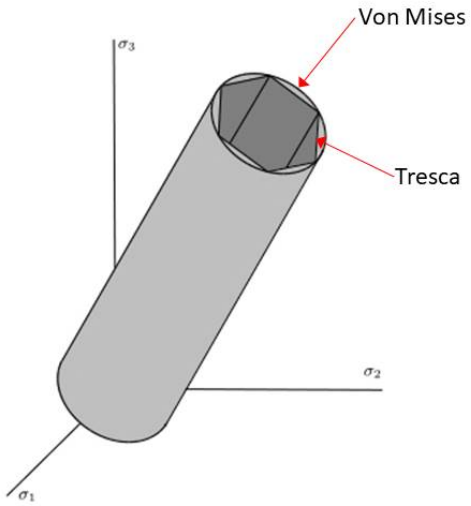

Figure 3.2: Tresca and von Mises yield surfaces in principal stress space

The plastic flow rule: normality law

The starting point for the plastic flow rule, which governs the evolution of $\boldsymbol{\epsilon}^p$, is the principle of maximum plastic dissipation.

Plastic dissipation

The quantity $\dot{\boldsymbol{\epsilon}}^p : \boldsymbol{\sigma}$ in (3.7) is a measure of dissipation as deformation progresses. It is known as plastic dissipation. The principle of maximum plastic dissipation states that the actual stress $\boldsymbol{\sigma} \in \mathcal{S}$ and plastic strain rate $\dot{\boldsymbol{\epsilon}}^p$ are such as to maximize the dissipation over all admissible stresses $\boldsymbol{\tau} \in \mathcal{S}$; that is,

$$\begin{aligned} \dot{\boldsymbol{\epsilon}}^p : \boldsymbol{\sigma} \geq \dot{\boldsymbol{\epsilon}}^p : \boldsymbol{\tau} \quad \text{for all } \boldsymbol{\tau} \in \mathcal{S} \\ \Longrightarrow (\boldsymbol{\sigma} - \boldsymbol{\tau}) : \dot{\boldsymbol{\epsilon}}^p \geq 0. \end{aligned} \tag{3.22}$$

The inequality (3.22) has two consequences:

1. The yield surface is convex; that is, if $\boldsymbol{\sigma}, \boldsymbol{\tau} \in \mathcal{S}$ then $\theta\boldsymbol{\sigma} + (1-\theta)\boldsymbol{\tau} \in \mathcal{S}$ for $0 < \theta < 1$;

2. The plastic strain rate $\dot{\boldsymbol{\epsilon}}^p$ is normal to the yield surface.

Figure 3.3 illustrates the convexity of $\mathcal{S}$ and the normality law.

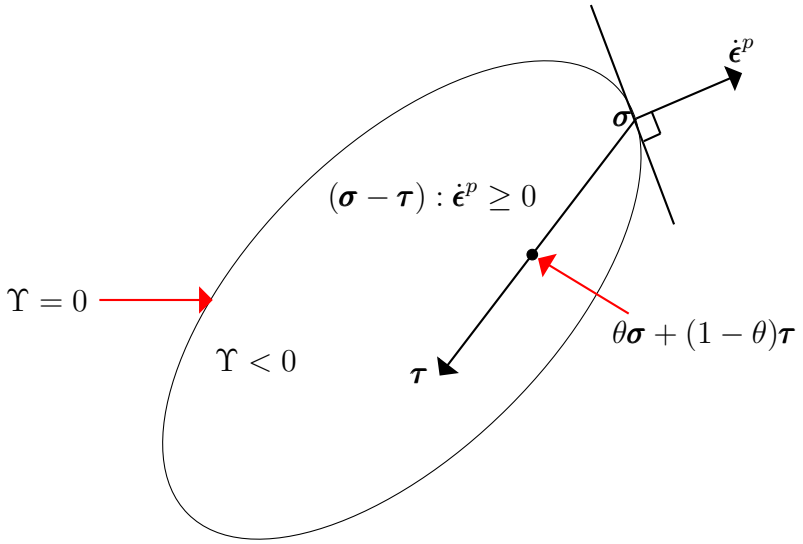

Figure 3.3: A schematic depiction of a convex yield surface and the normality law.

The von Mises and Tresca yield surfaces, shown in Figure 3.2, are examples of convex yield surfaces.

For a smooth yield surface such as von Mises, the normality relation can be written as

$$\dot{\boldsymbol{\epsilon}}^p = \lambda \frac{d\Upsilon}{d\boldsymbol{\sigma}} \tag{3.23}$$

where λ is a non-negative scalar, together with the complementarity conditions

$$\lambda \geq 0, \quad \Upsilon \leq 0 \text{ and } \lambda\Upsilon = 0. \tag{3.24}$$

Thus in the elastic phase we have

$$\Upsilon < 0 \quad \Rightarrow \lambda = 0, \tag{3.25}$$

whilst at the onset of the plastic phase we have

$$\lambda > 0 \Rightarrow \Upsilon = 0. \tag{3.26}$$

For example, for the von Mises yield function (3.16) we have

$$\Upsilon(\boldsymbol{\sigma}) = \sqrt{3/2}|\boldsymbol{\sigma}^{\text{dev}}| - \sigma_y \leq 0, \tag{3.27}$$

so that the plastic flow rule is given by

$$\begin{aligned}\dot{\boldsymbol{\epsilon}}^p &= \lambda \frac{\partial \Upsilon(\boldsymbol{\sigma})}{\partial \boldsymbol{\sigma}} \\ &= \sqrt{3/2}\lambda \frac{\boldsymbol{\sigma}^{\text{dev}}}{|\boldsymbol{\sigma}^{\text{dev}}|}.\end{aligned} \tag{3.28}$$

The flow relation may be inverted to give the stresses in terms of the plastic strain rate. To do this, we define a convex dissipation function $\mathcal{D}(\dot{\boldsymbol{\epsilon}}^p)$ with the properties

$$\mathcal{D}(\dot{\boldsymbol{\epsilon}}^p) \geq 0, \quad \mathcal{D}(\mathbf{0}) = 0, \quad \mathcal{D}(\alpha\dot{\boldsymbol{\epsilon}}^p) = |\alpha|\mathcal{D}(\dot{\boldsymbol{\epsilon}}^p), \quad \alpha \in \mathbb{R}. \tag{3.29}$$

The last property indicates that $\mathcal{D}$ is positively homogeneous. Then the flow relation can be written as

$$\boldsymbol{\sigma} = \frac{\partial \mathcal{D}}{\partial \dot{\boldsymbol{\epsilon}}^p} \quad \text{for } \dot{\boldsymbol{\epsilon}}^p \neq \mathbf{0}. \tag{3.30}$$

For example, we have for the von Mises criterion

$$\mathcal{D} = \sigma_y |\dot{\boldsymbol{\epsilon}}^p|. \tag{3.31}$$

Using (3.28) we have

$$\boldsymbol{\sigma}^{\text{dev}} = \frac{\dot{\boldsymbol{\epsilon}}^p}{\sqrt{3/2}\lambda} |\boldsymbol{\sigma}^{\text{dev}}| \tag{3.32}$$

and

$$|\dot{\boldsymbol{\epsilon}}^p| = \lambda. \tag{3.33}$$

As a consequence, and noting that $|\boldsymbol{\sigma}^{\text{dev}}| = \sigma_y$ at yield, we obtain

$$\boldsymbol{\sigma}^{\text{dev}} = 2\sigma_y \frac{\dot{\boldsymbol{\epsilon}}^p}{\sqrt{3/2}|\dot{\boldsymbol{\epsilon}}^p|} = \frac{\partial \mathcal{D}}{\partial \dot{\boldsymbol{\epsilon}}^p}. \tag{3.34}$$

Hardening

Beyond the yield point, the stress levels may depend on the evolution of plastic strain. This is known as hardening. If hardening is absent, then the material model is said to be perfectly

plastic. If hardening is observed with continued loading, it can be classified as either isotropic or kinematic.

Isotropic hardening

A material model exhibits isotropic hardening if the initial yield surface expands uniformly. This is shown in Figure 3.4.

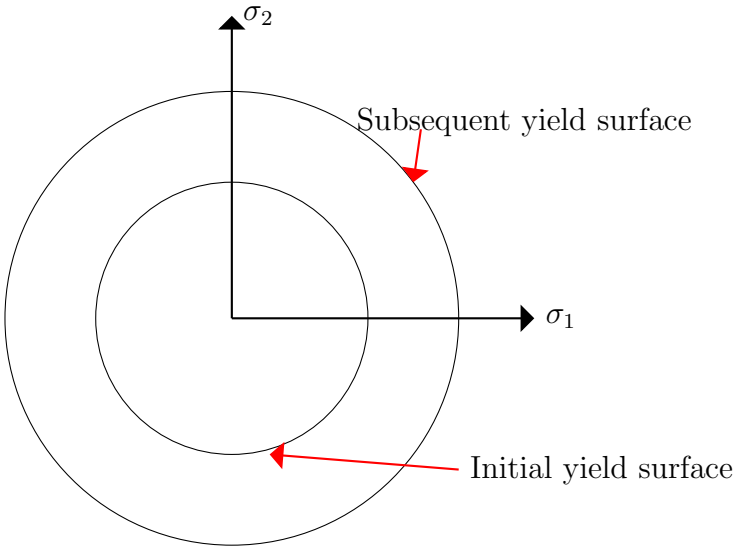

Figure 3.4: Isotropic hardening: the yield surface expands uniformly

There are two methods of implementing this type of hardening: work hardening and strain hardening. We restrict our attention to strain hardening. That is, the hardening state depends on a particular scalar measure called the accumulated plastic strain η, defined in (de Souza Neto et al., 2011) by

$$\begin{aligned}\eta(t) &\equiv \int_0^t \sqrt{\frac{2}{3}\,\dot{\boldsymbol{\epsilon}}^p(s) : \dot{\boldsymbol{\epsilon}}^p(s)}\; ds \\ &= \sqrt{\frac{2}{3}} \int_0^t |\dot{\boldsymbol{\epsilon}}^p(s)|\; ds. \end{aligned} \tag{3.35}$$

The above definition (3.35), is justified since for uniaxial stress we have

$$|\dot{\boldsymbol{\epsilon}}^p|^2 = \dot{\epsilon}^p_{ij}\dot{\epsilon}^p_{ij} \tag{3.36}$$

$$= (\dot{\epsilon}^p_{11})^2(1 + \tfrac{1}{4} + \tfrac{1}{4}) \tag{3.37}$$

$$= \tfrac{3}{2}(\dot{\epsilon}^p_{11})^2 \tag{3.38}$$

since

$$\dot{\epsilon}^p_{ii} = 0 \quad \Leftrightarrow \quad \dot{\epsilon}^p_{22} = \dot{\epsilon}^p_{33} = -\tfrac{1}{2}\dot{\epsilon}^p_{11}. \tag{3.39}$$

Thus (3.35) reduces to

$$\eta = \int_0^t |\dot{\epsilon}^p_{11}(s)|\, ds \tag{3.40}$$

for uniaxial stress. For linear hardening we define the current yield stress σ_y by

$$\sigma_y(\eta) = \sigma_0 + H\eta \tag{3.41}$$

in which σ_0 is the initial yield stress and H is the hardening modulus. For example, the von Mises yield function then becomes

$$\Upsilon(\boldsymbol{\sigma}) = \sqrt{\tfrac{1}{2}J_2(\boldsymbol{\sigma})} - (\sigma_0 + H\eta). \tag{3.42}$$

Other forms of non-linear strain-hardening functions may also be defined.

Kinematic hardening

If the yield surface translates and maintains its original shape during hardening, then the material is said to demonstrate kinematic hardening. This type of hardening is usually observed in uniaxial loading analyses whose resistance to plastic yielding decreases in the opposite direction after being hardened. This is known as the *Bauschinger effect*. Figure 3.5 shows the kinematic hardening phenomenon and the Bauschinger effect.

The hardening parameter in this type of hardening is the backstress $\boldsymbol{\varrho}$ which determines the degree of translation. For example, the von Mises yield function (3.16) then becomes

$$\Upsilon(\boldsymbol{\sigma}) = \sqrt{\tfrac{1}{2}J_2(\boldsymbol{\sigma}^{\mathrm{dev}} - \boldsymbol{\varrho})} - \sigma_y. \tag{3.43}$$

The simplest model of this form of hardening is the linear (Prager) kinematic hardening rule, in which the yield surface translates in the direction of the total plastic strain, so that

$$\boldsymbol{\varrho} = c\, \boldsymbol{\epsilon}^p \tag{3.44}$$

where c is a material parameter.

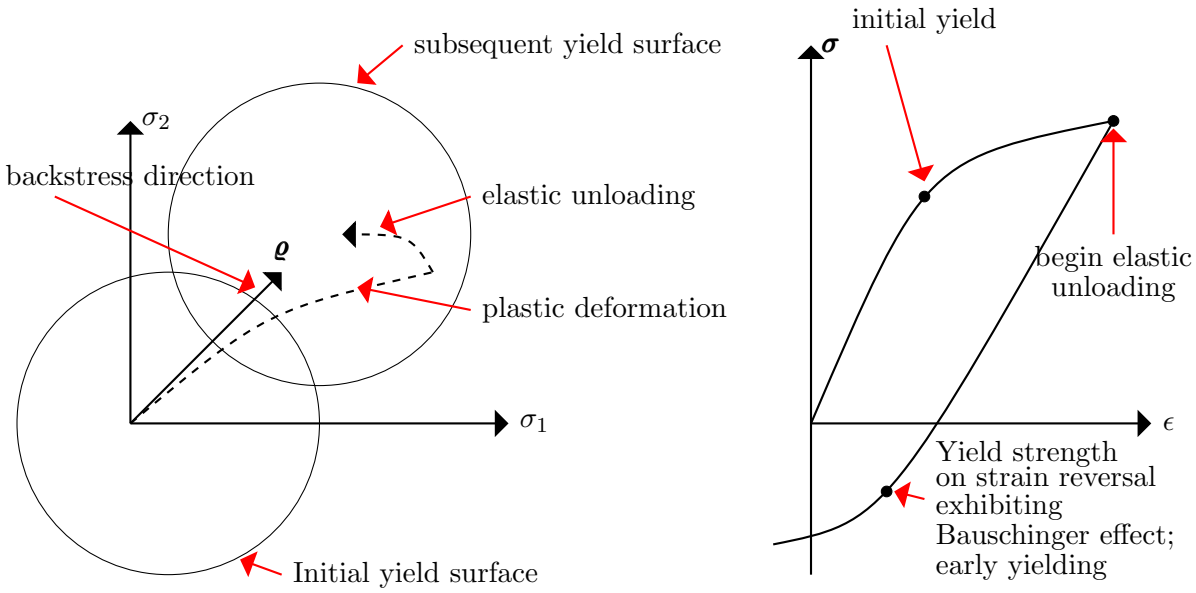

Figure 3.5: Kinematic hardening and the Bauschinger effect in a uniaxial cyclic test

3.2 Gradient plasticity

The classical plasticity theory assumes that there are no size effects in the behaviour of a continuum. However, experiments on specimens at the microscale ($\approx 10 - 100\mu m$) show size-dependent behaviour ascribed to geometrically necessary dislocations (GND). An example of size-dependent behaviour is given in the work by Ehrler et al. (2008) who report an experiment involving Nickel (Ni) foil under pure bending. Figure 3.6 below reproduces the results from the publication: foils with the same thickness but different grain size and results for foils with different thickness but same grain size.

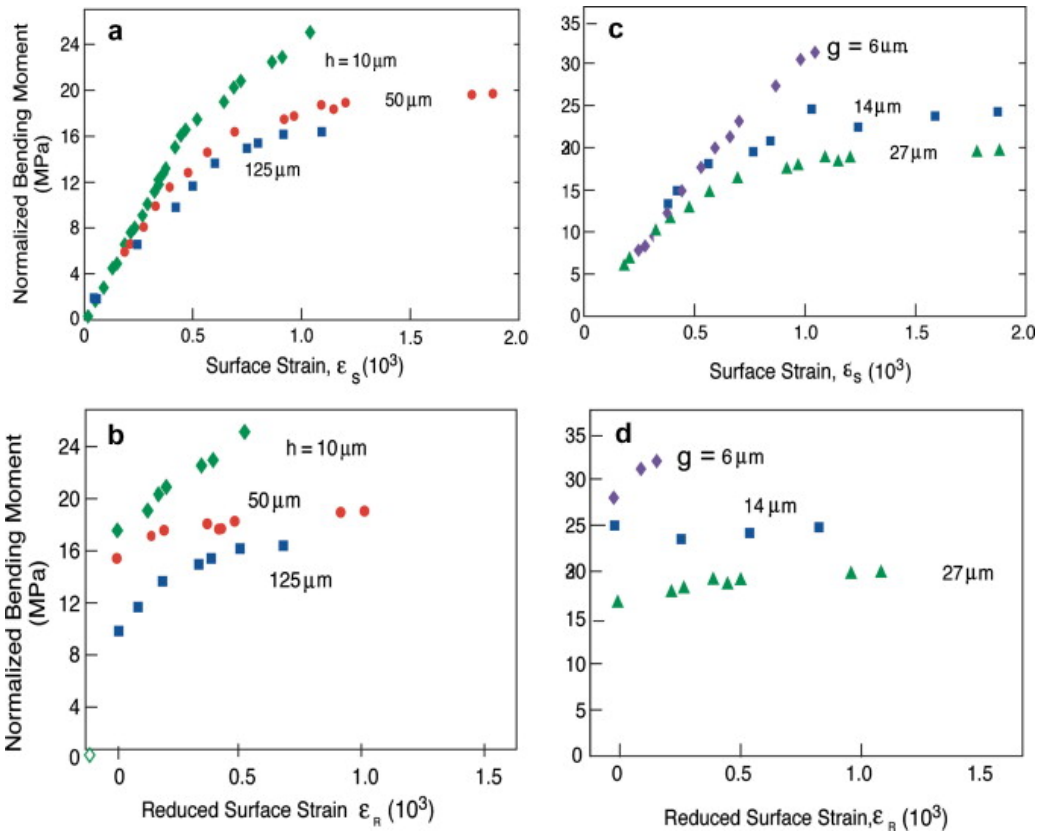

Figure 3.6: Normalized moment as a function of surface strain for Ni foils: (a and b) for grain size = 27μm and 3 different thicknesses; (c and d) for foil thickness= 50 μm and three different grain sizes. (Ehrler et al., 2008)

The strengthening with increase in length scale is clear. Therefore to model such behaviour it is necessary to include length scales and strain-gradient dependencies in the classical plasticity theory.

A considerable amount of work has been dedicated to developing strain-gradient plasticity (SGP) models. The first such model was proposed by Aifantis (1984) which in turn motivated the development of further SGP theories by Fleck and Hutchinson (1994), Gurtin (2004) and Gurtin and Anand (2005), to name a few. One of the strategies employed to account for geometrically necessary dislocations(GND) is to predicate that the stress depends upon the strain and its gradient. This strategy can be employed in numerous ways such as including size effects in the free energy (energetic contribution), or by extending the flow law (dissipative contribution), or by employing both methods. This work adopts the model by Gurtin and Anand (2005) which employs the latter for a rate-dependent material. However, we use the rate-independent model with an associative flow law developed by Reddy et al. (2008) and Reddy (2011) (see also (Han and Reddy, 2012)). A related model is that discussed in Fleck and Willis (2009a).

The starting point of the Gurtin-Anand model is the principle of virtual power. We define a

microstress $\boldsymbol{\rho}$ power conjugate to the plastic strain rate $\dot{\boldsymbol{\epsilon}}^p$ and a third-order microstress $\mathbb{K}$ power conjugate to the gradient of plastic strain rate $\nabla\dot{\boldsymbol{\epsilon}}^p$. We define a defect stress to $\boldsymbol{\zeta}$ conjugate to a dislocation density tensor $\boldsymbol{\alpha} = \text{curl } \boldsymbol{\epsilon}^p$ (Gurtin, 2002) where

$$\text{curl } \boldsymbol{\epsilon}^p = \varepsilon_{ikl}\ \epsilon^p_{jl,k}\ \mathbf{e}_i \otimes \mathbf{e}_j. \tag{3.45}$$

Then the total internal power P_{int} within an arbitrary part R of Ω is given by

$$P_{\text{int}} = \int_R (\boldsymbol{\sigma} : \dot{\boldsymbol{\epsilon}^e} + \boldsymbol{\rho} : \dot{\boldsymbol{\epsilon}}^p + \boldsymbol{\zeta} : \dot{\boldsymbol{\alpha}} + \mathbb{K} \vdots \nabla\dot{\boldsymbol{\epsilon}}^p)\ dx. \tag{3.46}$$

The external power expenditure of forces on R is expressed in terms of the body force $\boldsymbol{b}$ acting on R, the surface traction $\boldsymbol{t}$ on the boundary ∂R, and the microtraction $\boldsymbol{k}$ acting on a plastic strain rate:

$$P_{ext} = \int_R \boldsymbol{b} : \dot{\boldsymbol{u}}\ dx + \int_{\partial R} \boldsymbol{t} \cdot \dot{\boldsymbol{u}}\ ds + \int_{\partial R} \boldsymbol{k} : \dot{\boldsymbol{\epsilon}}^p\ ds, \tag{3.47}$$

where the velocity $\dot{\boldsymbol{u}}$, plastic strain rate, $\dot{\boldsymbol{\epsilon}}^p$ and elastic strain rate $\dot{\boldsymbol{\epsilon}^e}$ must satisfy

$$\boldsymbol{\epsilon}(\dot{\boldsymbol{u}}) = \dot{\boldsymbol{\epsilon}}^e + \dot{\boldsymbol{\epsilon}}^p. \tag{3.48}$$

The principle of virtual power states that the external and internal power expenditure are equal:

$$P_{\text{int}} = \int_R (\boldsymbol{\sigma} : \dot{\boldsymbol{\epsilon}^e} + \boldsymbol{\rho} : \dot{\boldsymbol{\epsilon}}^p + \boldsymbol{\zeta} : \dot{\boldsymbol{\alpha}} + \mathbb{K} : \nabla\dot{\boldsymbol{\epsilon}}^p)\ dx \tag{3.49}$$

$$= \int_R \boldsymbol{b} : \dot{\boldsymbol{u}}\ dx + \int_{\partial R} \boldsymbol{t} \cdot \dot{\boldsymbol{u}}\ ds + \int_{\partial R} \boldsymbol{k} : \dot{\boldsymbol{\epsilon}}^p\ ds. \tag{3.50}$$

Setting $\dot{\boldsymbol{\epsilon}}^p = \mathbf{0}$ in equation (3.49), and using an approach similar to that used in obtaining the equation of motion (2.46), we obtain the equation of equilibrium

$$\text{div } \boldsymbol{\sigma} + \mathbf{b} = \mathbf{0} \tag{3.51}$$

with the boundary microtraction condition

$$\boldsymbol{t} = \boldsymbol{\sigma n}. \tag{3.52}$$

We next set $\dot{\boldsymbol{u}} = \mathbf{0}$ in (3.49), then use the condition in (3.48) and finally integrate by parts, to

obtain the microscopic force balance equation

$$\boldsymbol{\sigma}^{dev} - \boldsymbol{\rho} + \text{div } \mathbb{K} - \text{sym}[\text{dev}(\text{curl } \boldsymbol{\zeta})] = \mathbf{0} \tag{3.53}$$

with the boundary condition

$$\boldsymbol{k}(\boldsymbol{n}) = \mathbb{K}\boldsymbol{n}. \tag{3.54}$$

Free energy potential

The free energy comprises an elastic term Φ^e, a defect term Φ^d and an isotropic hardening term Φ^h:

$$\Phi(\boldsymbol{\epsilon}, \boldsymbol{\epsilon}^p, \boldsymbol{\alpha}) = \Phi^e(\boldsymbol{\epsilon} - \boldsymbol{\epsilon}^p) + \Phi^d(\boldsymbol{\alpha}) + \Phi^h(\eta). \tag{3.55}$$

Here $\Phi^d(\boldsymbol{\alpha})$ is the defect energy, a function of the plastic strain and η is a hardening parameter to be specified.

The local dissipation inequality states that

$$\dot{\Phi} - \boldsymbol{\sigma} : \dot{\boldsymbol{\epsilon}}^e - \boldsymbol{\rho} : \dot{\boldsymbol{\epsilon}}^p - \mathbb{K} : \nabla\dot{\boldsymbol{\epsilon}}^p - \boldsymbol{\zeta} : \dot{\boldsymbol{\alpha}} \leq 0. \tag{3.56}$$

From (3.55) we have

$$\dot{\Phi} = \frac{\partial \Phi^e}{\partial \boldsymbol{\epsilon}^e} : \dot{\boldsymbol{\epsilon}}^e + \frac{\partial \Phi^d}{\partial \boldsymbol{\alpha}} : \dot{\boldsymbol{\alpha}} + \frac{\partial \Phi^h}{\partial \eta}\dot{\eta}. \tag{3.57}$$

Substituting equation (3.57) into (3.56), we obtain

$$\frac{\partial \Phi^e}{\partial \boldsymbol{\epsilon}^e} : \boldsymbol{\epsilon}^e + \frac{\partial \Phi^d}{\partial \boldsymbol{\alpha}} : \dot{\boldsymbol{\alpha}} + \frac{\partial \Phi^h}{\partial \eta}\dot{\eta} - \boldsymbol{\sigma} : \dot{\boldsymbol{\epsilon}}^e - \boldsymbol{\rho} : \dot{\boldsymbol{\epsilon}}^p - \mathbb{K} : \nabla\dot{\boldsymbol{\epsilon}}^p - \boldsymbol{\zeta} : \dot{\boldsymbol{\alpha}} \leq 0, \tag{3.58}$$

or

$$\left(\frac{\partial \Phi^e}{\partial \boldsymbol{\epsilon}^e} - \boldsymbol{\sigma}\right) : \dot{\boldsymbol{\epsilon}}^e + \boldsymbol{\rho} : \dot{\boldsymbol{\epsilon}}^p + \left(\frac{\partial \Phi^d}{\partial \boldsymbol{\alpha}} - \boldsymbol{\zeta}\right) : \dot{\boldsymbol{\alpha}} + \left(\frac{\partial \Phi^h}{\partial \eta}\right)\dot{\eta} - \mathbb{K} : \nabla\dot{\boldsymbol{\epsilon}}^p \leq 0. \tag{3.59}$$

We assume

$$\Phi^d = \mu l \; \boldsymbol{\alpha} \cdot \boldsymbol{\alpha}, \tag{3.60}$$

where l is an energetic material length scale. We define

$$\boldsymbol{\zeta} = \frac{\partial \Phi^d}{\partial \boldsymbol{\alpha}} \tag{3.61}$$

whilst the thermodynamical force g conjugate to η is defined by

$$g = -\frac{\partial \Phi^h}{\partial \eta}. \tag{3.62}$$

Then the reduced dissipation inequality takes the form

$$\boldsymbol{\rho} : \dot{\boldsymbol{\epsilon}}^p + \mathbb{K} : \nabla \dot{\boldsymbol{\epsilon}}^p + g\ \dot{\eta} \geq 0 \tag{3.63}$$

This inequality as seen in the classical plasticity theory (3.7) will be of utmost importance in formulating the plastic flow law (see for example the role of (3.7) in the classical theory).

Yield function and plastic flow rule

To discuss the plastic flow rule for strain-gradient plasticity, we first define the generalised stress S and strain $\mathsf{\Gamma}$ by

$$\mathsf{S} = (\boldsymbol{\rho}, L^{-1}\ \mathbb{K}) \tag{3.64}$$

$$\mathsf{\Gamma} = (\boldsymbol{\epsilon}^p, L\ \nabla \boldsymbol{\epsilon}^p) \tag{3.65}$$

with magnitudes

$$|\mathsf{S}| = \sqrt{|\boldsymbol{\rho}|^2 + \frac{1}{L^2}|\mathbb{K}|^2}, \tag{3.66}$$

$$|\mathsf{\Gamma}| = \sqrt{\tfrac{2}{3}|\boldsymbol{\epsilon}^p|^2 + \tfrac{2}{3}L^2|\nabla \boldsymbol{\epsilon}^p|^2}. \tag{3.67}$$

The parameter L is the dissipative material length scale. Thus the reduced dissipation inequality (3.63) can be expressed as

$$\mathsf{S} \diamond \dot{\mathsf{\Gamma}} + g\ \dot{\eta} \geq 0, \tag{3.68}$$

where

$$\mathsf{S} \diamond \dot{\mathsf{\Gamma}} = \boldsymbol{\rho} : \dot{\boldsymbol{\epsilon}}^p + \mathbb{K} : \nabla \dot{\boldsymbol{\epsilon}}^p. \tag{3.69}$$

Following the classical theory, define the yield function Υ as a convex function of the dissipative generalised stress S. We define a set of admissible stresses $\mathcal{E}$ by

$$f = \Upsilon(\mathsf{S}) + (g - \sigma_0) \leq 0 \tag{3.70}$$

in which σ_0 is the initial yield stress.

The generalised strain rate (flow relation) is assumed to be associative, so that

$$\dot{\Gamma} = \lambda \frac{\partial f}{\partial \mathsf{S}}, \tag{3.71}$$

$$\dot{\eta} = \lambda \frac{\partial f}{\partial g} = \lambda \tag{3.72}$$

with

$$\lambda \geq 0, \quad f \leq 0, \quad \lambda f = 0, \tag{3.73}$$

where λ is a scalar multiplier. As an example, we generalise the von Mises yield function and set

$$\Upsilon(\mathsf{S}) = \sigma_y |\mathsf{S}|, \tag{3.74}$$

when σ_y is the current yield stress, then the flow relation (3.71) becomes

$$\dot{\Gamma} = \lambda \sigma_y \frac{\mathsf{S}}{|\mathsf{S}|}, \tag{3.75}$$

or

$$\begin{cases} \dot{\boldsymbol{\epsilon}}^p & = \lambda \sigma_y \dfrac{\boldsymbol{\rho}}{|\mathsf{S}|}, \\ \nabla \dot{\boldsymbol{\epsilon}}^p & = \lambda \sigma_y L^{-2} \dfrac{\mathbb{K}}{|\mathsf{S}|} \end{cases}. \tag{3.76}$$

The scalar multiplier λ is given by

$$\lambda = |\dot{\Gamma}| = \dot{\eta}. \tag{3.77}$$

Plastic dissipation

The microstresses can be expressed in terms of $\dot{\boldsymbol{\epsilon}}^p$ and $\nabla\dot{\boldsymbol{\epsilon}}^p$ by inverting (3.76):

$$\boldsymbol{\rho} = \frac{\dot{\boldsymbol{\epsilon}}^p|\mathsf{S}|}{\lambda} = (\sigma_0 - g)\frac{\dot{\boldsymbol{\epsilon}}^p}{|\dot{\Gamma}|}, \tag{3.78}$$

$$\mathbb{K} = L^2\frac{\nabla\dot{\boldsymbol{\epsilon}}^p\ |\mathsf{S}|}{\lambda} = (\sigma_0 - g)L^2\frac{\nabla\dot{\boldsymbol{\epsilon}}^p}{|\dot{\Gamma}|}. \tag{3.79}$$

It is worth noting that (3.78) and (3.79) only hold for plastic flow. By analogy with the classical theory of plasticity, we next use the flow relation in (3.75) and the principle of maximum dissipation, to define the positively homogeneous effective dissipation function

$$\mathcal{D}_{\text{eff}}(\dot{\Gamma}) = (\sigma_0 - g)|\dot{\Gamma}|. \tag{3.80}$$

Hence, from (3.78) and (3.79)

$$\mathsf{S} = \frac{\partial\mathcal{D}_{\text{eff}}}{\partial\dot{\Gamma}} \tag{3.81}$$

$$= (\sigma_0 - g)\frac{\dot{\Gamma}}{|\dot{\Gamma}|}, \quad \dot{\Gamma} \neq 0. \tag{3.82}$$

Using the form presented in (3.80) one can approximate the dissipation function by a smooth function

$$\mathcal{D}_\delta = (\sigma_0 - g)\sqrt{|\dot{\Gamma}|^2 + \delta^2} - \delta, \tag{3.83}$$

which is rate-dependent. The approximate dissipation function (3.83) is smooth everywhere as shown in Figure 3.7.

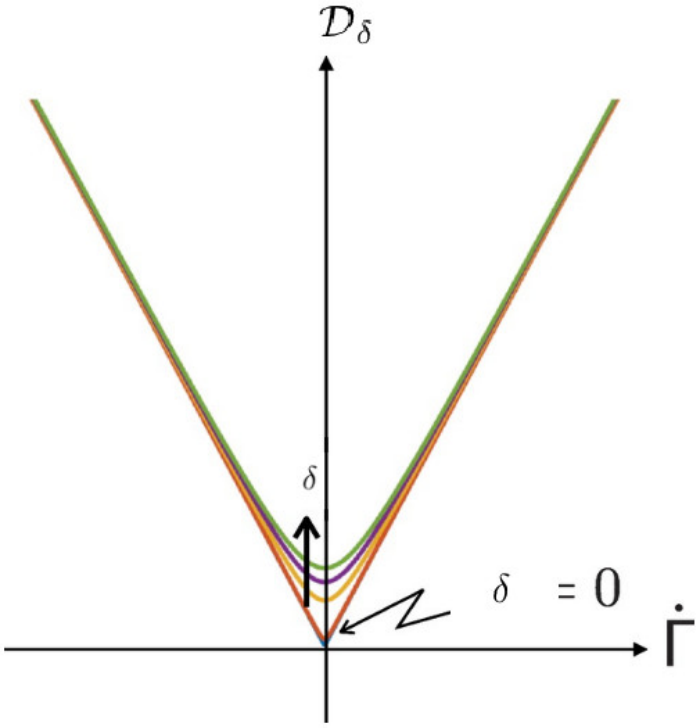

Figure 3.7: The approximate dissipation function

The microstresses for (3.83) are then given by

$$\boldsymbol{\rho} = \frac{\partial \mathcal{D}_\delta}{\partial \dot{\boldsymbol{\epsilon}}^p} = \frac{2(\sigma_0 - g)\dot{\boldsymbol{\epsilon}}^p}{\mathcal{D}_\delta}, \tag{3.84}$$

$$\mathbb{K} = \frac{\partial \mathcal{D}_\delta}{\partial \nabla \dot{\boldsymbol{\epsilon}}^p} = \frac{2(\sigma_0 - g)\nabla \dot{\boldsymbol{\epsilon}}^p}{\mathcal{D}_\delta}, \tag{3.85}$$

so that $\boldsymbol{\rho}$ and $\mathbb{K}$ are defined for all $\dot{\boldsymbol{\epsilon}}^p$.

Choice of hardening variable and dissipation function

Following Panteghini and Bardella (2016), we set

$$\eta = E^p \tag{3.86}$$

where $\dot{E}^p = |\dot{\Gamma}|$ and $-g = h(E^p)^{nh}$ in which h is the hardening modulus and nh is a non-negative parameter. Thus from (3.62) we have

$$h(E^p)^{nh} = \frac{\partial \Phi^h}{\partial \eta}. \tag{3.87}$$

It follows that

$$\Phi^h = \frac{h}{nh+1}(E^p)^{nh+1}. \tag{3.88}$$

Furthermore, we approximate the dissipation function of the same structure as (3.80) by

$$\mathcal{D}_\varepsilon(E^p, \dot{\Gamma}) = \begin{cases} [\sigma_0 - h(E^p)^{nh}]\frac{|\dot{\Gamma}|}{2\dot{\varepsilon_0}} & \text{if } |\dot{\Gamma}| \leq \dot{\varepsilon_0} \\ [\sigma_0 - h(E^p)^{nh}][1 - \frac{\dot{\varepsilon_0}}{2|\dot{\Gamma}|}] & \text{if } |\dot{\Gamma}| > \dot{\varepsilon_0} \end{cases} \tag{3.89}$$

where $\dot{\varepsilon}_0$ is the refence strain rate. This choice is robust, convex and suitably smooth, see Figure 3.8.

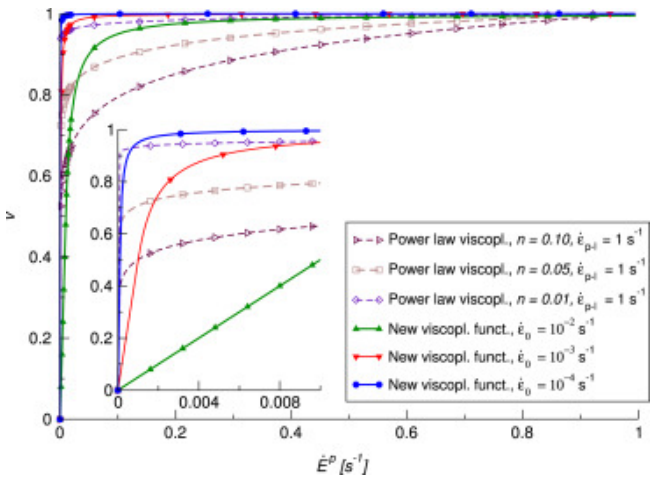

Figure 3.8: Comparison between a power law viscoplastic dissipation function and the proposed viscoplastic function (3.89) (Panteghini and Bardella, 2016).

3.3 Governing equations for gradient plasticity

We recall the equilibrium equations in Section 2.5 and the microforce balance equation

$$\boldsymbol{\sigma}^{\text{dev}} - \boldsymbol{\rho} + \text{div } \mathbb{K} - \text{sym}[\text{dev}(\text{curl } \boldsymbol{\zeta})] = 0, \tag{3.90}$$

with the flow relation

$$\mathsf{S} = (\sigma_0 - h(E^p)^{nh})\frac{\partial \mathcal{D}_\varepsilon}{\partial \dot{\Gamma}} \tag{3.91}$$

as the governing equations in the domain Ω. We partition the boundary into two parts: microfree $\partial\Omega_F$ and microhard $\partial\Omega_H$, such that $\partial\Omega = \partial\Omega_F \cup \partial\Omega_H$, and $\partial\Omega_F \cap \partial\Omega_H = \emptyset$. We

set

$$\mathbb{K}\boldsymbol{n} + \mathrm{sym}[\mathrm{dev}(\boldsymbol{\zeta} \times \boldsymbol{n})] = \mathbf{0} \quad \text{on } \partial\Omega_F, \tag{3.92}$$

$$\dot{\boldsymbol{\epsilon}}^p = \mathbf{0} \quad \text{on } \partial\Omega_H. \tag{3.93}$$

Then (3.90) - (3.93) comprise the governing equations and boundary conditions for plastic flow, for the strain-gradient theory.

Chapter 4

Weak formulations and finite element approximations

We will use the finite element method to solve the problem comprising equations (2.63) - (2.66) and (3.91) - (3.93). Background and details of the finite element method can be found in (Owen and Hinton, 1980), (Fish and Belytschko, 2007) and (Reddy, 1993). The first step towards the finite element method is to derive the weak formulation of the problem at hand.

Thus we use a simple BVP, Poisson's equation, in Section 4.1 to illustrate the derivation of a weak formulation from the strong form. We then proceed to discuss the approximation of the solution using Galerkin's method in Section 4.2, whilst in Section 4.3 we discuss the finite element method in approximating the solution. In Section 4.4 we illustrate the implementation of the finite element method in a two-dimensional setting. We formulate the weak form of the elastic and elastoplastic problems in Section 4.5. We then formulate the finite element approximation for the derived weak form in Section 4.6. Finally, in Section 4.7 we consider the discrete form of the global flow relation.

4.1 Poisson's equation

Consider the BVP

$$-\nabla^2 u = f \quad \text{in } \Omega, \tag{4.1}$$

$$u = 0 \quad \text{on } \partial\Omega, \tag{4.2}$$

on a domain Ω with boundary $\partial\Omega$. Here $f \in L^2(\Omega)$ and u are scalar functions. Set

$$\mathcal{V} = H_0^1(\Omega) = \left\{ w \in L^2(\Omega) \;\middle|\; \frac{\partial w}{\partial x_i} \in L^2(\Omega), w = 0 \text{ on } \partial\Omega \right\}. \tag{4.3}$$

We multiply (4.1) by an arbitrary test function w from $\mathcal{V}$ and integrate to obtain

$$-\int_\Omega (\nabla^2 u)\ w dx = \int_\Omega f w\ dx. \tag{4.4}$$

Using integration by parts, applying Green's theorem to the left hand side of (4.4) and using $w = 0$ on $\partial\Omega$ from the definition of $\mathcal{V}$, we have the weak form phrased as follows: find $u \in \mathcal{V}$ such that

$$\int_\Omega \nabla u \cdot \nabla w\ dx = \int_\Omega f w\ dx \quad \forall w \in \mathcal{V}. \tag{4.5}$$

If u is sufficiently smooth, the weak form (4.5) is equivalent to the strong form (4.1).

We define the bilinear form $a : \mathcal{V} \times \mathcal{V} \longrightarrow \mathbb{R}$ by

$$a(u, w) = \int_\Omega \nabla u \cdot \nabla w\ dx \tag{4.6}$$

and the linear functional $\ell : \mathcal{V} \longrightarrow \mathbb{R}$ by

$$\langle \ell, w \rangle = \int_\Omega f w\ dx. \tag{4.7}$$

Hence the weak form is phrased as: find $u \in \mathcal{V}$ such that

$$a(u, w) = \langle \ell, w \rangle \quad \forall w \in \mathcal{V}. \tag{4.8}$$

4.2 The Galerkin approximation

Let the space of solutions $\mathcal{V}$ be approximated by a finite dimensional space $\mathcal{V}^h$, i.e. $w \in \mathcal{V}^h$ vanishes at $\partial\Omega$ and $\mathcal{V}^h \subset \mathcal{V}$, and $\text{span}\{\phi_i\}_{i=1}^N$ be a basis for $\mathcal{V}^h$ so that

$$\text{span}\{\phi_i\} = \mathcal{V}^h. \tag{4.9}$$

We now seek $u_h \in \mathcal{V}^h$ such that

$$a(u_h, w_h) = \langle \ell, w_h \rangle \quad \text{for all } w_h \in V^h. \tag{4.10}$$

We note that the problem is posed on $\mathcal{V}^h$ so that u_h and w_h must be linear combinations of the basis of $\mathcal{V}^h$:

$$u_h = \sum_{i=1}^{N} c_i \phi_i \quad \text{and} \quad w_h = \sum_{j=1}^{N} d_j \phi_j. \tag{4.11}$$

We substitute (4.11) into (4.10) and use the bilinear form a and the linear functional ℓ to obtain

$$\sum_{i=1}^{N} \sum_{j=1}^{N} a(\phi_i, \phi_j) c_i d_j = \sum_{j=1}^{N} \langle \ell, \phi \rangle d_j. \tag{4.12}$$

Let $K_{ij} = a(\phi_i \phi_j)$ and $F_j = \langle \ell, \phi \rangle$; then equation (4.12) can be written as

$$\sum_{j=1}^{N} d_j \left(\sum_{i=1}^{N} K_{ij} c_i - F_j \right) = 0. \tag{4.13}$$

Since w_h is arbitrary, the coefficients d_j are also arbitrary. We set the second sum to zero for (4.13) to hold. This gives a set of simultaneous linear equations to solve:

$$\sum_{i=1}^{N} K_{ij} c_i = F_j, \quad j = 1, 2, \ldots, N. \tag{4.14}$$

In matrix-vector form,

$$\boldsymbol{K}\boldsymbol{c} = \boldsymbol{F}, \tag{4.15}$$

noting that $\boldsymbol{K}$ is symmetric from (4.12). Solving the simultaneous linear system then allows us to find the solution u_h in (4.11).

4.3 Finite element approximations

The choice of basis for the finite-dimensional space $\mathcal{V}^h$ in the Galerkin approximation is important in obtaining an accurate approximation of the solution. Choosing the basis functions is not necessarily easy, more especially if Ω is a complex geometry. Henceforth we assume that

Ω is a polygonal domain in $\mathbb{R}^2$ The finite element method (FEM) overcomes this difficulty by using basis functions which cater for irregularity of the domain. The starting point of the finite element method is partitioning of the domain into subdomains called elements, which we denote by Ω_e for $(e = 1, 2, \ldots, E)$ where E is the total number of elements. In a two-dimensional setting the elements are connected along the edges as opposed to a connection to a section of an edge, Figure 4.1 shows admissible and inadmissible connections between two elements with 3 edges.

(a) Inadmissible connection (b) Admissible connection

Figure 4.1: Two element connections showing admissible and inadmissible connection between two elements in two-dimensional setting.

The ends of connecting edges are connected by nodes at vertices. The node connection is such that adjacent elements share at least one node and therefore share degrees of freedom (the unknowns) such as displacement. The connectivity and assembly of the elements is called the finite element mesh. Figure 4.2 shows an example of a mesh where the elements OEQ, EKQ,KPQ and POQ share the node labelled Q.

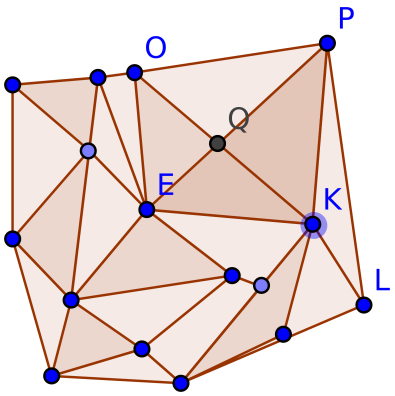

Figure 4.2: An example of a finite element mesh

In the lowest-order case, as described, the dimension of $\mathcal{V}^h$ is $N_{nd} - N_{bc}$, where N_{nd} denotes the total number of nodes and N_{bc} denotes the number of nodes along $\partial\Omega$. We denote the basis or shape functions by N_i:

$$\mathcal{V}^h = \text{span}\{N_i\}_{i=1}^{N_{nd}-N_{bc}} \tag{4.16}$$

The shape functions have the following properties:

1. N_i is a continuous piecewise polynomial;

2. Each shape function N_i is associated with a node $\mathbf{x}_i$ such that it is zero at all other nodes and equal to one at that node; that is,

$$N_i(\mathbf{x}_j) = \begin{cases} 1 & \text{if } i = j, \\ 0 & \text{if } i \neq j. \end{cases} \tag{4.17}$$

3. Each shape function N_i is non-zero only on elements connected to the associated node $\mathbf{x}_i$.

Thus the approximate solution u_h is written as

$$u_h(\mathbf{x}) = \sum_{i=1}^{N_{nd}} d_i N_i(\mathbf{x}) \tag{4.18}$$

and

$$u_h(\mathbf{x}_j) = \sum_{i=1}^{N_{nd}} d_i N_i(\mathbf{x}_j) = d_j \tag{4.19}$$

in which d_j is the value of u_h at node j. We recall that to obtain u_h, we first have to solve the system (4.15).

We set $K_{ij} = a(N_i, N_j)$ and $F_j = \langle \ell, N_j \rangle$. A field quantity is then interpolated by the chosen basis function over each element, that is, the bilinear form $a(N_i, N_j)$ and the linear functional $\langle \ell, N_j \rangle$ are integrated over the domain Ω discretized into E finite elements (Ω_e $(e = 1, \ldots, E)$); denoting the integrand in the bilinear form by $\mathcal{F}(N_i, N_j)$,

$$\begin{aligned} a(N_i, N_j) &= \int_\Omega \mathcal{F}(N_i, N_j) dx \\ &= \sum_{e=1}^{N_e} \int_{\Omega_e} \mathcal{F}(N_i^{(e)}, N_j^{(e)}) \, dx \\ &:= \sum_{e=1}^{N_e} a^{(e)}(N_i^{(e)}, N_j^{(e)}) \end{aligned} \tag{4.20}$$

whilst denoting the integrand appearing in the linear functional by $\mathcal{G}(N_j)$ we have

$$\begin{aligned}\langle \ell, N_j \rangle &= \int_\Omega \mathcal{G}(N_j) \\ &= \sum_{e=1}^{N_e} \int_{\Omega_e} \mathcal{G}(N_j^{(e)}) \\ &:= \sum_{e=1}^{N_e} \langle \ell^{(e)}, N_j^{(e)} \rangle. \end{aligned} \tag{4.21}$$

We then have $K_{ij}^{(e)} = a^{(e)}(N_i^{(e)}, N_j^{(e)})$ and $F_j^{(e)} = \langle \ell^{(e)}, N_j^{(e)} \rangle$ as the element matrices and vectors. They are then assembled such that the system consists of simultaneous algebraic equations to be solved, hence the matrix $\boldsymbol{K}$ and the vector $\boldsymbol{F}$ are presented as

$$\boldsymbol{K} = \mathop{\mathrm{A}}_{e=1}^{E} \boldsymbol{K}^{(e)}, \tag{4.22}$$

$$\boldsymbol{F} = \mathop{\mathrm{A}}_{e=1}^{E} \boldsymbol{F}^{(e)} \tag{4.23}$$

where A denotes the assembly operator.

4.4 Two-dimensional elements

We use two-dimensional elements to illustrate how the basis functions introduced above are chosen. We consider the simplest polygon and commonly used element: the linear triangle.

We first define a reference element $\hat{\Omega}$ as an element isolated from the actual mesh but still has the same nodal system as the elements Ω_e in the actual mesh. It has its own coordinate system $\boldsymbol{\xi} = (\xi, \eta)$ and we assume that each element in the mesh is generated from the reference element by an invertible affine mapping

$$\mathbf{x} = F_e(\boldsymbol{\xi}) \equiv (1 - \xi - \eta)\mathbf{x}_1^{(e)} + \xi \mathbf{x}_2^{(e)} + \eta \mathbf{x}_3^{(e)} \tag{4.24}$$

which maps each point from $\boldsymbol{\xi} = (\xi, \eta) \in \hat{\Omega}$ to the corresponding point $\mathbf{x} \in \Omega_e$.

The vertices or nodes of the triangle are numbered using a local numbering system such that the node numbers are identical with those of the reference element; see Figure 4.3 below.

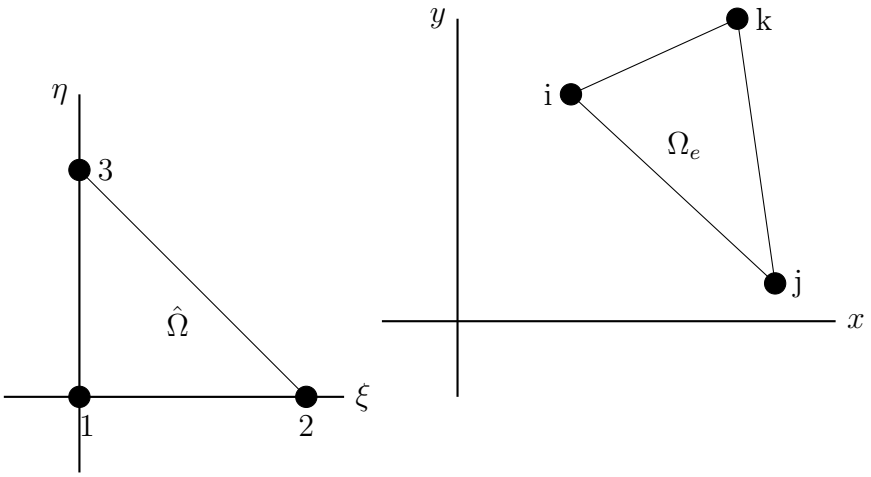

Figure 4.3: A linear triangular element with the corresponding reference element.

The point 1 maps to i, 2 maps to j, and 3 maps to k. The local basis functions on $\hat{\Omega}$ are defined by

$$\hat{N}_1(\boldsymbol{\xi}) = 1 - \xi - \eta, \tag{4.25}$$

$$\hat{N}_2(\boldsymbol{\xi}) = \xi, \tag{4.26}$$

$$\hat{N}_3(\boldsymbol{\xi}) = \eta, \tag{4.27}$$

whilst the basis functions on Ω_e are obtained from

$$N_i^{(e)}(\mathbf{x}) = \hat{N}_i(\boldsymbol{\xi}), \quad \text{for } i = 1, 2, 3. \tag{4.28}$$

The coordinate $\boldsymbol{x}$ is related to $\boldsymbol{\xi}$ through the map defined in (4.24). For the triangular element, $\boldsymbol{K}^{(e)}$ in (4.22) is a 3×3 matrix.

Since we will be using the bilinear quadrilateral element in this work, we discuss it as well. This element has nodes at the four corners of the quadrilateral. The local basis functions for $\hat{\Omega}_i$ are bilinear, namely:

$$\hat{N}_1(\boldsymbol{\xi}) = \frac{1}{4}(1 - \xi)(1 - \eta), \tag{4.29}$$

$$\hat{N}_2(\boldsymbol{\xi}) = \frac{1}{4}(1 + \xi)(1 - \eta), \tag{4.30}$$

$$\hat{N}_3(\boldsymbol{\xi}) = \frac{1}{4}(1 + \xi)(1 + \eta), \tag{4.31}$$

$$\hat{N}_4(\boldsymbol{\xi}) = \frac{1}{4}(1 - \xi)(1 + \eta), \tag{4.32}$$

and the basis functions for Ω_e are obtained from $\hat{N}_i(\boldsymbol{\xi}) = N_i^{(e)}(\boldsymbol{x})$. We set up a square reference

element $\hat{\Omega} = (-1, 1) \times (-1, 1)$ and obtain the rectangular element Ω_e by the map

$$\mathbf{x} = F_e\boldsymbol{\xi} \equiv \boldsymbol{T}\boldsymbol{\xi} + \boldsymbol{b} \tag{4.33}$$

where $\boldsymbol{T}$ is the matrix

$$\boldsymbol{T} = \frac{1}{2}\begin{bmatrix} x_2^{(e)} & -x_1^{(e)} & y_2^{(e)} & -y_2^{(e)} \\ x_4^{(e)} & -x_1^{(e)} & y_4^{(e)} & -y_1^{(e)} \end{bmatrix} \tag{4.34}$$

and $\boldsymbol{b}$ is the position vector of the centroid of Ω_e (Figure 4.4).

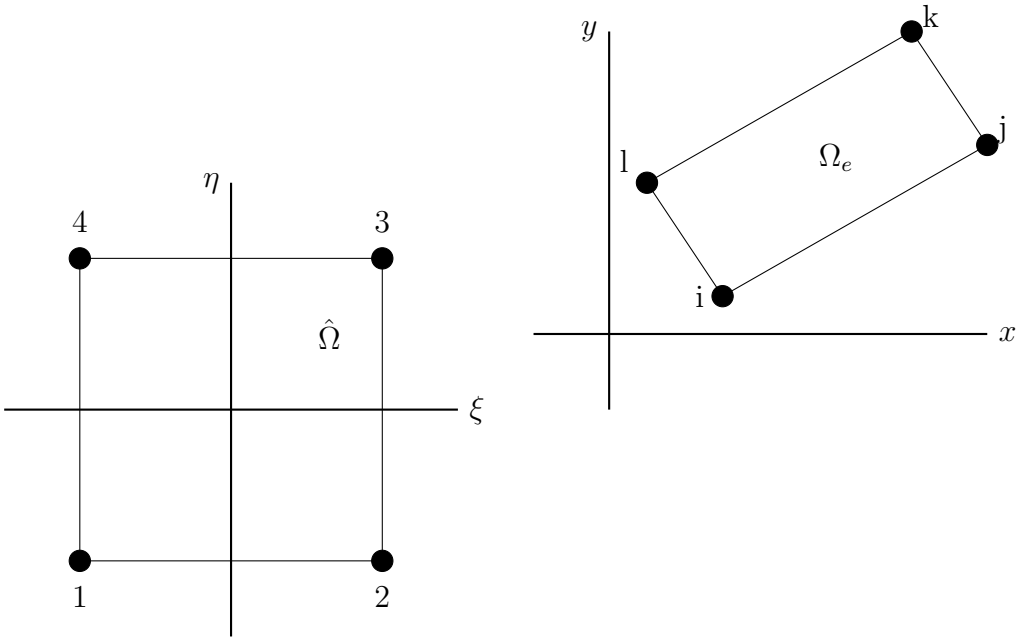

Figure 4.4: A bilinear rectangular element with the corresponding reference element.

More generally, one obtains a quadrilateral, shown in Figure 4.5 from (4.29)-(4.32) by the map

$$\begin{aligned} \mathbf{x} &= F_e(\boldsymbol{\xi}) \\ &= \sum_{i=1}^{4} \hat{N}_i(\boldsymbol{\xi})\mathbf{x}_i \end{aligned} \tag{4.35}$$

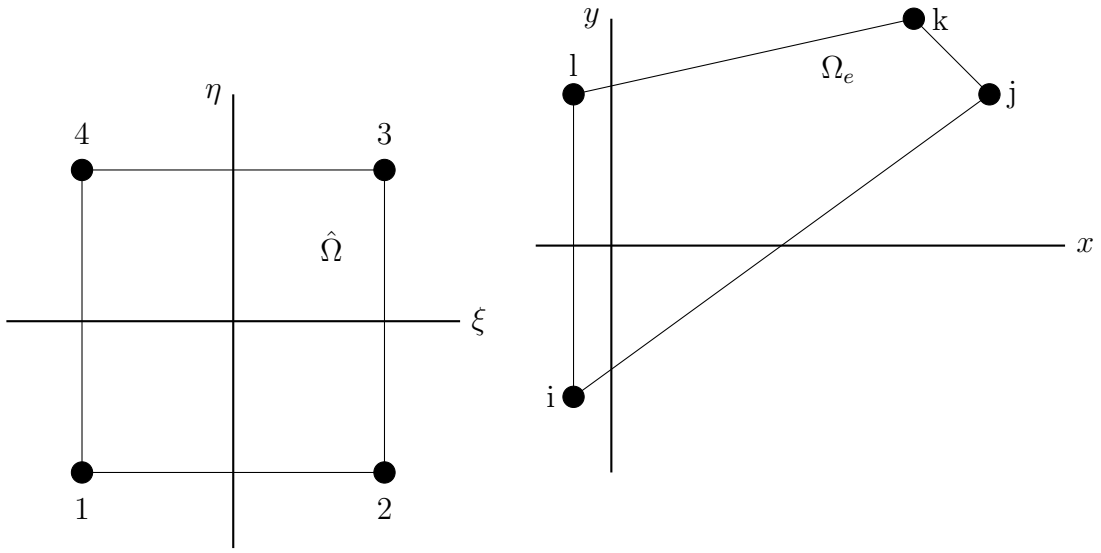

Figure 4.5: A bilinear quadratic element with the corresponding reference element.

4.5 Weak formulations

This section derives the weak form of the boundary value problem introduced in Section 2.5 and the weak form of the microforce balance (3.90).

The equilibrium equation

From (2.63) we have

$$-\text{div}\,\boldsymbol{\sigma} = \mathbf{F}. \tag{4.36}$$

We set

$$\mathcal{V} = H^1(\Omega) = \left\{ \mathbf{w} \in L^2(\Omega) \middle| \frac{\partial \mathbf{w}}{\partial x_i} \in L^2(\Omega),\ \mathbf{w} = \mathbf{0} \text{ on } \partial\Omega_D \right\}. \tag{4.37}$$

Taking the inner product of (4.36) with an arbitrary displacement function $\mathbf{w}$ and integrating over the domain Ω we obtain

$$-\int_\Omega (\text{div}\,\boldsymbol{\sigma}) \cdot \mathbf{w}\ dx = \int_\Omega \mathbf{F} \cdot \mathbf{w}\ dx. \tag{4.38}$$

We apply Green's theorem on the left-hand side of (4.38) to get

$$-\int_{\partial\Omega} (\boldsymbol{\sigma}\boldsymbol{n}) \cdot \mathbf{w}\ ds + \int_\Omega \boldsymbol{\sigma} : \nabla \mathbf{w}\ dx = \int_\Omega \mathbf{F} \cdot \mathbf{w}\ dx. \tag{4.39}$$

Since $\boldsymbol{\sigma}$ is symmetric and $\boldsymbol{\sigma n} = \overline{\mathbf{t}}$, thus (4.39) becomes

$$-\int_{\partial\Omega_N} \overline{\mathbf{t}} \cdot \mathbf{w}\ ds + \int_\Omega \boldsymbol{\sigma} : \tfrac{1}{2}(\nabla \mathbf{w} + (\nabla \mathbf{w})^T)\ dx = \int_\Omega \mathbf{F} \cdot \mathbf{w}\ dx. \tag{4.40}$$

We recall the strain-displacement relation

$$\boldsymbol{\epsilon} = \tfrac{1}{2}(\nabla \boldsymbol{u} + (\nabla \boldsymbol{u})^T); \tag{4.41}$$

thus the weak form of (4.36) is presented as

$$-\int_{\partial\Omega_N} \overline{\mathbf{t}} \cdot \mathbf{w}\ ds + \int_\Omega \boldsymbol{\sigma}(\boldsymbol{\epsilon}(\boldsymbol{u})) : \boldsymbol{\epsilon}(\mathbf{w})\ dx = \int_\Omega \mathbf{F} \cdot \mathbf{w}\ dx. \tag{4.42}$$

Microforce balance and flow relation

Here we derive the weak form of the microforce balance equation (3.90)

$$\boldsymbol{\sigma} - \boldsymbol{\rho} + \operatorname{div} \mathbb{K} - \operatorname{sym}[\operatorname{dev}(\operatorname{curl} \boldsymbol{\zeta})] = \mathbf{0}. \tag{4.43}$$

We define

$$\mathsf{Q} = \left\{ q_{ij} \in H^1(\Omega) \middle| q_{ij} = q_{ji},\ q_{ii} = 0 \text{ and } \mathbf{q} = \mathbf{0} \text{ on } \partial\Omega_H \right\}. \tag{4.44}$$

We first take the inner product of (4.43) and boundary conditions with an arbitrary plastic strain $\mathbf{q} \in \mathsf{Q}$ and then integrate to obtain

$$\int_\Omega \left\{ \mathbf{q} : \left(\boldsymbol{\sigma} - \boldsymbol{\rho} + \operatorname{div} \mathbb{K} - \operatorname{sym}[\operatorname{dev}(\operatorname{curl} \boldsymbol{\zeta})] \right) \right\} dx = 0. \tag{4.45}$$

Expanding (4.45) and integrating by parts the term involving $\mathbb{K}$, we have

$$\int_\Omega \left\{ \boldsymbol{\sigma} : \mathbf{q} - \boldsymbol{\rho} : \mathbf{q} - \mathbb{K} : \nabla \mathbf{q} - \operatorname{sym}[\operatorname{dev}(\operatorname{curl} \boldsymbol{\zeta})] : \mathbf{q} \right\} dx + \int_{\partial\Omega} \mathbb{K}\mathbf{n} \cdot \mathbf{q}\ ds = 0. \tag{4.46}$$

We write

$$\boldsymbol{\rho} : \mathbf{q} + \mathbb{K} : \nabla \mathbf{q} = \mathsf{S} \circ \mathsf{Q}, \tag{4.47}$$

where $\mathsf{Q} = (\mathbf{q}, L\nabla\mathbf{q})$ and $\mathsf{S} = (\boldsymbol{\rho}, L^{-1}\mathbb{K})$, see (3.64) - (3.65); hence (4.46) becomes

$$\int_\Omega \big\{\boldsymbol{\sigma} : \mathbf{q} - \mathsf{S}\circ\mathsf{Q}\big\}dx - \int_\Omega \big\{\text{sym}[\text{dev}(\text{curl}\ \boldsymbol{\zeta})] : \mathbf{q}\big\}\ dx + \int_{\partial\Omega} \mathbb{K}\mathbf{n}\cdot\mathbf{q}\ ds = 0. \tag{4.48}$$

We note that $\mathbf{q}$ is deviatoric and symmetric, thus (4.48) may be expressed as

$$\int_\Omega \big\{\boldsymbol{\sigma} : \mathbf{q} - \mathsf{S}\circ\mathsf{Q}\big\}dx - \int_\Omega \text{curl}\ \boldsymbol{\zeta} : \mathbf{q}\ dx + \int_{\partial\Omega} \mathbb{K}\mathbf{n}\cdot\mathbf{q}\ ds = 0. \tag{4.49}$$

Integrating by parts the middle term of (4.49), we obtain

$$\int_\Omega \big\{\boldsymbol{\sigma} : \mathbf{q} - \mathsf{S}\circ\mathsf{Q}\big\}dx + \int_\Omega \boldsymbol{\zeta} : \text{curl}\ \mathbf{q}\ dx + \int_{\partial\Omega} [\mathbb{K}\mathbf{n} + \text{sym}[\text{dev}(\boldsymbol{\zeta}\times\mathbf{n})]]\cdot\mathbf{q}\ ds = 0. \tag{4.50}$$

Since $\partial\Omega = \partial\Omega_F \cup \partial\Omega_H$, $\mathbf{q} = \mathbf{0}$ at $\partial\Omega_H$ and $\mathbb{K}\mathbf{n} + \text{sym}[\text{dev}(\boldsymbol{\zeta}\times\mathbf{n})] = \mathbf{0}$ at $\partial\Omega_F$, the boundary term in (4.50) vanishes. Also, since $\mathbf{q}$ is symmetric and deviatoric, we have

$$\int_\Omega \big\{\boldsymbol{\sigma} : \mathbf{q} - \mathsf{S}\circ\mathsf{Q}\big\}dx + \int_\Omega \boldsymbol{\zeta} : \text{curl}\ \mathbf{q}\ dx = 0. \tag{4.51}$$

The defect stress $\boldsymbol{\zeta}$ is defined by (see equation 4.52)

$$\boldsymbol{\zeta} = \mu l^2 \text{curl}\ \boldsymbol{\epsilon}^p \tag{4.52}$$

where l is the energetic material length scale. Substituting (4.52) into (4.51) we obtain

$$\int_\Omega \big\{\boldsymbol{\sigma} : \mathbf{q} - \mathsf{S}\circ\mathsf{Q}\big\}dx - \int_\Omega \big\{\ \mu l^2 \text{curl}\ \boldsymbol{\epsilon}^p : \text{curl}\mathbf{q}\big\}\ dx = 0. \tag{4.53}$$

We recall from (3.81) that

$$\mathsf{S} = \frac{\partial \mathcal{D}_\varepsilon}{\partial \dot{\Gamma}}, \tag{4.54}$$

where $\mathcal{D}_\varepsilon$ is a chosen dissipation function. Substituting (4.54) into (4.53), we have

$$\int_\Omega \left\{\boldsymbol{\sigma} : \mathbf{q} - \left(\frac{\partial \mathcal{D}_\varepsilon}{\partial \dot{\Gamma}}\right)\circ\mathsf{Q}\right\}dx - \int_\Omega \big\{\ \mu l^2 \text{curl}\ \boldsymbol{\epsilon}^p : \text{curl}\mathbf{q}\big\}\ dx = 0. \tag{4.55}$$

The next step is to discretize (4.55) with respect to time $t \in [0, T]$ with $0 = t_0 < t_1 < \cdots < t_N = T$. For the time discretisation we adopt the backward Euler integration scheme. We denote a time increment at $k+1$ by $\Delta t = t_{k+1} - t_k$. Thus from (3.67) we have

$$\Delta\Gamma = \sqrt{\tfrac{2}{3}|\Delta\boldsymbol{\epsilon}^p|^2 + \tfrac{2}{3}L^2|\Delta\nabla\boldsymbol{\epsilon}^p|^2}, \tag{4.56}$$

hence (4.55) becomes

$$\int_\Omega \left\{ \boldsymbol{\sigma}^{k+1} : \mathbf{q} \;\; - \left(\frac{\partial \mathcal{D}_\varepsilon}{\partial \Delta\Gamma}\right)^{k+1} \circ \mathsf{Q} \;\; - \mu l^2 \text{curl}\, \boldsymbol{\epsilon}^{p(k+1)} : \text{curl}\mathbf{q} \right\} dV = 0 \tag{4.57}$$

4.6 Finite element formulation

Here we formulate the finite element approximation of (4.42) and (4.57). Our unknowns are the displacement $\mathbf{u}$ and the plastic strain $\boldsymbol{\epsilon}^p$. Their nodal values are denoted by $\hat{\mathbf{u}}$ and $\hat{\boldsymbol{\epsilon}}^p$. Henceforth, we adopt Voigt notation; for example, the stress $\boldsymbol{\sigma}$ and strain $\boldsymbol{\epsilon}$ become four component vectors

$$\boldsymbol{\sigma}^T = [\sigma_{xx}\ \sigma_{yy}\ \sigma_{zz}\ \sigma_{xy}] \tag{4.58}$$

$$\boldsymbol{\epsilon}^T = [\epsilon_{xx}\ \epsilon_{yy}\ \epsilon_{zz}\ 2\epsilon_{xy}] \tag{4.59}$$

respectively. We introduce a spatial discretisation of the unknown fields based on the shape functions $\mathbf{N}^{(i)}(\xi,\eta)$ with $i = 1, 2, \ldots N_{\text{nodes}}$ and $\xi, \eta \in [-1, 1]$. We have

$$\begin{gathered} \boldsymbol{u} = \mathbf{N}\hat{\boldsymbol{u}}, \qquad \boldsymbol{w} = \mathbf{N}\hat{\boldsymbol{w}}, \qquad \boldsymbol{\epsilon}(\boldsymbol{u}) = \mathbf{B}\hat{\boldsymbol{u}}, \quad \boldsymbol{\epsilon}(\boldsymbol{w}) = \mathbf{B}\hat{\boldsymbol{w}} \\ \boldsymbol{\epsilon}^p = \mathbf{N}\hat{\boldsymbol{\epsilon}}^p, \quad \nabla\boldsymbol{\epsilon}^p = \mathbf{H}\hat{\boldsymbol{\epsilon}}^p, \quad \boldsymbol{q} = \mathbf{N}\hat{\boldsymbol{q}}, \quad \nabla\boldsymbol{q} = \mathbf{B}\hat{\boldsymbol{q}} \end{gathered} \tag{4.60}$$

where $\mathbf{B}$ is the strain-displacement differentiation matrix and $\mathbf{H}$ is a matrix of the shape functions' spatial derivatives. We use the same shape functions for $\mathbf{u}$ and $\boldsymbol{\epsilon}^p$. The Cauchy stress is defined by

$$\boldsymbol{\sigma} = \mathsf{L}(\mathbf{B}\hat{\boldsymbol{u}} - \mathbf{N}\hat{\boldsymbol{\epsilon}}^p) \tag{4.61}$$

in which L is the 4×4 matrix characterising linear elastic behaviour.

Equilibrium

We substitute (4.60)-(4.61) into (4.42) to obtain

$$\int_\Omega \hat{\boldsymbol{w}}^T \boldsymbol{B}^T \mathsf{L}(\mathbf{B}\hat{\boldsymbol{u}} - \mathbf{N}\hat{\boldsymbol{\epsilon}}^p)\ dx = \int_\Omega \hat{\boldsymbol{w}}^T \boldsymbol{N}^T \boldsymbol{F}\ dx \qquad \forall\ \hat{\boldsymbol{w}}. \tag{4.62}$$

Since $\hat{\boldsymbol{w}}$ is arbitrary, we have

$$\hat{\boldsymbol{w}}^T \left[\int_\Omega \boldsymbol{B}^T \mathsf{L}(\mathbf{B}\hat{\boldsymbol{u}} - \mathbf{N}\hat{\boldsymbol{\epsilon}}^p)\ dx - \int_\Omega \boldsymbol{N}^T \boldsymbol{F}\ dx \right] = \mathbf{0} \qquad \forall\ \hat{\boldsymbol{w}}. \tag{4.63}$$

If we choose $\hat{\boldsymbol{w}}^T \neq \mathbf{0}$, then

$$\int_\Omega \boldsymbol{B}^T \mathsf{L}(\mathbf{B}\hat{\boldsymbol{u}} - \mathbf{N}\hat{\boldsymbol{\epsilon}}^p)\ dx - \int_\Omega \boldsymbol{N}^T \boldsymbol{F}\ dx = \mathbf{0}. \tag{4.64}$$

Flow

From equation (4.57), we let

$$\text{curl}\ \boldsymbol{\epsilon}^p = \mathbf{C}\ \hat{\boldsymbol{\epsilon}}^p \tag{4.65}$$

$$\text{curl}\ \boldsymbol{q} = \mathbf{C}\ \hat{\mathbf{q}} \tag{4.66}$$

where $\mathbf{C}$ is represents the curl in Voigt notation. We also substitute (4.60)-(4.61) into equation (4.57) to obtain

$$\begin{aligned} \int_\Omega \Bigg\{ \left(\hat{\boldsymbol{q}}^T \mathbf{N}^T \mathsf{L}(\mathbf{B}\hat{\boldsymbol{u}} - \mathbf{N}\hat{\boldsymbol{\epsilon}}^p) \right)^{k+1} - \left(\frac{\partial \mathcal{D}_{\text{eff}}}{\partial \Delta\Gamma} \right)^{k+1} \circ \mathsf{Q} \\ - \mu l^2 \left(\hat{\mathbf{q}}^T \mathbf{C}^T \mathbf{C}\ \hat{\boldsymbol{\epsilon}}^p \right)^{k+1} \Bigg\}\ dx = \mathbf{0}. \end{aligned} \tag{4.67}$$

Our effective dissipation function is defined by (3.89); thus its derivative is defined by

$$\frac{\partial \mathcal{D}_{\text{eff}}}{\partial \Delta\Gamma} = \frac{\partial \mathcal{D}_\epsilon}{\partial \Delta\Gamma} = \begin{pmatrix} \dfrac{\partial \mathcal{D}_\epsilon}{\partial \dot{\boldsymbol{\epsilon}}^p} \\ \dfrac{\partial \mathcal{D}_\epsilon}{\partial \nabla \Delta \boldsymbol{\epsilon}^p} \end{pmatrix}. \tag{4.68}$$

Thus if $|\frac{\Delta\Gamma}{\Delta t}| \leq \dot{\varepsilon}_0$ we have

$$\frac{\partial \mathcal{D}_\epsilon}{\partial \Delta\Gamma} = \begin{pmatrix} \frac{1}{3}[\sigma_0 + h(E^p)^{nh}]\frac{\Delta\boldsymbol{\epsilon}^p}{\dot{\varepsilon}_0 \Delta\Gamma} \\ \\ \frac{1}{3}L^2[\sigma_0 + h(E^p)^{nh}]\frac{\nabla\Delta\boldsymbol{\epsilon}^p}{\dot{\varepsilon}_0 \Delta\Gamma} \end{pmatrix}, \tag{4.69}$$

otherwise

$$\frac{\partial \mathcal{D}_\epsilon}{\partial \Delta\Gamma} = \begin{pmatrix} \frac{1}{3}\dot{\varepsilon}_0[\sigma_0 + h(E^p)^{nh}]\frac{\Delta\boldsymbol{\epsilon}^p}{(\Delta\Gamma)^3} \\ \\ \frac{1}{3}\dot{\varepsilon}_0 L^2[\sigma_0 + h(E^p)^{nh}]\frac{\nabla\Delta\boldsymbol{\epsilon}^p}{(\Delta\Gamma)^3} \end{pmatrix}. \tag{4.70}$$

Let

$$\sigma_y = \sigma_0 + h(E^p)^{nh}. \tag{4.71}$$

We have $\mathsf{Q} = (\boldsymbol{q}, L\nabla\boldsymbol{q})$; thus if $|\Delta\Gamma| \leq \dot{\varepsilon}_0$ we have

$$\begin{aligned} \frac{\partial \mathcal{D}_\epsilon}{\partial \dot{\Gamma}} \circ \mathsf{Q} &= \frac{\sigma_y^{k+1}}{3\dot{\varepsilon}_0}\left[\frac{\Delta\boldsymbol{\epsilon}^p}{\Delta\Gamma} : \boldsymbol{q} + L^2\frac{\Delta\nabla\boldsymbol{\epsilon}^p}{\Delta\Gamma} : \nabla\boldsymbol{q}\right] \\ &= \frac{\sigma_y^{k+1}}{3\dot{\varepsilon}_0}\left[\frac{\mathbf{N}(\Delta\hat{\boldsymbol{\epsilon}}^p)}{\Delta\Gamma} : \mathbf{N}\hat{\boldsymbol{q}} + L^2\frac{\mathbf{H}(\Delta\hat{\boldsymbol{\epsilon}}^p)}{\Delta\Gamma} : \mathbf{B}\hat{\boldsymbol{q}}\right] \\ &= \frac{\sigma_y^{k+1}}{3\dot{\varepsilon}_0}\hat{\boldsymbol{q}}^T\left[\mathbf{N}^T\left(\frac{\mathbf{N}(\Delta\hat{\boldsymbol{\epsilon}}^p)}{\Delta\Gamma}\right) + L^2\mathbf{B}^T\left(\frac{\mathbf{H}(\Delta\hat{\boldsymbol{\epsilon}}^p)}{\Delta\Gamma}\right)\right]. \end{aligned} \tag{4.72}$$

Hence (4.67) may be written as

$$\begin{aligned} \int_\Omega \Bigg\{ \left(\hat{\boldsymbol{q}}^T\mathbf{N}^T\mathbf{L}(\mathbf{B}\hat{\boldsymbol{u}} - \mathbf{N}\hat{\boldsymbol{\epsilon}}^p)\right)^{k+1} - \Bigg(\frac{\sigma_y^{k+1}}{3\dot{\varepsilon}_0}\hat{\boldsymbol{q}}^T\Bigg[\mathbf{N}^T\left(\frac{\mathbf{N}(\Delta\hat{\boldsymbol{\epsilon}}^p)}{\Delta\Gamma}\right) \\ + L^2\mathbf{B}^T\left(\frac{\mathbf{H}(\Delta\hat{\boldsymbol{\epsilon}}^p)}{\Delta\Gamma}\right)\Bigg]\Bigg)^{k+1} \circ \mathsf{Q} - \mu l^2\left(\hat{\mathbf{q}}^T\mathbf{C}^T\mathbf{C}\,\hat{\boldsymbol{\epsilon}}^p\right)^{k+1}\Bigg\}\, dV = 0. \end{aligned} \tag{4.73}$$

Otherwise, if $\frac{\Delta\Gamma}{\Delta t} > \dot{\varepsilon}_0$

$$\begin{aligned} \frac{\partial \mathcal{D}_\epsilon}{\partial \Delta\Gamma} \circ \mathsf{Q} &= \frac{\sigma_y^{k+1}\dot{\varepsilon}_0}{3}\left[\frac{\Delta\boldsymbol{\epsilon}^p}{(\Delta\Gamma)^3} : \boldsymbol{q} + L^2\frac{\Delta\nabla\boldsymbol{\epsilon}^p}{(\Delta\Gamma)^3} : \nabla\boldsymbol{q}\right] \\ &= \frac{\sigma_y^{k+1}\dot{\varepsilon}_0}{3}\left[\frac{\mathbf{N}(\Delta\hat{\boldsymbol{\epsilon}}^p)}{(\Delta\Gamma)^3} : \mathbf{N}\hat{\boldsymbol{q}} + L^2\frac{\mathbf{H}(\Delta\hat{\boldsymbol{\epsilon}}^p)}{(\Delta\Gamma)^3} : \mathbf{B}\hat{\boldsymbol{q}}\right] \\ &= \frac{\sigma_y^{k+1}\dot{\varepsilon}_0}{3}\hat{\boldsymbol{q}}^T\left[\mathbf{N}^T\left(\frac{\mathbf{N}(\Delta\hat{\boldsymbol{\epsilon}}^p)}{(\Delta\Gamma)^3}\right) + L^2\mathbf{B}^T\left(\frac{\mathbf{H}(\Delta\hat{\boldsymbol{\epsilon}}^p)}{(\Delta\Gamma)^3}\right)\right], \end{aligned} \tag{4.74}$$

thus

$$\int_\Omega \Bigg\{ \left(\hat{\boldsymbol{q}}^T \mathbf{N}^T \mathsf{L} (\mathbf{B}\hat{\boldsymbol{u}} - \mathbf{N}\hat{\boldsymbol{\epsilon}}^p) \right)^{k+1} - \left(\frac{\sigma_y^{k+1}\dot{\varepsilon}_0}{3} \hat{\boldsymbol{q}}^T \left[\mathbf{N}^T \left(\frac{\mathbf{N}(\Delta\hat{\boldsymbol{\epsilon}}^p)}{(\Delta\Gamma)^3} \right) + L^2 \mathbf{B}^T \left(\frac{\mathbf{H}(\Delta\hat{\boldsymbol{\epsilon}}^p)}{(\Delta\Gamma)^3} \right) \right] \right)^{k+1} \circ \mathsf{Q} - \mu l^2 \left(\hat{\mathbf{q}}^T \mathbf{C}^T \mathbf{C}\, \hat{\boldsymbol{\epsilon}}^p \right)^{k+1} \Bigg\}\, dV = \mathbf{0}. \tag{4.75}$$

We also note that $\hat{\boldsymbol{q}}$ is arbitrary, therefore (4.76) and (4.77) may be presented as

$$\int_\Omega \Bigg\{ \left(\mathbf{N}^T \mathsf{L} (\mathbf{B}\hat{\boldsymbol{u}} - \mathbf{N}\hat{\boldsymbol{\epsilon}}^p) \right)^{k+1} - \left(\frac{\sigma_y^{k+1}}{3\dot{\varepsilon}_0} \left[\mathbf{N}^T \left(\frac{\mathbf{N}(\Delta\hat{\boldsymbol{\epsilon}}^p)}{\Delta\Gamma} \right) + L^2 \mathbf{B}^T \left(\frac{\mathbf{H}(\Delta\hat{\boldsymbol{\epsilon}}^p)}{\Delta\Gamma} \right) \right] \right)^{k+1} \circ \mathsf{Q} - \mu l^2 \left(\mathbf{C}^T \mathbf{C}\, \hat{\boldsymbol{\epsilon}}^p \right)^{k+1} \Bigg\}\, dV = \mathbf{0} \tag{4.76}$$

and

$$\int_\Omega \Bigg\{ \left(\mathbf{N}^T \mathsf{L} (\mathbf{B}\hat{\boldsymbol{u}} - \mathbf{N}\hat{\boldsymbol{\epsilon}}^p) \right)^{k+1} - \left(\frac{\sigma_y^{k+1}\dot{\varepsilon}_0}{3} \left[\mathbf{N}^T \left(\frac{\mathbf{N}(\Delta\hat{\boldsymbol{\epsilon}}^p)}{(\Delta\Gamma)^3} \right) + L^2 \mathbf{B}^T \left(\frac{\mathbf{H}(\Delta\hat{\boldsymbol{\epsilon}}^p)}{(\Delta\Gamma)^3} \right) \right] \right)^{k+1} \circ \mathsf{Q} - \mu l^2 \left(\mathbf{C}^T \mathbf{C}\, \hat{\boldsymbol{\epsilon}}^p \right)^{k+1} \Bigg\}\, dV = \mathbf{0} \tag{4.77}$$

respectively.

4.7 Global flow relation

We note that the yield condition is in terms of the indeterminate generalised stress S, thus the yield condition cannot be determined locally from (3.82). This is resolved by formulating the flow relation in global form (Reddy, Ebobisse, McBride (2008), Reddy (2011)). The flow relation (3.81) is multiplied by Q and then integrated to obtain

$$\int_\Omega \left(\frac{\partial \mathcal{D}}{\partial \dot{\Gamma}} : \mathsf{Q}\, dx - \mathsf{S} : \mathsf{Q} \right) dx = 0. \tag{4.78}$$

The weak formulation of the microforce balance equation (4.51) is used to obtain:

$$\int_\Omega \left(\frac{\partial \mathcal{D}}{\partial \dot{\Gamma}} : \mathsf{Q}\, dx + \boldsymbol{\sigma} : \mathbf{q} - \boldsymbol{\zeta} : \operatorname{curl} \mathbf{q} \right) dx = 0. \tag{4.79}$$

For convenience, we set $\boldsymbol{\zeta} = \mathbf{0}$. We next set

$$j(\mathsf{Q}) = \int_\Omega \mathcal{D}(\mathsf{Q}) dx. \tag{4.80}$$

From here, one can attempt to find the global yield function corresponding to j by finding the relationship between the dissipation function and (canonical) yield function as polar conjugates.

The polar conjugate to j is defined by

$$\Phi(\mathsf{S}) = \sup_{\mathsf{Q}\neq 0} \frac{\int_\Omega \boldsymbol{\sigma} : \mathbf{q}\ dx}{j(\mathsf{Q})}. \tag{4.81}$$

The function Φ is convex, positively homogeneous and corresponds to the yield function associated with j. We formulate (4.81) in discrete form using the finite element approximations (4.60). First, the dissipation function is given by:

$$\mathcal{D} = (\sigma_0 - g)\sqrt{(\hat{\boldsymbol{\epsilon}}^p)^T \boldsymbol{N}^T \boldsymbol{N} \hat{\boldsymbol{\epsilon}}^p + L^2\ (\hat{\boldsymbol{\epsilon}}^p)^T \boldsymbol{H}^T \boldsymbol{H} \hat{\boldsymbol{\epsilon}}^p}. \tag{4.82}$$

We denote the pointwise matrix K by

$$\mathsf{K}(\mathbf{x}) = \boldsymbol{N}^T \boldsymbol{N} + L^2\ \boldsymbol{H}^T \boldsymbol{H}, \tag{4.83}$$

so that

$$\mathcal{D} = (\sigma_0 - g)\sqrt{(\hat{\boldsymbol{\epsilon}}^p)^T\ \mathsf{K}\ \hat{\boldsymbol{\epsilon}}^p}. \tag{4.84}$$

The global discrete dissipation function corresponding to j is then given by

$$\mathcal{J}(\hat{\boldsymbol{\epsilon}}^p) = \int_\Omega \mathcal{D}(\hat{\boldsymbol{\epsilon}}^p, \mathbf{x})\ dx \tag{4.85}$$

Next, the middle term on the left of (4.79) in discrete form is

$$\int_\Omega \boldsymbol{\sigma} : \mathbf{q}\ dx = \int_\Omega \hat{\mathbf{q}}^T \mathbf{N}^T \boldsymbol{\sigma}\ dx = \hat{\mathbf{q}}^T \mathsf{s} \tag{4.86}$$

where the global vector of nodal stresses is defined by

$$\mathsf{s} = \int_\Omega \mathbf{N}^T \boldsymbol{\sigma}^{\text{dev}} \, dx. \tag{4.87}$$

Substituting in (4.79) we have

$$\mathsf{s} = \left.\frac{\partial \mathcal{J}}{\partial \hat{\mathbf{q}}}\right|_{\hat{\boldsymbol{\epsilon}}^p} \qquad \text{for } \hat{\boldsymbol{\epsilon}}^p \neq \mathbf{0}. \tag{4.88}$$

Then the discrete flow relation is

$$\mathsf{s} = \left.\frac{\partial \mathcal{J}}{\partial \hat{\mathbf{q}}}\right|_{\hat{\boldsymbol{\epsilon}}^p} \quad \Leftrightarrow \quad \hat{\boldsymbol{\epsilon}}^p = \lambda \frac{\partial \Phi}{\partial \mathsf{s}}. \tag{4.89}$$

The yield function corresponding to the global discrete dissipation function is

$$\Phi(\mathsf{s}) = \sup_{\hat{\mathbf{q}} \neq 0} \frac{\hat{\mathbf{q}}^T \mathsf{s}}{\mathcal{J}(\hat{\mathbf{q}})} \tag{4.90}$$

for

$$\mathcal{J}(\mathbf{q}) = (\sigma_0 - g) \int_\Omega |K^{1/2}(\mathbf{x})\mathbf{q}|. \tag{4.91}$$

We have the upper bound (Carstensen et al., 2017)

$$\Phi(\mathsf{s}) \leq (\sigma_0 - g)^{-1} \max_{x \in \Omega} |[K(\mathbf{x})]^{-1/2}|. \tag{4.92}$$

However, it can be shown that (4.92) cannot be achieved. In Chapter 5 we will explore various approximations to Φ numerically.

Chapter 5

Numerical results

The main objective of this work is to explore the response of an SGP model involving both energetic and dissipative higher order contributions. In this chapter we present results obtained from an implementation of the SGP model as a user element in the commercial software ABAQUS. We restrict our work to plane strain boundary value problems.

The model problem investigated is that of a rectangular block subjected to simple shear. The block has height $H = 20$mm and width $W = 55$mm. The bottom surface is encastered whilst the top surface is subjected to a prescribed uniform displacement $u_x = \Gamma H$ in which the applied shear Γ is applied at a rate $\dot{\Gamma} = 1s^{-1}$. In addition, the top surface is constrained against displacement in the y-directon ($u_y = 0$).

The sides of the block are traction-free. Three types of higher-order boundary conditions (BCs) are applied:

- Microfree BCs - plastic flow is unconstrained on all boundaries, i.e. dislocations exit the body freely throughout the analysis: $\mathbb{K}\boldsymbol{n} + \text{sym}[\text{dev}(\boldsymbol{\zeta} \times \boldsymbol{n})] = \mathbf{0}$.
- Microhard BCs - No plastic flow on all boundaries for the duration of the analysis period, i.e. dislocations pile up at the boundaries: $\dot{\boldsymbol{\epsilon}}^p = \mathbf{0}$.
- Passivation BCs - Plastic flow is unconstrained in all boundaries for a time interval, after which microhard conditions are applied on all boundaries.

For this work, analyses have a duration of 1 second. The parameters used are listed in Table 5.1 below, unless otherwise stated.

Parameter	Value	Units
Young's modulus, E	68380	MPa
Initial yield stress, σ_0	2500	MPa
Hardening modulus, H	437.34	MPa
strain reference rate, $\dot{\epsilon}_0$	$5E-04$	s^{-1}
sensitivity parameter, n	0.2	-
Poisson's ratio	0.3	-

Table 5.1: Material parameters used for the simple shear problem

The shear modulus is calculated as

$$\mu = \frac{E}{2(1+\nu)}. \tag{5.1}$$

We study the simple shear problem for a homogeneous and a non-homogeneous body. The homogeneous block shown in Figure 5.1 has the properties in Table 5.1 in the whole domain, whilst the non-homogeneous domain in Figure 5.2 has two sections: a purely elastic rectangular section in the middle while the surrounding material has the elastoplastic properties listed in Table 5.1. The elastic section has Young's modulus $E_2 = \alpha E$ for $\alpha \in \{10^2, 10^3, 10^4, 10^5, 10^6\}$.

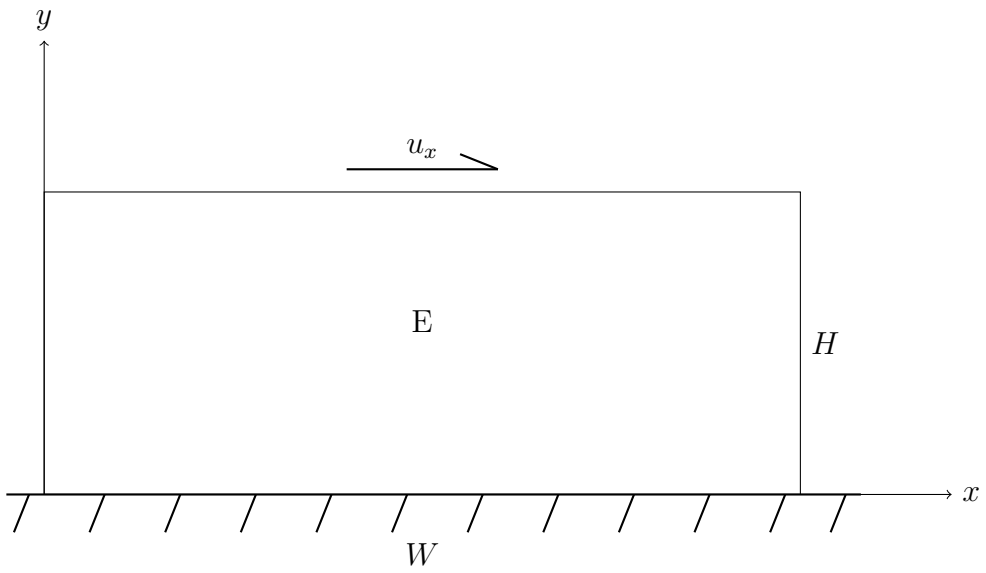

Figure 5.1: The simple shear problem for a homogeneous block.

This chapter is arranged as follows. We present mesh sensitivity results in Section 5.1 and results showing variation with α for the non-homogenous block in Section 5.2. Variation in the stresses is shown in Section 5.3 whilst in Section 5.4 we present examples of the elastic gap: the elastic response that follows a change in boundary conditions from microfree to microhard (Fleck et al., 2014). Then, in Section 5.5 we demonstrate the strengthening effect (Polizzotto, 2010), (Chiricotto et al., 2016) that accompanies an increase in the dissipative length scale, and

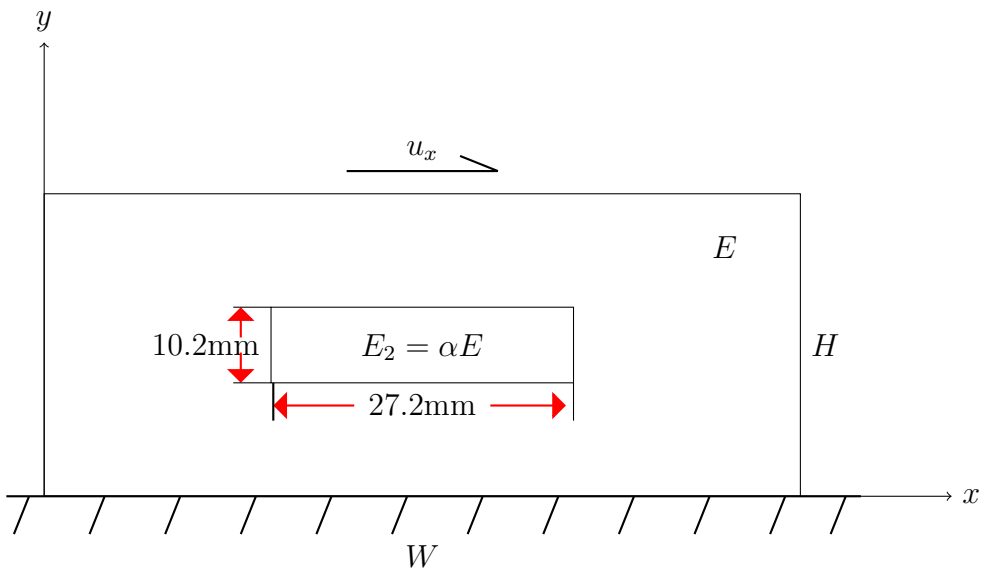

Figure 5.2: The simple shear problem for a non-homogeneous block.

the hardening effect associated with an increase in the energetic length scale. Lastly, Section 5.6 numerically explores the problem introduced in Section 4.7 by comparing estimates of the yield strength with that obtained for various simulations.

The dimensionless shear stress τ_{xy}/μ presented as a function of the applied strain Γ is used to demonstrate the results for mesh sensitivity, dissipative and energetic effects. Unless otherwise stated, results for both blocks are those obtained at the point $(x = 0.5W,\ y = 0.75H)$.

5.1 Mesh sensitivity

Here we present results obtained for the homogenous block with microhard boundary conditions and $L = 0.2H,\ l = 0$. The geometry is discretized using uniform meshes of 50×50, 40×40, 20×20 and 20×4 elements.

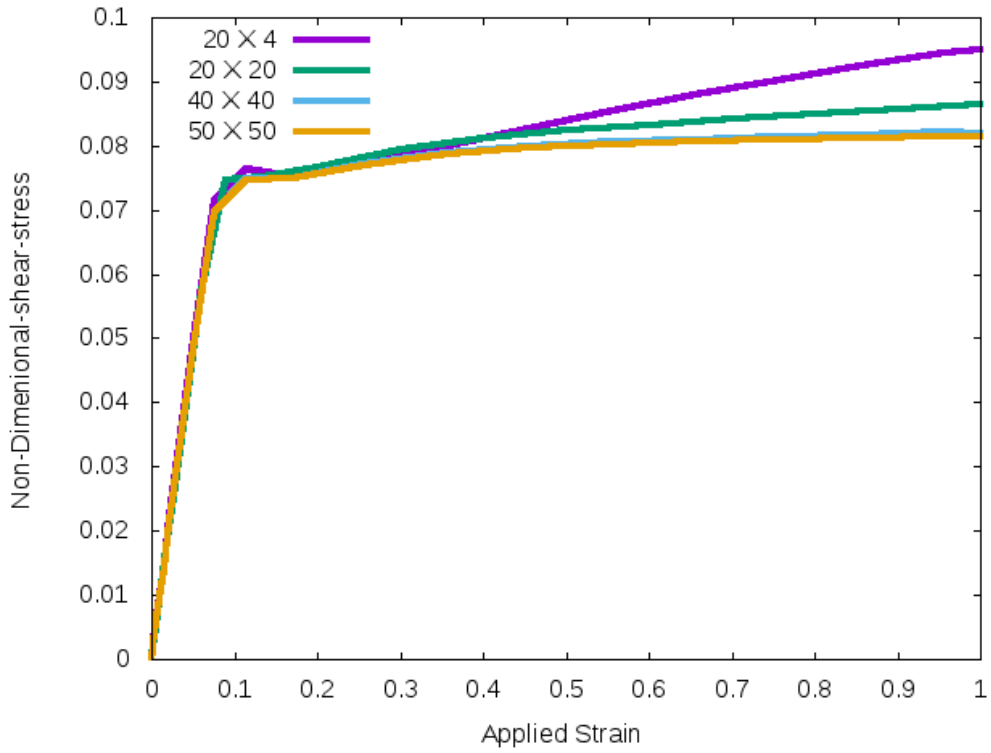

Figure 5.3: Microhard results with pure dissipative conditions ($L = 0.2H$, $l = 0$) from uniform meshes of 50×50, 40×40, 20×20 and 20×4 elements.

The results show close agreement in the elastic region. In the post-yield region there is negligible difference between the results using the 40×40 and 50×50 element meshes. We use the 50×50 element mesh in the simulations that follow.

5.2 Non-homogeneous block: variation with Young's modulus in the elastic sub-domain

In later simulations we want to use a value of α that is large enough for the inner section to be effectively rigid, thus we compare five values of α. Figure 5.4 shows curves of dimensionless shear stress τ_{xy}/μ as a function of the applied strain Γ. The results are extracted at the point $(x = 0.5W, y = 0.75H)$. We use a 50×50 element mesh with microhard BCs, dissipative length scale $L = 0.3H$, and energetic length scale $l = 0$.

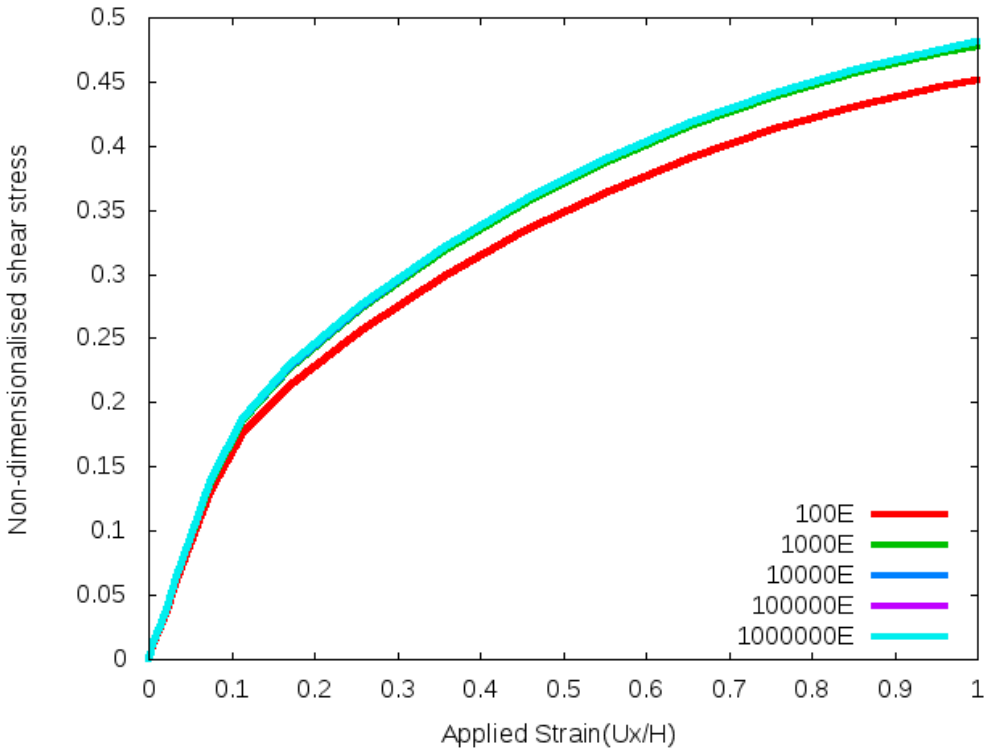

Figure 5.4: Variation of α on the non-homogeneous block with microhard bc's and pure dissipative conditions; $L = 0.3H,\ l = 0$.

We note that there is a negligible difference between the results for $\alpha = 10^3$ to $\alpha = 10^6$. From here onwards we use $\alpha = 10^3$.

5.3 Stress distributions

For the homogeneous block, the problem is primarily one-dimensional, and the only dominant Cauchy stress component is the shear stress τ_{xy}.

To observe the variation in stresses across the domain, we plot the stress components σ_{11}, σ_{22}, σ_{12} and the norm of the deviatoric stress ($|\boldsymbol{\sigma}^{\mathbf{dev}}|$) along the line $y = 0.75H$ for both homogeneous and non-homogeneous blocks. We consider purely dissipative conditions with $L = 0.2H,\ l = 0$, and we present results at 0.2s.

Microfree boundary conditions

Figure 5.5 below shows variation in the stresses along $y = 0.75H$ for microfree BCs when implementing the strain-gradient model, whilst Figure 5.6 shows the same results obtained from the classical (non-gradient) model in ABAQUS.

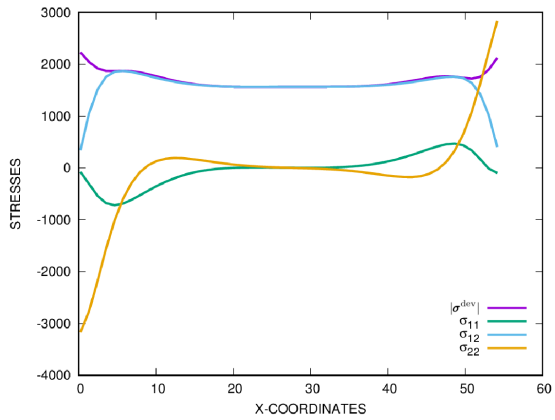

(a) Homogeneous block

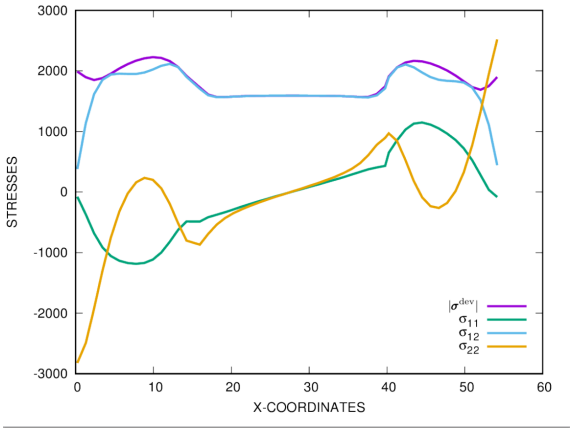

(b) Non-homogeneous block

Figure 5.5: Strain gradient model's stress results for homogeneous and non-homogeneous blocks along $y = 0.75H$ with $L = 0.2H$, $l = 0$ and microfree BCs.

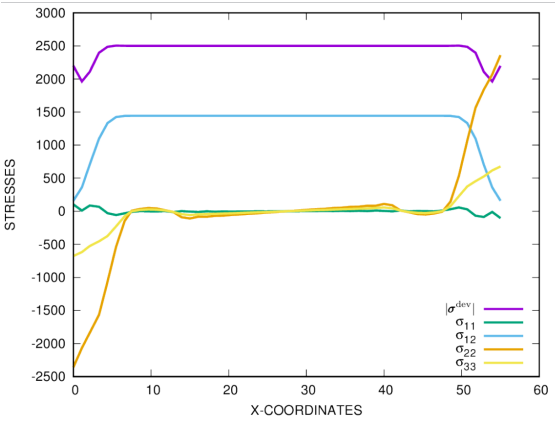

(a) Homogeneous block

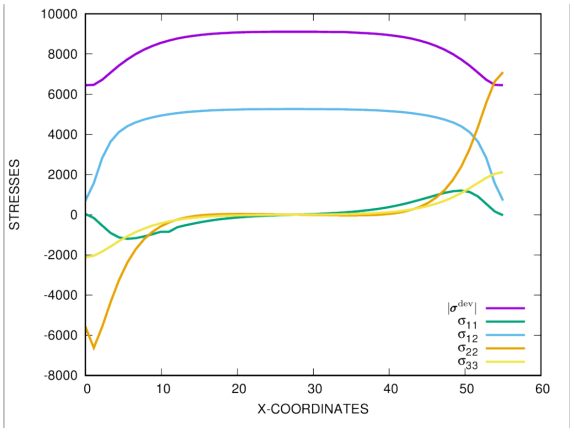

(b) Non-homogeneous block

Figure 5.6: Classical model's stress results for homogeneous and non-homogeneous blocks along $y = 0.75H$ with microfree BCs using ABAQUS elements.

We note that both blocks, in both strain gradient and classical models, show a dominant shear stress, as expected. Moreover, along the line of symmetry, the direct stresses for both blocks are zero. For the strain-gradient model, the stress σ_{22} exhibits extreme magnitudes on both ends of the block. At $y = 0.75H$, the maximum magnitude of $|\boldsymbol{\sigma}^{\text{dev}}|$ occurs at the sides: at $x = 0W$, $x = W$ for the homogeneous block and approximately $x = 0.2W$, $x = 0.8W$ for the non-homogeneous block. For the classical model, the non-homogenous block is stiffer than the homogenous block. The stress σ_{22} exhibits extreme magnitudes on both ends of the block. The maximum magnitude of $|\boldsymbol{\sigma}^{\text{dev}}|$ occurs at approximately $x = 0.1W$, $x = 0.9W$ for the homogeneous block and approximately $x = 0.2W$, $x = 0.8W$ for the non-homogeneous block. The strain-gradient model results are different to the classical model. This is because the problem exhibits gradients in the plastic strain in both directions as a result of the boundary conditions. This is in contrast to the problem of an infinite strip in shear, which is a one-

dimensional problem.

Microhard boundary conditions

Here we present results obtained by imposing microhard conditions on both blocks. Figure 5.7 below presents the stresses along the line y=0.75H.

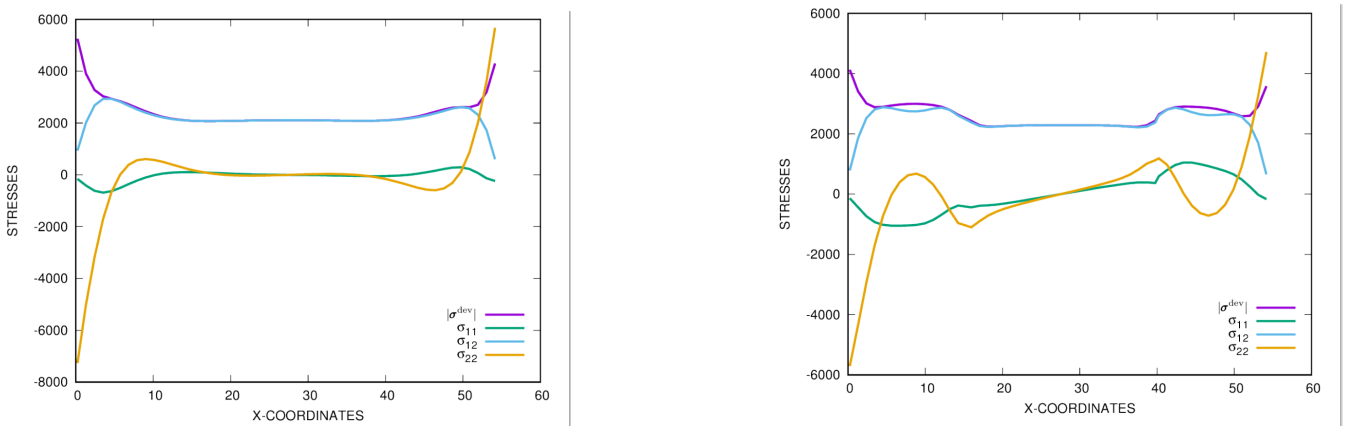

(a) Homogeneous block

(b) Non-homogeneous block

Figure 5.7: Microhard stress results for homogeneous and non-homogeneous blocks along $y = 0.75H$ with $L = 0.2H, l = 0$.

We note that both blocks show a dominant shear stress, and zero direct stresses along the line of symmetry. The stress σ_{22} also still has extreme magnitudes at both ends of the block. All stress magnitudes are significantly higher as compared to their corresponding magnitudes in the microfree analysis. This is expected because of the plastic strain restriction which causes dislocations piling up on the edges, unlike the microfree BCs which allow dislocations to exit freely. The maximum value of $|\boldsymbol{\sigma}^{\text{dev}}|$ occurs at the sides ($x = 0W,\ x = W$) of the homogeneous block and at $x = 0.2W$, $x = 0.8W$ of the non-homogeneous block. In summary, there is not much difference between the homogeneous and non-homogeneous solutions.

5.4 Elastic gap

We study the elastic gap phenomenon on the homogeneous block. The three types of boundary conditions results are presented in Figure 5.8: microfree (red), microhard (green) and microfree for the first $0.5s$ then microhard (blue) are used for this test with the material length scales $L = 0.2H$ and $l = 0$. We refer to the latter boundary condition as passivation and the time frame where microfree is changed to microhard as $t_{\text{pass}} = 0.5s$ or the passivation point.

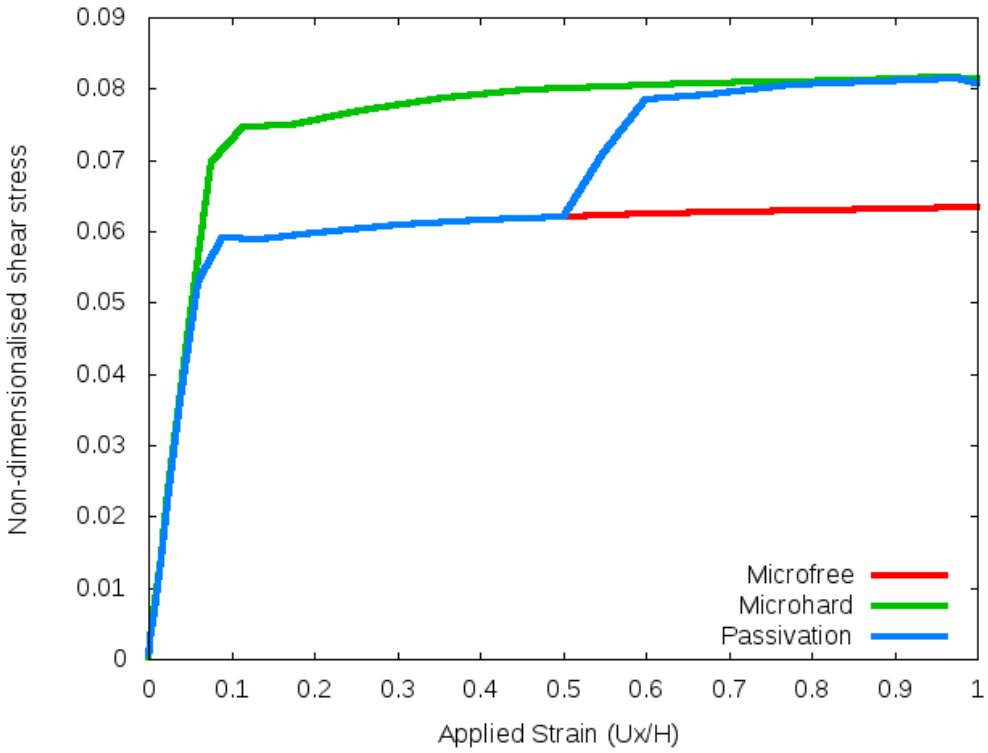

Figure 5.8: Passivation, microfree and microhard results for the homogeneous block with pure dissipative conditions ($L = 0.2H$, $l = 0$) and using a mesh of 50×50 elements

The results show negligible difference in the elastic phase. Moreover, the passivation results are in alignment with the microfree results up to the point of passivation ($t_{\text{pass}} = 0.5$s), as expected. The stress evolution is linear with applied strain after t_{pass}. This phenomenon is referred to as the elastic gap. However, our elastic gap is not the same as the elastic phase slope (≈ 1) as expected and as observed in Carstensen et al. (2017). This could be as a result of the viscoplastic nature of our dissipation function.

5.5 Strengthening and hardening

In this section we investigate the effect of different magnitudes of the dissipative and energetic length scales in both the homogeneous and non-homogeneous plate. Strengthening refers to the increase of the limit of proportionality or the threshold for the onset of plastic flow, whilst hardening is associated with the increase in the stress needed to obtain a given plastic shear. Moreover, strengthening is associated with the dissipative material length scale whereas hardening corresponds to the energetic material length scale.

Strengthening

We consider a pure dissipative analysis; that is, $l = 0$. The figures below show the results for microfree BCs for both blocks in consideration.

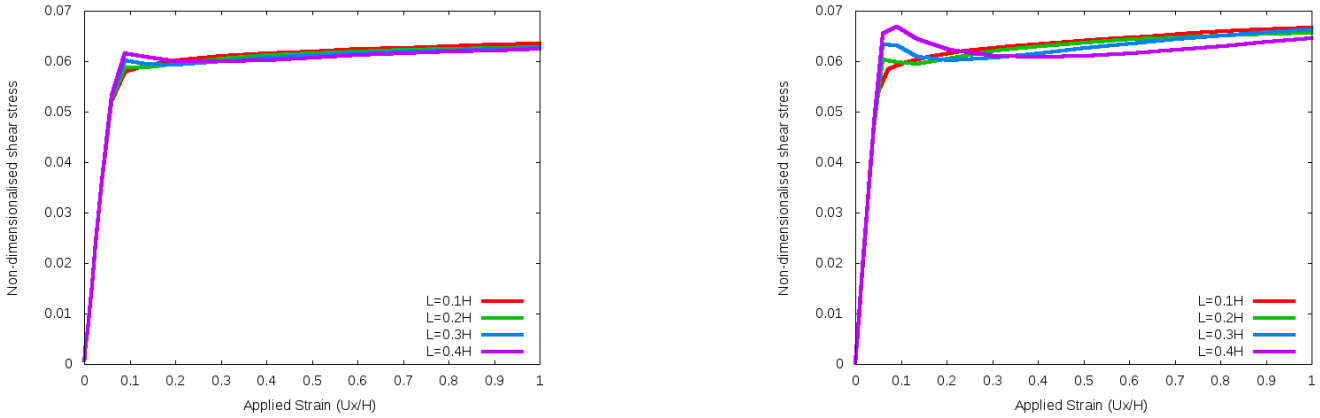

(a) Homogeneous block (b) Non-homogeneous block

Figure 5.9: Microfree results for both homogenous and non-homogeneous blocks with pure dissipative conditions.

The microfree results for the homogeneous block show minor strengthening whilst the non-homogeneous block results show quite a significant difference in the limit of proportionality which shows strengthening with the increase in dissipative length scale. However, after the applied strain = 0.3, insignificant differences and some softening are observed.

We also review results for the microhard BC for both homogeneous and non-homogeneous blocks in figure 5.10 below.

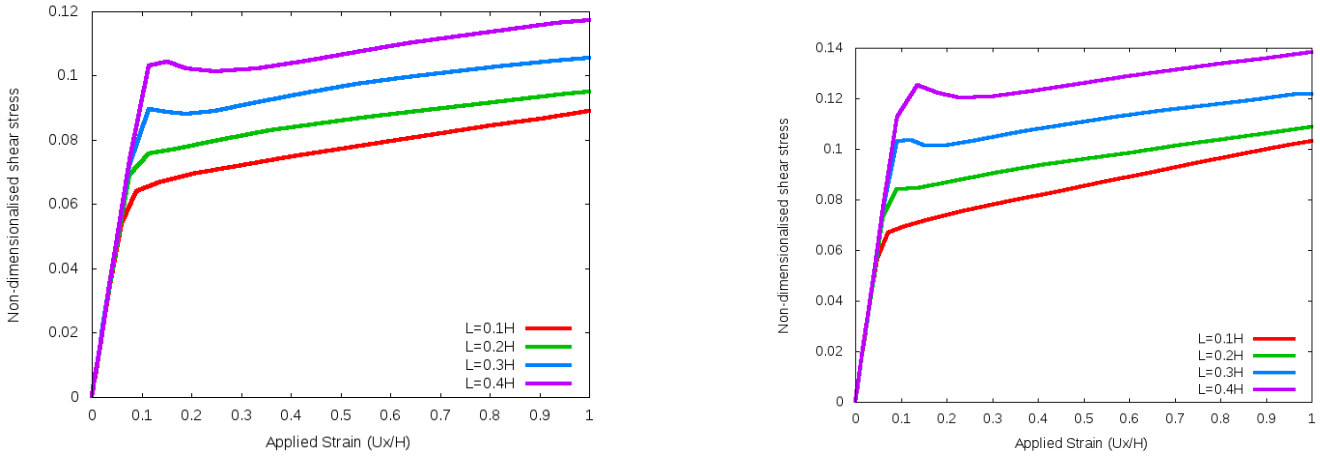

(a) Homogeneous block (b) Non-homogeneous block

Figure 5.10: Microhard BC results for homogeneous and non-homogeneous blocks for pure dissipative conditions

Both sets of results show significant strengthening as the dissipative length scale magnitude

increases. Also, the curve for $L = 0.4H$ has a huge hump around the yield point, which is evident in the microfree case as well.

Hardening

Here we study the effect of using different energetic length scale magnitudes with $L = 0$. We present microfree results for both blocks in question in Figure 5.11 below.

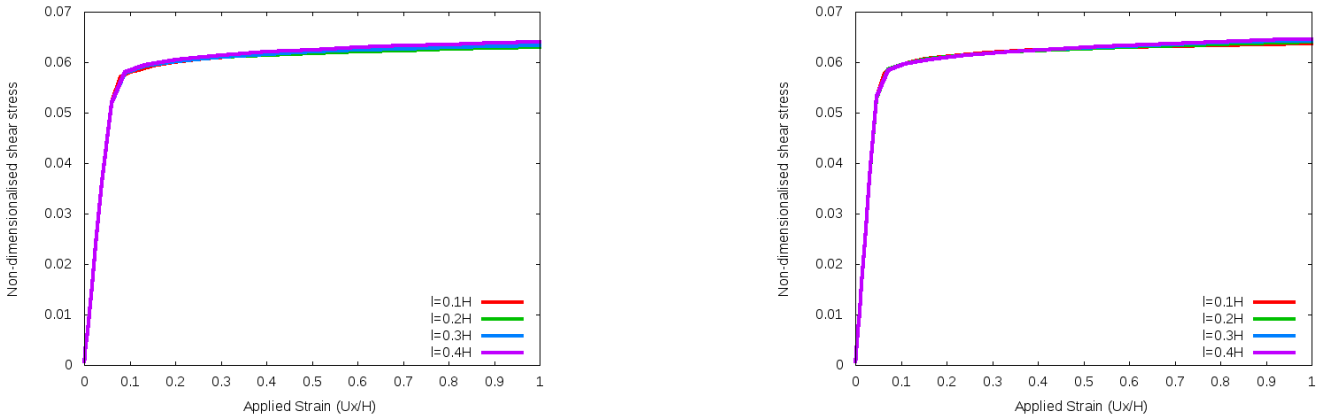

(a) Homogeneous block (b) Non-homogeneous block

Figure 5.11: Microfree results for both homogeneous and non-homogeneous blocks under energetic conditions.

Results for both homogeneous and non-homogeneous blocks show insignificant differences throughout the analysis.

From the microhard BC of both blocks we have the results shown in Figure 5.12:

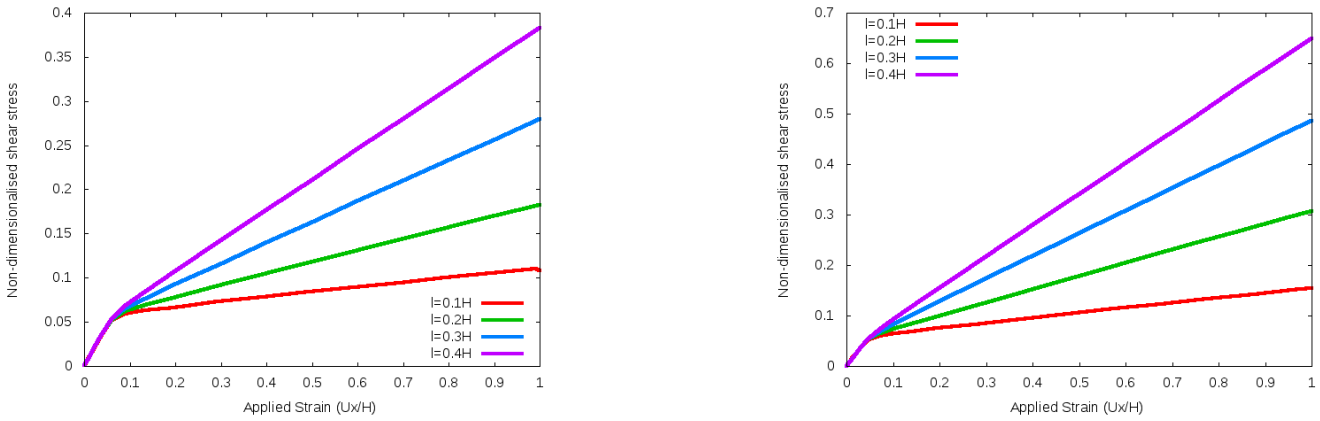

(a) Homogeneous block (b) Non-homogeneous block

Figure 5.12: Microhard results for both homogeneous and non-homogeneous blocks under energetic conditions.

The microhard results for both blocks shown in Figure 5.12 are in alignment in the elastic

range and clearly distinct in the plastic range: the slope increases markedly as the energetic length scale increases, thus exhibiting hardening. The non-homogeneous block has significantly greater magnitudes of τ_{xy}/μ compared to the homogeneous block.

Comparing the homogeneous block to the non-homogeneous block

Since from the above subsections the non-homogeneous block appears to have greater magnitudes of dimensionless shear stress than the homogeneous block, we compare them in one plot in this section so as to investigate the difference.

Purely dissipative

Here we compare the responses for the homogeneous and non-homogeneous blocks under pure dissipative conditions; $L = 0.3H$, $l = 0$: see Figure 5.13.

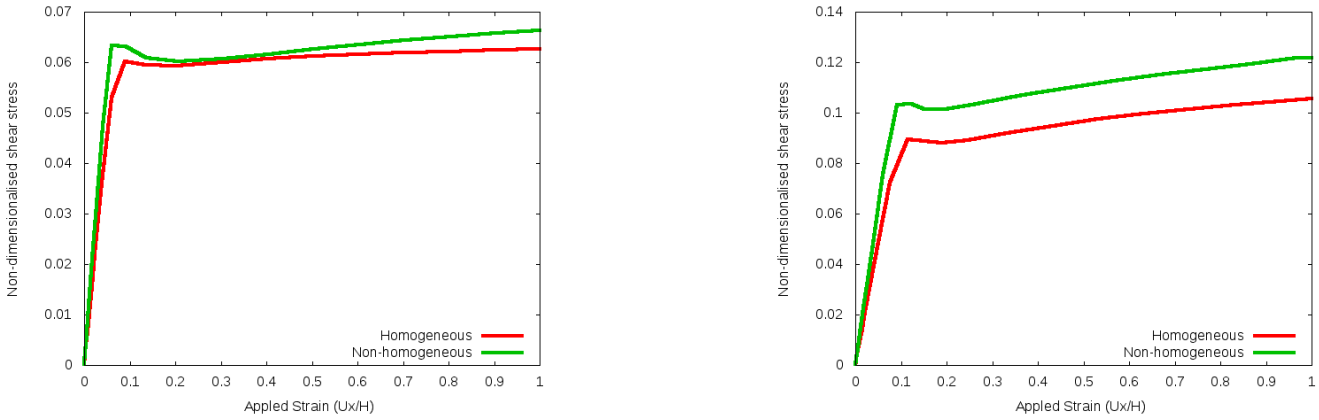

(a) Microfree.

(b) Microhard.

Figure 5.13: Comparing microfree and microhard results for both plates in consideration under pure dissipative conditions: $L = 0.3H$, $l = 0$.

Unsuprisingly the non-homogeneous plate is stiffer than the homogeneous plate for both BCs under purely dissipative conditions.

Purely energetic

Here we compare the responses for the homogeneous and non-homogeneous blocks under pure energetic conditions; $L = 0$, $l = 0.3H$: see Figure 5.14 .

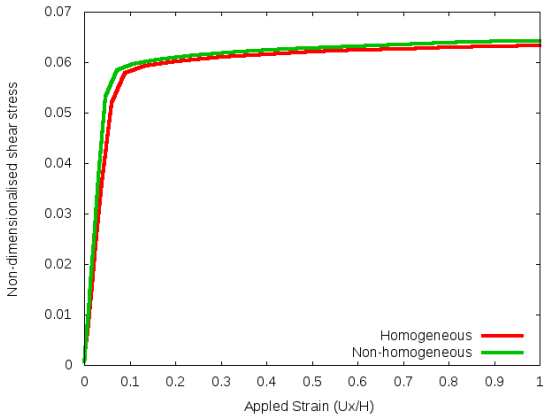

(a) Microfree.

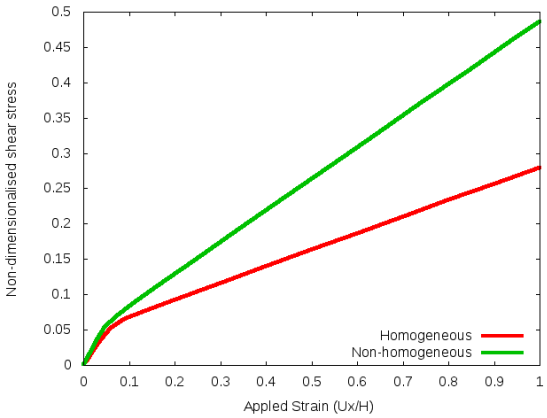

(b) Microhard.

Figure 5.14: Comparing microfree and microhard results for both plates in consideration under pure energetic conditions: $L = 0$, $l = 0.3H$

The non-homogeneous plate is much stiffer than the homogeneous plate with microhard BC and pure energetic conditions.

5.6 The global flow relation

As indicated in Section 4.7, the flow relation for the dissipative rate-independent problem is a global condition when expressed in terms of the Cauchy stress as a function of the dissipation function. It is not possible to invert this relation in closed form, to obtain the generalized plastic strain rate as the normal to a global yield function.

We numerically explore some upper-bound approximations to Φ as given by (4.90). The first approximation is obtained by setting $\mathbf{q} = \boldsymbol{\sigma}^{\mathrm{dev}}$ in (4.81) or $\hat{\mathbf{q}} = \mathsf{s}$. Then we have

$$\Phi(\mathsf{s}) \leq \overline{\Phi}(\mathsf{s}) := \frac{|\mathsf{s}|^2}{\mathcal{J}(\mathsf{s})}. \tag{5.2}$$

For the second approximation, we set as an upper bound the classical Mises yield criterion: that is,

$$\Phi(\boldsymbol{\sigma}) \leq \hat{\Phi}(\boldsymbol{\sigma}) := \frac{\max_{\Omega}|\boldsymbol{\sigma}^{\mathrm{dev}}|}{\sigma_0\sqrt{2/3}}. \tag{5.3}$$

Clearly, $\hat{\Phi}$ and $\overline{\Phi}$ will provide upper bounds to the actual yield. Alternatively, they would be expected to predict first yield earlier than when it actually occurs.

We present results for the two approximations using microhard BCs with purely dissipative

conditions; that is, $L = 0.2H$, $l = 0$. As observed in Figure 5.7, we have the maximum of $|\boldsymbol{\sigma}_{\mathbf{dev}}|$ approximately at $(x = 0,\ y = 0.75H)$ and $(x = W,\ y = 0.75H)$ for both the homogenous and the non-homogenous block. Thus we use values of $\boldsymbol{\sigma}^{\text{dev}}$ at these points. We also add a comparison with results from $(x = 0.5W,\ y = 0.75H)$ for completeness. These are reproduced in Figure 5.15, together with the figures showing the approximations as a function of the applied strain.

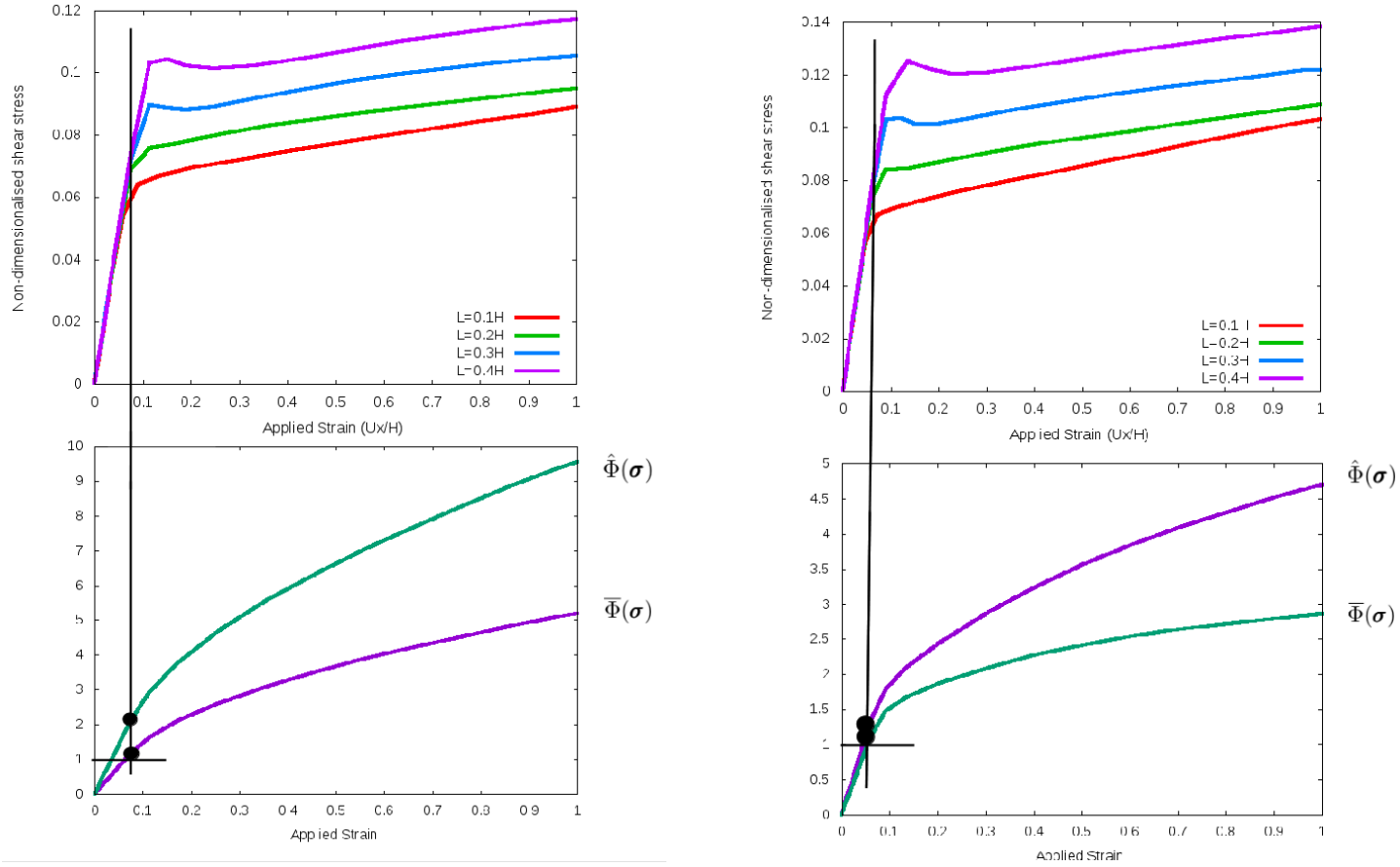

(a) Homogeneous plate

(b) Non-homogeneous plate

Figure 5.15: $\hat{\Phi}(\boldsymbol{\sigma})$ and $\overline{\Phi}(\boldsymbol{\sigma})$ both as a function of the applied strain compared to τ_{xy}/μ also a function of the applied strain. Results for microhard BCs presented for both homogeneous and non-homogeneous blocks from $x = 0.5W$, $y = 0.75H$.

A close-up of the elastic phase/yield stress of Figure 5.15 is shown in Figure 5.16.

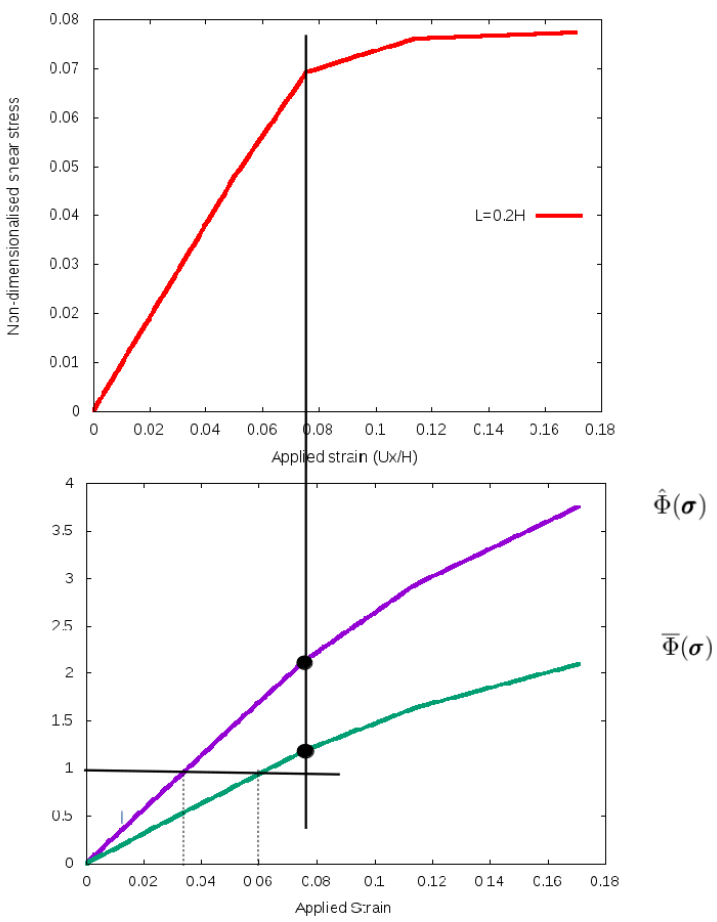

(a) Homogeneous plate.

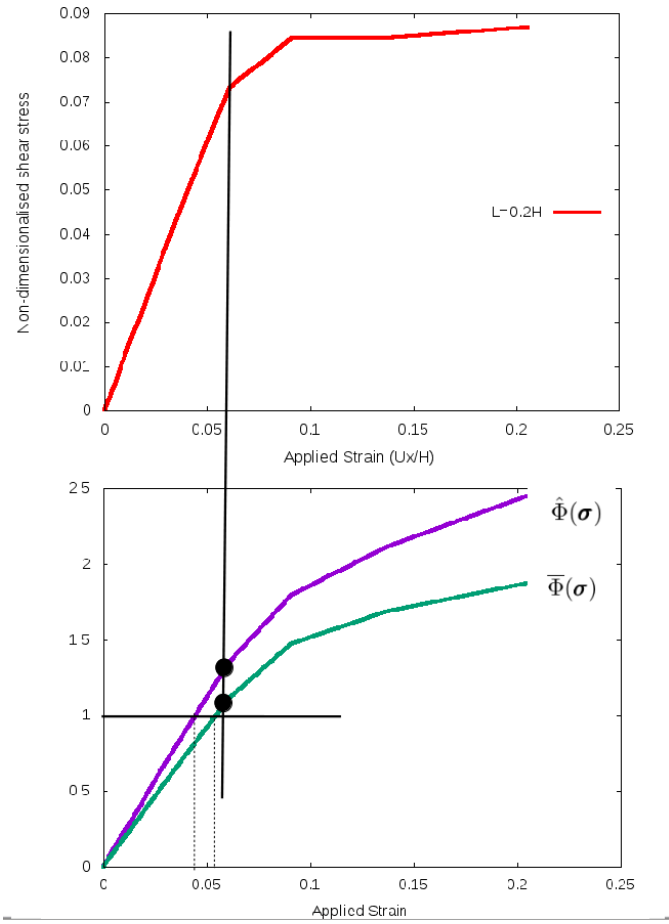

(b) Non-homogeneous plate.

Figure 5.16: A close up of Figure 5.15 on the elastic phase of the region around first point yield

For the homogeneous domain shows we observe that $\hat{\Phi}(\boldsymbol{\sigma}) \approx 2.1$ and $\overline{\Phi}(\boldsymbol{\sigma}) \approx 1.2$ at actual first yield, while for the non-homogeneous the values are $\overline{\Phi}(\boldsymbol{\sigma}) \approx 1.1$ and $\hat{\Phi}(\boldsymbol{\sigma}) \approx 1.25$. In both cases, these are upper bounds as expected.

On the other hand, for the homogeneous block, the approximations $\hat{\Phi}$ and $\overline{\Phi}$, predict first yield at applied strain values of 0.03 and 0.06 respectively, as opposed to the actual value of 0.075. For the non-homogeneous block, the corresponding values are 0.049 and 0.055, respectively, as opposed to the actual value of 0.06. From these results, it is seen that $\overline{\Phi}$ provides a closer approximation to first yield.

Next, we present results for $(x = 0,\ y = 0.75H)$ in Figure 5.17, noting that this is the approximate location of maximum Mises stress (see Figure 5.7)

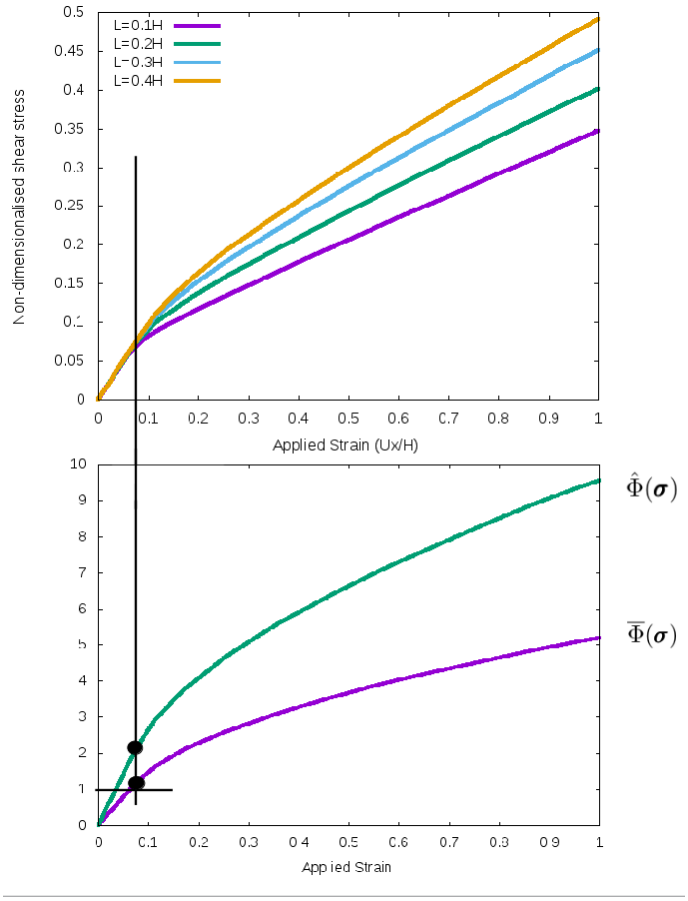

(a) Homogeneous plate.

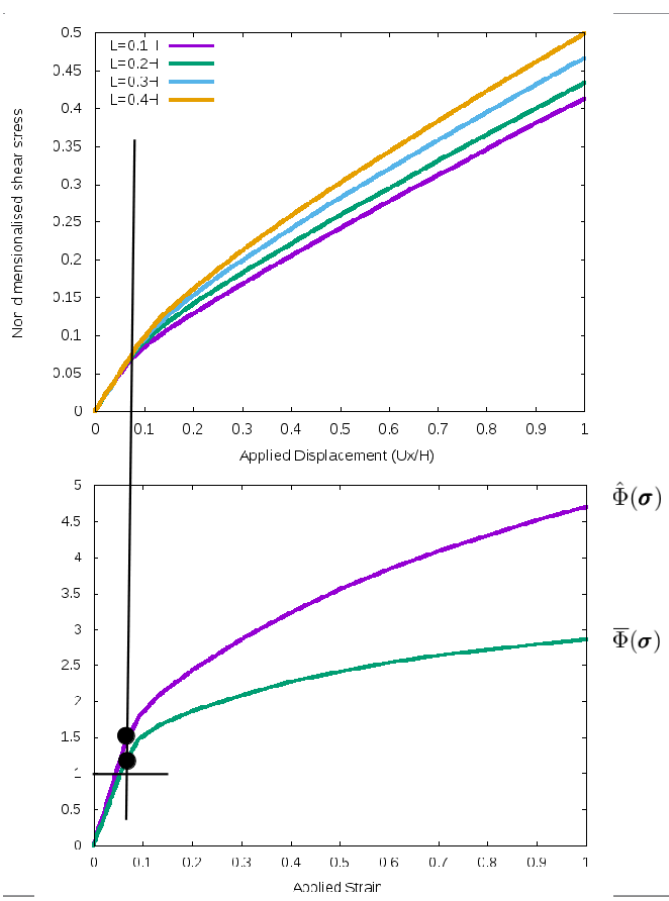

(b) Non-homogeneous plate.

Figure 5.17: $\hat{\Phi}(\boldsymbol{\sigma})$ and $\overline{\Phi}(\boldsymbol{\sigma})$ both as a function of the applied strain compared to τ_{xy}/μ also a function of the applied strain. Results for microhard BC presented for both homogemous and non-homogeneous blocks from $(x = 0,\ y = 0.75H)$.

We zoom in on the point of yield for Figure 5.17:

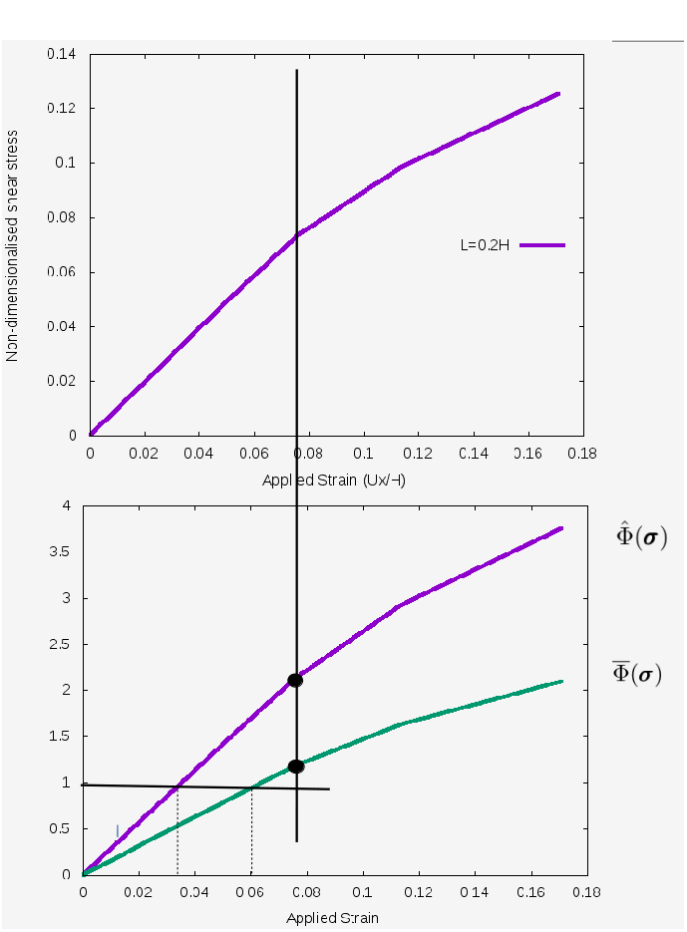

(a) Homogeneous plate.

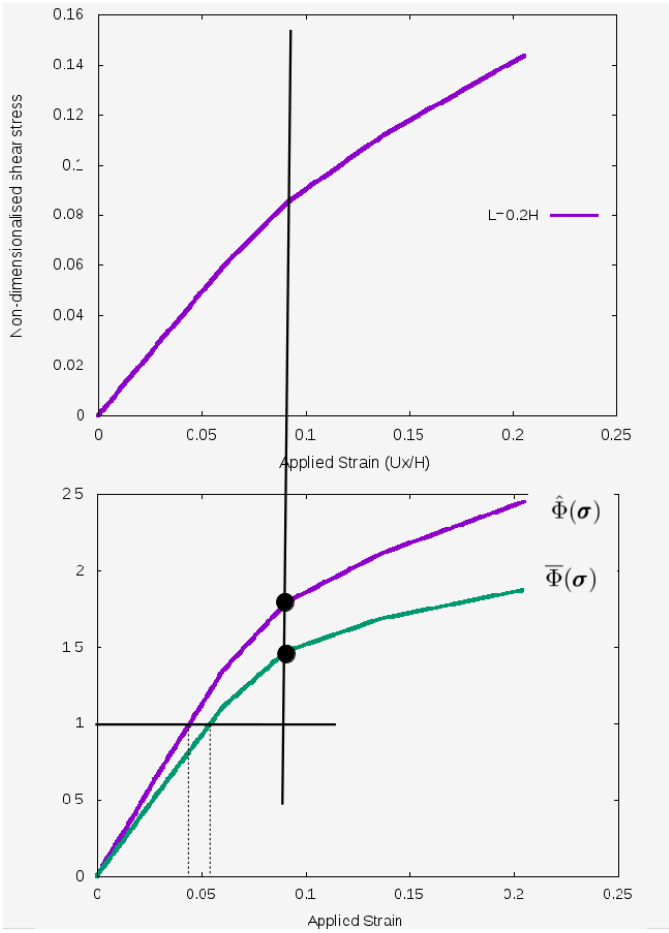

(b) Non-homogeneous plate.

Figure 5.18: A close up of Figure 5.17

For the homogeneous domain shows we observe that $\hat{\Phi}(\boldsymbol{\sigma}) \approx 2.1$ and $\overline{\Phi}(\boldsymbol{\sigma}) \approx 1.3$ at actual first yield, while for the non-homogeneous the values are $\overline{\Phi}(\boldsymbol{\sigma}) \approx 1.4$ and $\hat{\Phi}(\boldsymbol{\sigma}) \approx 1.75$. In both cases, these are upper bounds as expected.

On the other hand, for the homogeneous block, the approximations $\hat{\Phi}$ and $\overline{\Phi}$, predict first yield at applied strain values of 0.038 and 0.06 respectively, as opposed to the actual value of 0.075. For the non-homogeneous block, the corresponding values are 0.048 and 0.055, respectively, as opposed to the actual value of 0.09. From these results, it is seen that $\overline{\Phi}$ provides a closer approximation to first yield.

Lastly, we compare the $\overline{\Phi}(\boldsymbol{\sigma})$, $\hat{\Phi}(\boldsymbol{\sigma})$ results with microhard results from the point $x = W, y = 0.75H$ in Figure 5.19

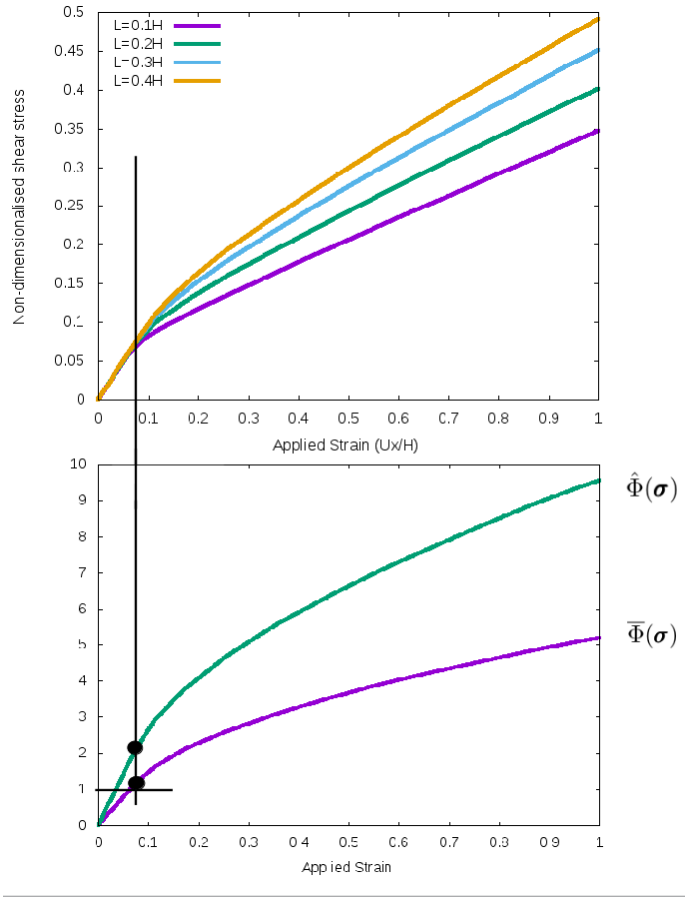

(a) Homogeneous plate.

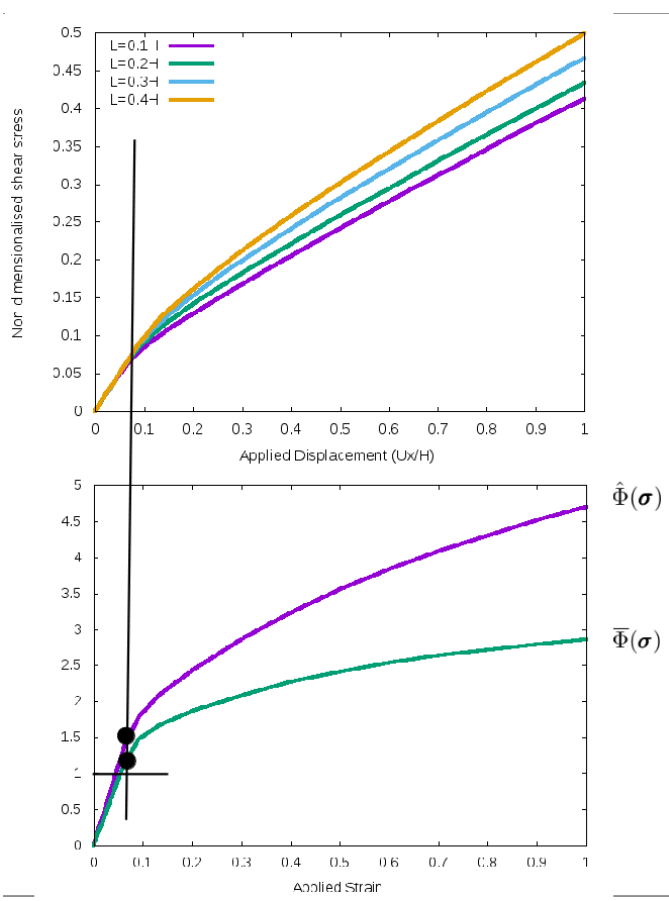

(b) Non-homogeneous plate.

Figure 5.19: $\hat{\Phi}(\boldsymbol{\sigma})$ and $\overline{\Phi}(\boldsymbol{\sigma})$ both as a function of the applied strain compared to τ_{xy}/μ also a function of the applied strain. Results for microhard BC presented for both homogeneous and non-homogeneous blocks from $(x = W,\ y = 0.75H)$.

A close up on the point of yield for Figure 5.17 is shown below in Figure 5.20.

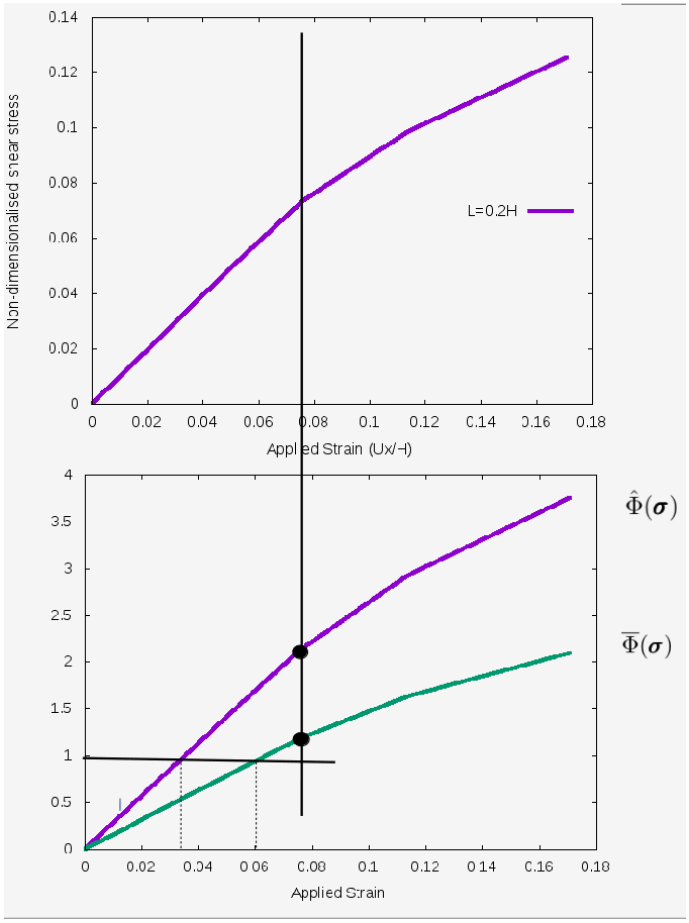

(a) Homogeneous plate.

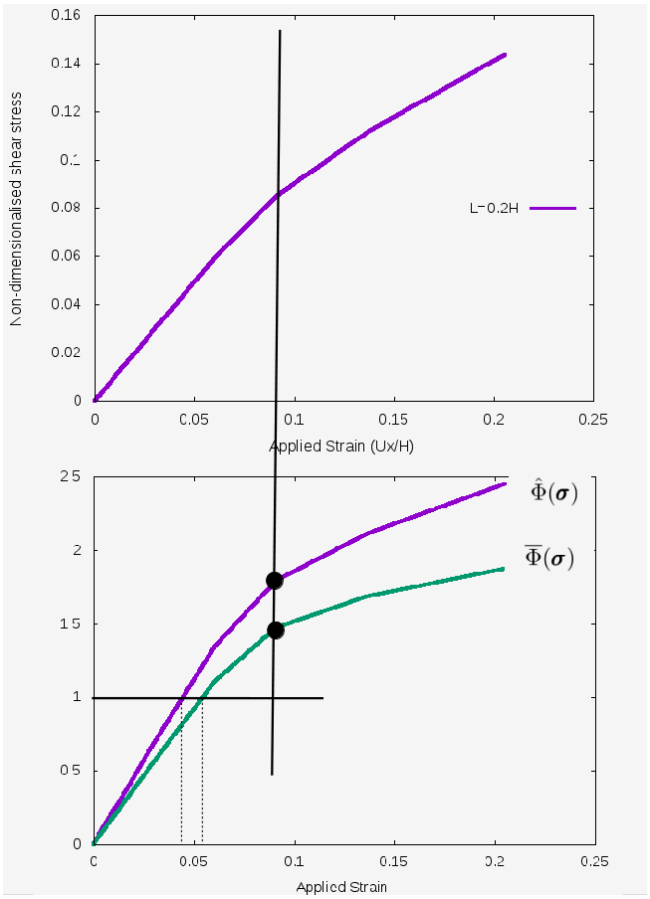

(b) Non-homogeneous plate.

Figure 5.20: A close up of Figure 5.19

We see that the results from $(x = 0,\ y = 0.75H)$ and $(x = W,\ y = 0.75H)$ are very close.

The approximation based on $\overline{\Phi}$ gives a reasonably close prediction of the applied strain at which first yield occurs. However, further numerical investigation of a range of problems is required in order to gain a better understanding of its utility.

Chapter 6

Conclusions

The main aim of this project has been to implement a higher-order strain gradient plasticity algorithm with energetic and dissipative contributions as a user element in ABAQUS; and to use it to numerically investigate various aspects of a strain-gradient plasticity theory, viz. strengthening and hardening as size-dependent effects; the elastic gap in the case of non-proportional loading; and the global flow relation for the purely dissipative problem. These investigations were conducted using homogeneous and non-homogeneous blocks under simple shear, with combinations of microfree, microhard, and passivation boundary conditions. A power-law approximation was used with parameters small enough to constitute a good approximation to rate-independent behaviour.

The first step, after establishing that a 50×50 element mesh gave results of sufficient accuracy, was to examine the stress distributions so as to have an idea of the variation in the stresses across the homogeneous and non-homogeneous domains. For this purpose, microfree and microhard BCs were used, and since the former is generally an extended version of classical plasticity, we compared results from our user element to those obtained from classical plasticity. We observed a similar behaviour for the two types of boundary conditions: the shear stress is the dominant stress, and the direct stress in the direction transverse to shear has greatest magnitudes at the sides of each domains.

Next, we investigated the elastic gap phenomenon and observed an elastic gap from the point at which boundary conditions were changed from microfree to microhard. However, the elastic gap slope was found to be lower than that corresponding to truly elastic behaviour. This might be because of the viscoplasticity nature of our model.

We also investigated for the homogeneous and non-homogeneous domains, the dependence of strengthening and hardening on the dissipative and energetic length scales, respectively. In

both domains, strengthening with increase in the dissipative length scale is evident at the point of yield, followed by softening in the case of microfree boundary conditions, whilst for microhard BCs, there is strengthening from the yield point through to the end of the analysis. We further compared strengthening and hardening results from each domain to confirm that the non-homogeneous domain is stiffer than the homogeneous domain.

Lastly, we numerically investigated two approximations to the global yield condition that is characteristic of the purely dissipative problem. The yield condition is given as the upper bound of a functional involving the dissipation function, and the approximations adopted were, first, the simple Mises yield condition and, secondly, one in which the arbitrary plastic strain is chosen to be collinear with the deviatoric stress. These approximations were found to behave as expected, though that based on the Mises condition was found to be poor in that, it predicts the first yield at an applied strain considerably lower than that obtained from the simulations.

It is hoped that this work has provided some useful perspectives on the behaviour of dissipative and energetic theories. The notion of a global yield condition is an intriguing one, and the results in this thesis provide some indication of its relationship to first yield and of the effectiveness or otherwise for simple approximations. While there exist results in the literature on yield and the related issue of strengthening for the problem of simple shear of an infinite strip, for problems only slightly complex such as that studied in this work; such closed-form results are not feasible using standard approaches. It is thus important to extend the investigation in this thesis of approximations to yield, to include a range of problem types and choices of approximations.

Acknowledgements

I would like to sincerely express my gratitude to my supervisor Prof B.D. Reddy for his patience, guidance and support. I was very new to the world of mechanics, FEM, Abaqus and Fortran. With his help, I was able to progress at a relatively faster pace and started to enjoy my work. To Andrew McBride, I thank him for his suggestions when I was at my worst concerning the numerical work. I thank him for introducing me to Daniele Barbera, he really helped me out. I thank Daniele for taking time from his busy life to help me out regardless of the distance and me being a stranger. Also, Greg Mitchell at the FEAS office, I thank him for helping me out with Abaqus; from the basics to my annoying subsequent everyday emails. He was patient with me and he answered every email I sent to him, regardless of how obvious it was. Nkosi, Emma, Mebratu, Michael, Maien, Ritesh, Karl, Fara, Bev, Kevin and the whole CERECAM family, I thank you for your help even though I would randomly pitch at your desks/offices. A special thanks to Natalie. She was my mom. She cared for my well being; emotionally, physically and financially. She has the purest heart. I am so grateful to have had you as my shoulder during this work, continue being the best. To my friends here in Cape Town, thank you for keeping me sane, through your jokes and company. I have found family in you. I would also like to thank my parents and friends from Swaziland. Even though they didn't unerstand why I had to do a second masters, they were supportive and kept on checking up on me. They continued to ask me when I will finish; well, here we are.

References

E. C. Aifantis. On the microstructural origin of certain inelastic models. *Journal of Engineering Materials and technology*, 106(4):326–330, 1984.

E. C. Aifantis. The physics of plastic deformation. *International Journal of Plasticity*, 3(3): 211–247, 1987.

E. C. Aifantis. Strain gradient interpretation of size effects. In *Fracture Scaling*, pages 299–314. Springer, 1999.

B. Allan. Lecture notes on continuum mechanics:conservation laws for continua, 2012.

L. Anand, M. Gurtin, S. Lele, and C. Gething. A one-dimensional theory of strain-gradient plasticity: formulation, analysis, numerical results. *Journal of the Mechanics and Physics of Solids*, 53(8):1789–1826, 2005.

L. Bardella. Some remarks on the strain gradient crystal plasticity modelling, with particular reference to the material length scales involved. *International Journal of Plasticity*, 23(2): 296–322, 2007.

L. Bardella. Size effects in phenomenological strain gradient plasticity constitutively involving the plastic spin. *International Journal of Engineering Science*, 48(5):550–568, 2010.

S. Bargmann and B. D. Reddy. Modeling of polycrystals using a gradient crystal plasticity theory that includes dissipative micro-stresses. *European Journal of Mechanics-A/Solids*, 30 (5):719–730, 2011.

M. R. Begley and J. W. Hutchinson. The mechanics of size-dependent indentation. *Journal of the Mechanics and Physics of Solids*, 46(10):2049–2068, 1998.

T. Belytschko, W. K. Liu, B. Moran, and K. Elkhodary. *Nonlinear finite elements for continua and structures*. John wiley & sons, 2013.

V. L. Berdichevsky. Continuum theory of dislocations revisited. *Continuum Mechanics and Thermodynamics*, 18(3-4):195, 2006.

C. Carstensen, F. Ebobisse, A. McBride, B. Reddy, and P. Steinmann. Some properties of the dissipative model of strain-gradient plasticity. *Philosophical Magazine*, 97(10):693–717, 2017.

M. Chiricotto, L. Giacomelli, and G. Tomassetti. Dissipative scale effects in strain-gradient plasticity: the case of simple shear. *SIAM Journal on Applied Mathematics*, 76(2):688–704, 2016.

P. G. Ciarlet. *Three-dimensional elasticity*, volume 20. Elsevier, 1988.

E. A. de Souza Neto, D. Peric, and D. R. Owen. *Computational methods for plasticity: theory and applications*. John Wiley & Sons, 2011.

F. Ebobisse, A. McBride, and B. Reddy. On the mathematical formulations of a model of strain gradient plasticity. In *IUTAM Symposium on Theoretical, Computational and Modelling Aspects of Inelastic Media*, pages 117–128. Springer, 2008.

B. Ehrler, X. Hou, T. Zhu, K. M. P'ng, C. J. Walker, A. Bushby, and D. J. Dunstan. Grain size and sample size interact to determine strength in a soft metal. *Philosophical Magazine*, 88(25):3043–3050, 2008.

A. G. Evans and J. W. Hutchinson. A critical assessment of theories of strain gradient plasticity. *Acta Materialia*, 57(5):1675–1688, 2009.

C. A. Felippa. Introduction to finite element methods. *University of Colorado, USA*, 2001.

J. Fish and T. Belytschko. A first course in finite elements. 2007.

N. Fleck and J. Hutchinson. Strain gradient plasticity. *Advances in applied mechanics*, 33: 296–361, 1997.

N. Fleck and J. Willis. A mathematical basis for strain-gradient plasticity theory. part ii: Tensorial plastic multiplier. *Journal of the Mechanics and Physics of Solids*, 57(7):1045–1057, 2009a.

N. Fleck and J. Willis. A mathematical basis for strain-gradient plasticity theory—part i: scalar plastic multiplier. *Journal of the Mechanics and Physics of Solids*, 57(1):161–177, 2009b.

N. Fleck, G. Muller, M. Ashby, and J. Hutchinson. Strain gradient plasticity: theory and experiment. *Acta Metallurgica et Materialia*, 42(2):475–487, 1994.

N. Fleck, J. Hutchinson, and J. Willis. Strain gradient plasticity under non-proportional loading. *Proc. R. Soc. A*, 470(2170):20140267, 2014.

N. Fleck, J. Hutchinson, and J. Willis. Guidelines for constructing strain gradient plasticity theories. *Journal of Applied Mechanics*, 82(7):071002, 2015.

N. A. Fleck and J. Willis. Strain gradient plasticity: energetic or dissipative? *Acta Mechanica Sinica*, 31(4):465–472, 2015.

P. Gudmundson. A unified treatment of strain gradient plasticity. *Journal of the Mechanics and Physics of Solids*, 52(6):1379–1406, 2004.

M. E. Gurtin. *An introduction to continuum mechanics*, volume 158. Academic press, 1982.

M. E. Gurtin. A gradient theory of single-crystal viscoplasticity that accounts for geometrically necessary dislocations. *Journal of the Mechanics and Physics of Solids*, 50(1):5–32, 2002.

M. E. Gurtin. A gradient theory of small-deformation isotropic plasticity that accounts for the burgers vector and for dissipation due to plastic spin. *Journal of the Mechanics and Physics of Solids*, 52(11):2545–2568, 2004.

M. E. Gurtin and L. Anand. A theory of strain-gradient plasticity for isotropic, plastically irrotational materials. part i: Small deformations. *Journal of the Mechanics and Physics of Solids*, 53(7):1624–1649, 2005.

M. E. Gurtin and L. C. Martins. Cauchy's theorem in classical physics. *Archive for Rational Mechanics and Analysis*, 60(4):305–324, 1976.

M. E. Gurtin, L. Anand, and S. P. Lele. Gradient single-crystal plasticity with free energy dependent on dislocation densities. *Journal of the Mechanics and Physics of Solids*, 55(9): 1853–1878, 2007.

M. E. Gurtin, E. Fried, and L. Anand. *The mechanics and thermodynamics of continua*. Cambridge University Press, 2010.

W. Han and B. D. Reddy. *Plasticity: mathematical theory and numerical analysis*, volume 9. Springer Science & Business Media, 2012.

W. M. Lai, D. H. Rubin, E. Krempl, and D. Rubin. *Introduction to continuum mechanics*. Butterworth-Heinemann, 2009.

S. P. Lele and L. Anand. A large-deformation strain-gradient theory for isotropic viscoplastic materials. *International Journal of Plasticity*, 25(3):420–453, 2009.

Q. Ma and D. R. Clarke. Size dependent hardness of silver single crystals. *Journal of Materials Research*, 10(4):853–863, 1995.

E. Martínez-Pañeda and C. F. Niordson. On fracture in finite strain gradient plasticity. *International Journal of Plasticity*, 80:154–167, 2016.

E. Martínez-Pañeda, C. F. Niordson, and L. Bardella. A finite element framework for distortion gradient plasticity with applications to bending of thin foils. *International Journal of Solids and Structures*, 96:288–299, 2016.

M. MathWorks. the mathworks. *Inc., Natick, MA*, 1992.

A. McBride, B. D. Reddy, and P. Steinmann. Dissipation-consistent modelling and classification of extended plasticity formulations. *Journal of the Mechanics and Physics of Solids*, 2018.

H.-B. Mühlhaus and E. Aifantis. A variational principle for gradient plasticity. *International Journal of Solids and Structures*, 28(7):845–857, 1991.

K. L. Nielsen and C. F. Niordson. A numerical basis for strain-gradient plasticity theory: rate-independent and rate-dependent formulations. *Journal of the Mechanics and Physics of Solids*, 63:113–127, 2014.

C. F. Niordson and J. W. Hutchinson. On lower order strain gradient plasticity theories. *European Journal of Mechanics-A/Solids*, 22(6):771–778, 2003.

C. F. Niordson and P. Redanz. Size-effects in plane strain sheet-necking. *Journal of the Mechanics and Physics of Solids*, 52(11):2431–2454, 2004.

J. Nye. Some geometrical relations in dislocated crystals. *Acta metallurgica*, 1(2):153–162, 1953.

D. Owen and E. Hinton. *Finite elements in plasticity*, volume 271. Pineridge press Swansea, 1980.

A. Panteghini and L. Bardella. On the finite element implementation of higher-order gradient plasticity, with focus on theories based on plastic distortion incompatibility. *Computer Methods in Applied Mechanics and Engineering*, 310:840–865, 2016.

C. Polizzotto. Strain gradient plasticity, strengthening effects and plastic limit analysis. *International Journal of Solids and Structures*, 47(1):100–112, 2010.

B. Reddy. The role of dissipation and defect energy in variational formulations of problems in strain-gradient plasticity. part 1: polycrystalline plasticity. *Continuum Mechanics and Thermodynamics*, 23(6):527–549, 2011.

B. D. Reddy. *Introductory functional analysis: with applications to boundary value problems and finite elements*, volume 27. Springer Science & Business Media, 2013.

B. D. Reddy, F. Ebobisse, and A. McBride. Well-posedness of a model of strain gradient plasticity for plastically irrotational materials. *International Journal of Plasticity*, 24(1): 55–73, 2008.

J. N. Reddy. *An introduction to the finite element method*, volume 2. McGraw-Hill New York, 1993.

D. Roylance. Introduction to elasticity. *Cambridge: Department of Materials Science and Engineering*, 2000.

D. Rubin, E. Krempl, and W. Lai. *Introduction to Continuum Mechanics*. Elsevier Science, 2012. ISBN 9780080983875. URL `https://books.google.co.za/books?id=yUvw1m1zH7IC`.

N. Stelmashenko, M. Walls, L. Brown, and Y. V. Milman. Microindentations on w and mo oriented single crystals: an stm study. *Acta Metallurgica et Materialia*, 41(10):2855–2865, 1993.

J. S. Stölken and A. Evans. A microbend test method for measuring the plasticity length scale. *Acta Materialia*, 46(14):5109–5115, 1998.

J. Swadener, E. George, and G. Pharr. The correlation of the indentation size effect measured with indenters of various shapes. *Journal of the Mechanics and Physics of Solids*, 50(4): 681–694, 2002.

D. Systemes. Abaqus 6.14 documentation–theory guide. *Providence, RI*, 2015.

Y. Xiang and J. Vlassak. Bauschinger and size effects in thin-film plasticity. *Acta Materialia*, 54(20):5449–5460, 2006.

O. Zienkiewicz, D. Kelly, and P. Bettess. The coupling of the finite element method and boundary solution procedures. *International journal for numerical methods in engineering*, 11(2):355–375, 1977.